Upper-level troughs and tropical plumes at low latitudes: Identification, climatology and their impact on global moisture transport

Inaugural-Dissertation

zur

Erlangung des Doktorgrades

der Mathematisch-Naturwissenschaftlichen Fakultät

der Universität zu Köln

vorgelegt von

Elsa Luise Fröhlich

aus Dresden

Berichterstatter (Gutachter):	Prof. Dr. A. Fink Prof. Dr. M. Kerschgens Dr. habil. P. Knippertz
Tag der mündlichen Prüfung:	24. Januar 2012

Abstract

Intrusions of upper-level extratropical troughs into low latitudes are prominent examples of extratropical-tropical interactions. Along the eastern edge of these troughs tropical moisture is transported poleward into the subtropics, where it may occasionally lead to extreme precipitation events. Furthermore, these situations are often accompanied by enhanced convection and the formation of elongated cloud bands, which develop along the eastern flank of the trough and extend from the Tropics pole- and eastward into the subtropics or even midlatitudes. Such bands of mid- and upper-level clouds are commonly referred to as **T**ropical **P**lumes (TP). In the present work, these extratropical-tropical interactions are investigated on the basis of two novel climatologies of low-latitude troughs and of tropical plumes.

In the first part of this thesis the focus is on the identification, climatology and evolution of upper-level troughs at low latitudes and their impact on moisture transport is evaluated. For the identification of such events a new algorithm has been developed that analyses, in contrast to prior studies, **v**ertical **a**verages of **p**otential **v**orticity (VAPV) in the 400 to 100 hPa layer. This leads to a detection of intense troughs with a coherent signal throughout the upper troposphere. Regions with VAPV values of $\geq$ |2 PVU| between 17° North and South are defined as intrusion event. This algorithm is applied to ERA-40 reanalysis data for the 22-year period from 1980 to 2001.

The resulting climatology indicates frequency maxima during boreal winter in both hemispheres over the Pacific and Atlantic Oceans, in regions where upper westerly winds are predominant over the equator ("westerly ducts"). In boreal summer the intrusion activity is generally reduced with the exception of the central North Pacific.

Interannual variations of intrusion frequency in boreal winter show a clear association with the **E**l **N**iño-**S**outhern **O**scillation (ENSO) in the Northern Hemisphere in such a way that over the North Pacific (North Atlantic) significantly more (less) intrusion events are detected during the cold phase of ENSO.

The typical evolution of a PV intrusion, analysed with the help of composites of the upper PV field, is in all regions related to an eastward propagating extratropical Rossby wave train, which is observed already five days before intrusion detection and disperses equatorward into the Tropics in the following days.
Composites of meridional moisture flux anomalies in relation to PV intrusions show an export of tropical moisture into the subtropics on the eastern flank of the wave disturbance, which is most pronounced in the mid-troposphere (750 to 500 hPa).

In the second part of the thesis the focus is on the identification and climatology of Tropical Plumes. The identification of TPs is accomplished by applying a first objective algorithm to the brightness temperature (T_b) dataset of the Cloud Archive User Service for the time period Jul. 1983 to June 2006.
Following the classic definition by McGuirk et al. (1987) TPs are defined as extended bands (length > 2000 km) with T_b anomalies below -20 K that cross 15° North or South. Additionally a criterion for the elongatedness of a TP is implemented based on the **l**ength-to-**w**idth **r**atio (LWR) of the smallest rectangle that contains the TP.
The resulting northern winter climatology reveals nine active TP regions with the main maximum located over the central South Pacific close to the South Pacific convergence zone. Further TP frequency maxima are found over the eastern parts of the North Pacific and North Atlantic and over the western South Atlantic. In boreal summer the TP frequency is generally reduced except for the Bay of Bengal and the Northwest Pacific. A long-term negative trend in TP occurrence was found to be an artefact caused by changes in the satellite viewing geometries.
Inter-annual variations in TP frequency are related to ENSO primarily over the Pacific, where TP frequencies in the western South Pacific and over Australia are reduced during El Niño and enhanced over the central and eastern subtropical Pacific.
Based on composite analysis two different conditions for TP genesis are detected. While TP development in the majority of the regions is linked to the propagation of extratropical upper-level trough into low latitudes, in the Northwest Pacific tropical convective processes are responsible for TP formation. A brief comparison of both climatologies supports this idea.
Finally, the new identification algorithms for low-latitude disturbances and Tropical Plumes and the associated climatologies can serve as a basis for future studies on extratropical-tropical interactions.

Zusammenfassung

Das Eindringen von extratropischen Höhentrögen in niedere Breiten ist ein typisches Beispiel für extratropische-tropische Wechselwirkungen. An der Vorderseite des Troges wird feuchtwarme Luft aus den Tropen nordwärts in die Subtropen transportiert, wodurch in Einzelfällen extreme Niederschlagsereignissen in den Rand- und Subtropen hervorgerufen werden können. Zudem bilden sich häufig entlang der Ostseite dieser Höhentröge zusammenhängende Wolkenbänder, die in der Literatur als Tropische Wolkenfahnen (engl.: **T**ropical **P**lumes, TP) bezeichnet werden. Tropische Wolkenfahnen bestehen aus hohen und mittelhohen Wolken und erstrecken sich über Tausende von Kilometern von den Tropen ost- und polwärts bis in die Subtropen oder sogar mittleren Breiten.

In der folgenden Arbeit werden diese extratropischen-tropischen Wechselwirkungen mit Hilfe von zwei neu erstellten Klimatologien erforscht. Die erste Klimatologie beschreibt das Auftreten von Höhentrögen in niederen Breiten und die zweite das von Tropischen Wolkenfahnen. Im ersten Teil dieser Arbeit wird auf die Identifizierung, Klimatologie und Entwicklung der Höhentröge in niederen Breiten eingegangen und deren Einfluss auf Wasserdampftransporte wird erörtert. Zur Identifizierung dieser Ereignisse wurde ein neuer Algorithmus entwickelt, der im Gegensatz zu früheren Studien vertikale Mittel der potentiellen Vorticity zwischen 400 bis 100 hPa (VAPV) analysiert. Dadurch werden intensivere Tröge erfasst, die ein kohärentes Signal in der oberen Troposphäre bewirken. Regionen mit VAPV Werten $\geq$ |2 PVU| zwischen 17° N und S werden als Intrusionssysteme definiert. Dieser Ansatz wird auf die ERA-40 Reanalysedaten für den 22-jährige Zeitraum von 1980 bis 2001 angewendet.

Die daraus resultierende Klimatologie zeigt im nordhemisphärischen Winter in beiden Hemisphären Häufigkeitsmaxima über dem pazifischen und atlantischen Ozeanen, in Regionen mit mittleren Westwinden über dem Äquator (“westerly ducts”). Im nordhemisphärischen Sommer ist die Intrusionsaktivität im Allgemeinen geringer mit Ausnahme

über dem zentralen Nordpazifik.
Die jährlichen Schwankungen der regionalen Intrusionshäufigkeiten zeigen in der Nordhemisphäre eine deutliche Verbindung zu **E**l **N**iño-**S**outhern **O**scillation (ENSO): Dabei werden signifikant weniger (mehr) Intrusionsereignisse über dem Nordpazifik (Nordatlantik) während eines El Niño-Winters identifiziert.
Im Weiteren wird die Entwicklung von Intrusionssystemen mit Hilfe von Kompositestudien dargestellt. Diese Studien zeigen, dass die Entstehung eines Intrusionssystems in allen Regionen an einen ostwärts propagierender Rossby-Wellenzug gekoppelt ist, der bereits fünf Tage vor dem Ereignis stromaufwärts im Bereich des Stormtracks beobachtet wird. An den folgenden Tagen intensiviert sich dieser Wellenzug, während er sich äquatorwärts fortsetzt, wo es dann zur Bildung der Intrusion kommt.
Des Weiteren werden mit Hilfe von Kompositestudien Anomalien im Feuchtefluss im Zusammenhang mit dem Auftreten von Trögen in niederen Breiten untersucht. Dabei zeigt sich im Mittel ein nordwärtsgericheter Feuchtefluss an der Vorderseite des Troges, wodurch Feuchte aus den Tropen in die Subtropen transportiert wird.

Im zweite Teil dieser Arbeit wird die Identifizierung und Klimatologie von Tropischen Wolkenfahnen (TP) diskutiert. Für die Identifizierung der TPs wurde ein erstes objektives Verfahren entwickelt, das mit Hilfe von Helligkeitstemperaturen (T_b) Wolkenstrukturen im Zeitraum von Juli 1983 bis Juni 2006 identifiziert. Dabei werden in Anlehnung an die klassische Definition von McGuirk et al. (1987) TPs definiert als lang-gezogene Bänder (Länge> 2000 km) mit T_b Anomalien unter -20 K, die den nördlichen oder südlichen 15ten Breitengrad überqueren. Ein weiteres Identifikationskriterium berücksichtigt die “Langgezogenheit” der Wolkenfahnen mit Hilfe des Längenseitenverhältnisses (engl. **l**enght-to-**w**idth **r**atio, LWR) des kleinsten Rechtecks, dass die Wolkenfahne umfasst. Die daraus resultierende Klimatologie zeigt im nordhemisphärischen Winter neun Regionen, in denen TPs bevorzugt auftreten, mit einem Aktivitätsmaximum über dem Südwestpazifik in der Nähe der südpazifischen Konvergenzzone identifiziert werden. Weitere Häufigkeitsmaxima befinden sich über dem östlichen Nordpazifik und Nordatlantik und über dem westlichen Südatlantik. Im Sommer werden im Allgemeinen weniger TPs identifiziert, außer über dem Golf von Bengalen und über dem Nordwestpazifik. Die TP-Klimatologie zeigt eine signifikante Abnahme der Wolkenbänder innerhalb des Untersuchungszeitraumes, die durch Änderungen der Beobachtungssatelliten (bzgl. Randverdunklung) hervorgerufen wird. Die jährlichen Schwankungen der regionalen TP-Häufigkeiten zeigen vor allem im gesamten Pazifikraum eine deutliche Korrelation zu ENSO: Während über dem westlichen Südpazifik und über Australien im Allgemeinen mehr TPs in den Warmphasen von ENSO (Oct.-March) identifiziert werden, treten über dem tropischen Zentralpazifik und östlichen Nord- und Südpazifik weniger TPs auf. Mit Hilfe von Kompositstudien wurden zwei verschiede Bedingungen für die Entwicklung von TPs festgestellt: Während die Bildung von Tropischen Wolkenfahnen über dem Nordatlantik und Nordpazifik im Zusammenhang mit Höhentrögen in niederen Breiten steht, sind über dem Nordwestpazifik tropische konvektive Prozesse eher verantwortlich für die Bildung von TPs. Ein Vergleich der beiden vorgestellten Klimatologien bestätigt

zudem diese Beobachtungen.
Die in dieser Arbeit entwickelten Verfahren zur Identifizierung von Trögen in niederen Breiten und tropischen Wolkenfahnen und die damit erzeugten Klimatologien stellen eine Grundlage dar für weitere Forschungen im Zusammenhang mit extratropischen-tropischen Wechselwirkungen.

Contents

Abbreviations

AIRS	Atmospheric Infrared Sounder
AMM	Atlantic Meridional Mode
CLAUS	Cloud Archive User Service
CPC	Climate Prediction Center
ECMWF	European Centre for Medium Range Weather Forecast
ENSO	El Niño/Southern Oscillation
EOF	Empirical Orthogonal Function
ERA-40	ECMWF reanalysis, 40-year period 1957–2001
GPH	Geopotential Height
hPa	hectopascal
IR	Infrared
ISCCP	International Satellite Cloud Climatology Project
ITCZ	Intertropical Convergence Zone
LASDC	Langley Atmospheric Sciences Data Center
LWR	Length-to-Width Ratio
mb	millibar
MCA	Maximum Covariance Analysis
MJO	Madden-Julian Oscillation
MLS	Microwave Limb Sounder
MSLP	Mean Sea Level Pressure
NAO	North Atlantic Oscillation
NCAR	National Center for Atmospheric Research
NCEP	National Center of Environmental Prediction
NH	Northern Hemisphere
OLR	Outgoing Longwave Radiation
PNA	Pacific/North American teleconnection pattern

PV ..... Potential Vorticity
PVU ..... PV Units
RH ..... Relative Humidity
RWB ..... Rossby Wave Breaking
SACZ ..... South Atlantic Convergence Zone
SH ..... Southern Hemisphere
SOI ..... Southern Oscillation Index
SPCZ ..... South Pacific Convergence Zone
STJ ..... Subtropical Jet
TME ..... Tropical Moisture Export
TP ..... Tropical Plume
TRMM ..... Tropical Rainfall Measuring Mission
TUTT ..... Tropical Upper Tropospheric Trough
UTH ..... Upper Tropospheric Humidity
VAPV ..... Vertically Averaged Potential Vorticity
WV ..... Water Vapor

1 Introduction

1.1 Overview and motivation

Different kinds of relevant interactions between the Tropics and extratropics have been observed and analysed for a long time. Most of these studies are mainly concerned with the influence of tropical heating anomalies on the extratropical circulation on seasonal to inter-annual time scales, for example, in connection to the **E**l **N**iño/**S**outhern **O**scillation (ENSO; e.g., Horel and Wallace 1981) phenomenon. More recent studies brought evidence for a linkage between the intra-seasonal tropical heating anomalies related to the **M**adden-**J**ulian **O**scillation (MJO; e.g., Madden and Julian 1994) and anomalies in extratropical circulation (e.g., Weickmann et al. 1985, Jones et al. 2004). But there are also examples, where the extratropics directly affect the Tropics mainly by modulating the convective activity on different space and time scales. Specific examples include lower-tropospheric cold-surge events (e.g., Chang and Lau 1982, Garreaud 2001) and the equatorward propagation of upper-tropospheric troughs (e.g., Kiladis and Weickmann 1992a). The latter phenomenon will be the main subject of the present thesis.
Different studies have shown that troughs at low latitudes are often parts of east- and southward propagating coherent Rossby wave trains from the extratropics (e.g., Kiladis and Weickmann 1992a). The propagation of such waves is usually described by linear Rossby wave theory (Hoskins and Ambrizzi 1993), which requires mean westerly background flow for a penetration of stationary wave disturbances into the Tropics or even into the other hemisphere. Therefore this kind of interaction is most important on synoptic to sub-monthly time scales and is confined to tropical regions, where westerly background flow is prevalent. Such conditions are observed during the boreal cool season over the Pacific and Atlantic Oceans. Hence, these regions have been referred to as "westerly ducts" by Webster and Holton (1982).
One visible sign of these interactions is the formation of cloud bands that often develop

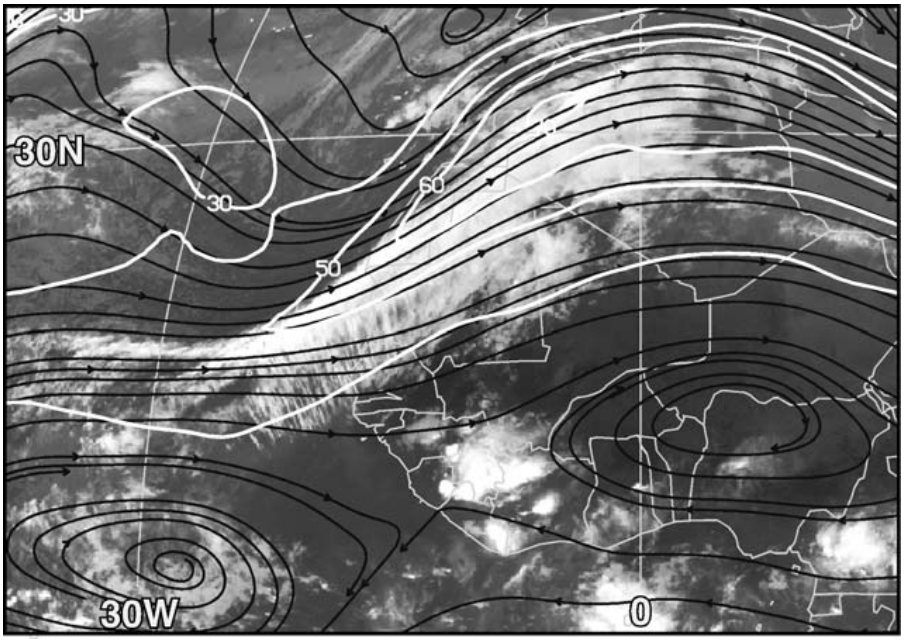

Figure 1.1: Meteosat IR satellite image at 00 UTC 1 April 2002 with superimposed isotachs at the 345 K isentropic level in white (m $s^{-}1$) and streamlines in black from Knippertz and Martin (2005) their Fig. 3.

at the eastern flank of the troughs and extend from the Tropics pole- and eastward into the subtropics or even midlatitudes. Such bands of mid- and upper-level clouds are commonly referred to as **T**ropical **P**lumes (TP) (e.g., Iskenderian 1995). These situations enable tropical moisture transport towards the subtropics, where they may lead to extreme precipitation events (Yoneyama and Parsons 1999, Fink and Knippertz 2003, Knippertz and Martin 2005, 2007a).

In Knippertz and Martin (2005) such an extreme rainfall event is described that affected Southern Morocco and Western Algeria in March/April 2002. The synoptic situation of this event is visualized in Fig. 1.1. The main features are i) a pronounced upper-level trough located over the Atlantic reaching south-westward into the Tropics (Fig. 1.1/streamlines) and ii) east of the trough an elongated Tropical Plume (Fig. 1.1/IR image) accompanied by a strong **s**ub**t**ropical **j**et (STJ) streak (Fig. 1.1/isotachs). Besides the detrimental effects of the heavy rainfall (i.e. damage by flooding), the event had also beneficial hydrological implications by refilling of local water reservoirs. This demonstrates the great relevance of such a single event for different socio-economic aspects (i.e. water supply, vegetation and agriculture) in an arid region like Northwest Africa (Fink and Knippertz 2003).

In addition to the effect on hydrological processes, further implications on the atmosphere related with the occurrence of troughs at low latitudes are observed:

- Low-latitude upper disturbances play an important role for the poleward transport of momentum and kinetic energy (e.g., Peixoto and Oort 1992), which underlies their relevance for the global and regional momentum balances (e.g. Kiladis and Feldstein 1994).

- The global radiation budget may be affected by the formation of Tropical Plumes.
- The chemical composition of the atmosphere is influenced by this kind of interaction due to the lateral mixing of stratospheric air, with low water vapour and high ozone, into the tropical upper troposphere (e.g., Wiegand 2008, Yoneyama and Parsons 1999).

In summary, upper-level disturbances are an important element of the general atmospheric circulation. Hence, investigations that focus on the occurrence, characteristics and impacts of this phenomenon, as done in this thesis, contribute to a more complete understanding of global atmospheric processes and may bring benefit to the population in the affected regions.

1.2 Scientific background

Various processes related to the equatorward propagation of upper-level troughs are described in detail in a recent review by Knippertz (2007). According to Knippertz (2007), observational studies in the literature that are concerned with the detection and analysis of extratropical-tropical interactions related to upper troughs at low latitudes, are commonly based on one of three different approaches: (1) Identification of low-latitude disturbances on either streamfunction or **p**otential **v**orticity (PV) fields; (2) satellite-based identification of Tropical Plumes and (3) correlations between convection anomalies and fields of streamfunction, wind or geopotential. Due to the great relevance for the present investigations these different approaches and their results are discussed in the following subsections. At the end of this chapter, studies that examined the impact on moisture fluxes and precipitation are discussed.

1.2.1 Identification and climatology of low-latitude troughs

Prior studies of tropical or subtropical upper-level disturbances are commonly based on analysis of either streamfunction on pressure levels or PV fields near the subtropical tropopause. Within the PV framework (Hoskins et al. 1985; for further information about PV see Chap. 2.1.1), low-latitude disturbances are characterized by elongated tongues of positive anomalies in the upper tropospheric PV field indicating intrusions of stratospheric air downward into the tropical troposphere. An example is given in Fig. 1.2 from a study of Tomas and Webster (1994). The PV distribution on 345 K isentropic level in Fig. 1.2a exhibits amongst other features a strongly tilted tongue of positive PV values (> 2 PVU) extending from about 30°N to the equator near 145°W. In contrast, in the 200-mb **g**eopotential **h**eight **d**istribution (GPH) of the particular date (Fig. 1.2b) the distinct streamer can hardly be recognized, which is due to the general weak gradients in geopotential height at low latitudes. Thus, the example demonstrates that GPH fields are generally less suitable for investigations of tropical or subtropical disturbances.

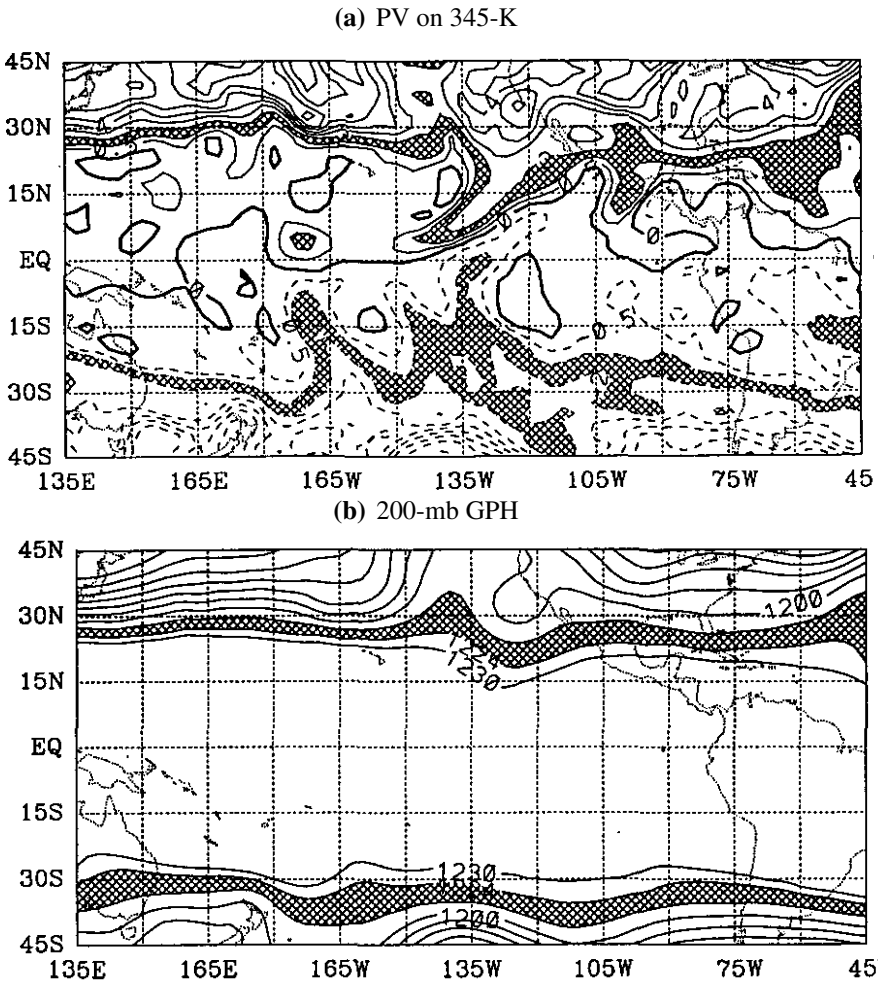

Figure 1.2: (a) Potential vorticity on the 345-K isentropic surface on 03 February 1984 based on ECMWF analysis. The contour interval is 1 x $10^{-6} Km^2 kg^{-1} s^{-1}$ (= 1 PVU) with the $\pm$ 0.5 PVU contours added; the interval between 1 and 2 PVU is cross-hatched. (b) 200-mb geopotential height on the same day. The contour interval is 120 m and the interval between 1240 m and 12120 m is cross-hatched. Both figures are from Tomas and Webster 1994.

Using NCEP/NCAR reanalyses (Kalnay et al. 1996), Waugh and Polvani (2000) constructed a 20-year climatology of intrusion events, which were defined as occurrences of high absolute PV values (|PV| > 2 PVU) at 10°N or S on the 350-K isentropic surface. In this process all such occurrences within 10° longitude or within 6 days (the typical lifetime for events) were then grouped together as a single intrusion event. The example of a low-latitude PV streamer in Fig. 1.2a at 130°W and 15°N on the 345 K isentropic surface corresponds to their definition of an intrusion event. Waugh and Polvani found most intrusion events to occur over the central Pacific (180°W-100°W) and eastern Atlantic (50°W-0°) Oceans during northern winter in coincidence with the existence of westerly ducts (see Fig. 1.3). Furthermore, inter-annual variability in the frequency of Pacific events was observed in association with the El Niño/Southern Oscillation (ENSO, see Chap. 2.3). That means, the intrusion frequency in the central Pacific is reduced during warm ENSO phases (El Niño), consistent with ENSO-related alterations in the westerly

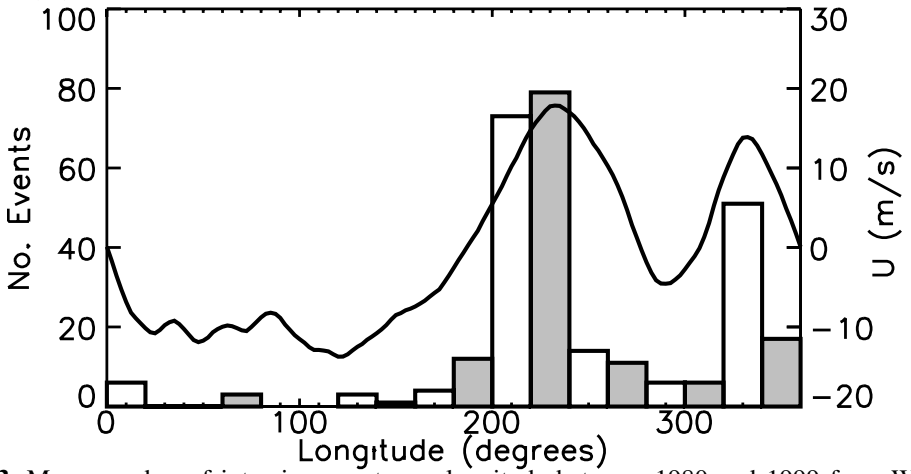

Figure 1.3: Mean number of intrusion events per longitude between 1980 and 1999 from Waugh and Polvani 2000. The solid (unfilled) bars show northern (southern) hemisphere events. Curve corresponds to climatological equatorial zonal winds at 350 K averaged from 1980 to 1999 between December and February.

background flow.

Another PV-based climatology was generated for the Northern Hemisphere by Wernli and Sprenger (2007). Based on the 15-year reanalyses data set of the ECMWF (ERA-15) and using a contour searching method, they identified PV streamers and cut off structures in the 2-PVU ($1PVU = 10^{-6}Km^2kg^{-1}s^{-1}$) contour, which represents the dynamical tropopause, on different isentropic surfaces. Above 320-K, Wernli and Sprenger (2007) found two frequency maxima of stratospheric PV streamers located over the subtropical North Atlantic and eastern North Pacific during northern winter. During summer, when the westerly ducts are absent, these maxima move to higher isentropic surfaces and shift north-westward, while the streamer frequency is quite constant year-round. Martius et al. (2007) applied the same contour searching algorithm to the ERA-40 reanalysis data set. They constructed a 44-year NH streamer climatology and thus frequency distributions comparable to the results of Wernli and Sprenger (2007) were achieved.

Since disturbances at low latitudes are often generated by breaking extratropical waves, other approaches consider rapid, large-scale and irreversible overturning of PV contours on isentropic surfaces in the subtropical upper troposphere (Postel and Hitchman 1999, Abatzoglou and Magnusdottir 2006b, Strong and Magnusdottir 2008) as evident in Fig. 1.2a over the NH Pacific between 180°W and 130°W. The 10-year climatology of **R**ossby **w**ave-**b**reaking (RWB) events by Postel and Hitchman (1999) based on global analyses from the ECMWF, reveals highest activity at 350-K during summer over the western parts of the ocean (Pacific and Atlantic) basins, in relative proximity to the subtropical high-pressure systems. These results are in agreement with the 46-year RWB (that they call 'planetary wave breaking') climatology of Abatzoglou and Magnusdottir (2006b) on the basis of daily averaged NCEP/NCAR reanalysis. Considering different isentropic levels, as done by Abatzoglou and Magnusdottir, reveals, that during boreal winter (DJF) these activity maxima shift to the Southeast and to lower isentropic levels

in agreement with the PV streamer climatology of Wernli and Sprenger (2007). Furthermore, Abatzoglou and Magnusdottir (2006b) found a strong correlation in boreal winter between the number of RWB events over the eastern Pacific and ENSO with higher RWB frequencies during the cold phases of ENSO (La Niña). These ENSO-related alterations in RWB occurrence are explained by the weaker eastern Pacific zonal flow observed during La Niña and consistent with the inter-annual variability of PV intrusion events of Waugh and Polvani (2000).
Nevertheless, comparing the discussed RWB climatologies with the PV intrusion climatology of Waugh and Polvani (2000), leads to the assumption that only RWB events during boreal winter tend to produce strong PV anomalies that reach into the upper-tropical troposphere.
Finally, some of these studies (e.g., Abatzoglou and Magnusdottir 2006a, Martius et al. 2007, Strong and Magnusdottir 2008) also analyzed variability in RWB or PV streamer occurrence in relation to further well-known modes of climate variability such as the **N**orth **A**tlantic **O**scillation (NAO) or the **P**acific/**N**orth **A**merican pattern (PNA, for more information see Chaps. 2.3 and 2.3). For example in the study of Abatzoglou and Magnusdottir (2006b) a link between the RWB frequency over the central North Atlantic and the NAO, which describes a large scale seesaw in atmospheric mass between the subtropical high and the polar low over the North Atlantic, was found with enhanced RWB activity during a NAO-positive winter due to the poleward shift in the eddy-driven jet and the enhanced equatorward wave activity flux. Benedict et al. (2004) suggests even that anticyclonic wave breaking over North America and the North Atlantic is essential for the growth and maintenance of the positive NAO phase. Strong and Magnusdottir 2008 constructed a climatology of cyclonic and anticyclonic wave breaking and found that the influence of RWB on the polarity of the NAO is in dependence of the latitude of RWB occurence.

1.2.2 Identification and climatology of tropical plumes

Only the introduction of meteorological satellites in the 1960s and 1970s enabled comprehensive observations and detailed descriptions of elongated cloud bands, that reach from the Tropics into the subtropics or even midlatitudes (e.g., Erickson and Winston 1972, Gray and Clapp 1978, Thepenir and Cruette 1981). In the past this phenomenon was named quite differently such as ‘cloud surges’, ‘tropical intrusions’, ‘cirrus surges’, ‘moisture bursts’ or ‘tropical plumes (TP)’. The latter denotation will be used in the present thesis. Furthermore it has to be mentioned, that all climatological studies of Tropical Plumes in the past (and described in this subsection) are based on visual inspection of **i**nfra**r**ed (IR) satellite imagery.
Thepenir and Cruette (1981) constructed the first TP climatology with focus on cloud bands stretching from the east of the subtropical part of the Pacific Ocean to Western Europe. They subjectively detected 145 of such cloud bands during the 3-year period from 1976 to 1978. The bands vary in length from 4000 to 16.000 km, in widths from

400 to 1200 km and have life spans from 3 to 9 days. Most TPs are detected between November and April (on average nearly 6 events per month) with a clear frequency maximum in December. TP genesis was observed commonly over the subtropical ocean between 5° and 25°N and 100° and 160°W and was linked to the occurrence of an upper-level trough with a NE-SW axis extending southward over the Pacific Ocean and to the development of a strong subtropical jet streak along the south-eastern flank of this trough (Thepenir and Cruette 1981). In 70% of all cases the cloud band embryo is related to convection of the **I**ntertropical **C**onvergence **Z**one (ITCZ). Further details on latitudinal or longitudinal distribution of TP occurrence are not given in this work.
The first objective definition for Tropical Plumes was given by McGuirk et al. (1987). Hereby a Tropical Plume (that they name 'moisture bursts') is defined as a continuous band (i) of upper- or midlevel clouds that is (ii) at least 2000 km in length and (iii) crosses the latitude of 15°N. Based on this definition, they identified cloud bands over the central and eastern North Pacific in the three 6-month cool seasons (November to April) of 1975/76, 1977/78 and 1981/82. On average about 10 events per month were detected equally distributed over the North Pacific between 160°E and 110°W and with lifetimes from 0.5 and 10 day (average lifetime: 2.5 days). A maximum in plume activity is observed in November and April and a relative minimum from February to March. Furthermore they observed a distinct reduction in plume activity during the El Niño cool season 1982/1983 with the location of occurrence shifted eastward.
The only global TP (termed 'tropical-extratropical cloudbands'/TECBs in this study) climatology was generated by Kuhnel (1989) for the 5-year time period 1979 to 1983 based on an objective TP definition according to which a cloud band is required to have (i) its origin between the Equator and 20°N, (ii) a length of at least 25° longitude, (iii) a maximal width of at least 5° latitude, (iv) a diagonal alignment, crossing at least 10° latitude and (v) a homogeneous texture. In contrast to the above-described studies, Kuhnel considers days with TP occurrence instead of single TP systems with beginning and ending times. As a result of the study, 14 different tropical zones (seven in each hemisphere) were subjectively defined as areas of TP origin (Fig. 1.4). The mean monthly TP frequencies of these regions range from 13 days of TP occurrence over the central South Pacific to 0.65 days over the northern Indian Ocean detected during the 5-year investigation period. The pronounced frequency maximum in the central South Pacific is caused by the quasi-permanent and quasi-stationary cloud bands of the **S**outh **P**acific **C**onvergence **Z**one (SPCZ) (e.g., Kodama 1992, 1993, Vincent 1994), that sometimes, especially during austral summer, continuously satisfy Kuhnel's TP definition for weeks. Similar observations of quasi-stationary, warm-season cloud bands are made in the South Atlantic (with origin area over South America) related to the **S**outh **A**tlantic **C**onvergence **Z**one (SACZ) and in the northwestern Pacific (Kodama 1992, Kodama 1993). McGuirk et al. (1987, p. 789) suggests to consider these quasi-stationary cloud bands as a different sort of meteorological phenomenon compared to the short-lived, transient TPs of the cold seasons. The latter type of TP will mainly be focused on in this thesis. Regarding the cool season climatology of Kuhnel, high TP activity is found in the NH over the eastern Pacific and Atlantic Oceans with occurrence maxima in October/November.

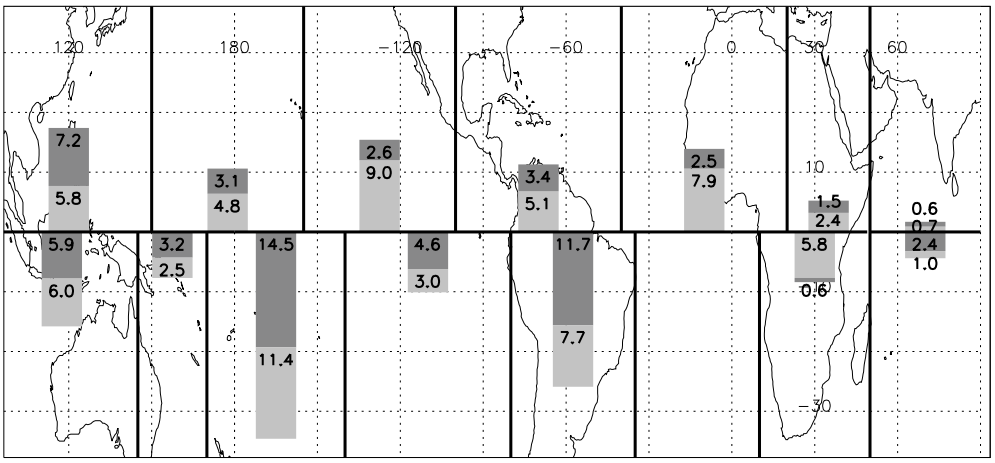

Figure 1.4: Mean monthly tropical plume frequency [number of days with TP occurrence] of the 14 defined regions with TP origin between 1979 and 1983 from Kuhnel (1989). Lighter/darker grey boxes label cool/warm season TP frequencies. NH/SH cool/warm season is Oct. to March. NH/SH warm/cool season is April to Sept.

According to Kuhnel, TP development in these regions is associated with intrusions of extratropical air masses into low latitudes. A reduction in TP occurrence is observed during the 1982/83 El Niño event in the eastern North Pacific similar to the results of McGuirk et al. (1987).
Iskenderian (1995) generated a 10-year cool season (Oct.-May) climatology of tropical cloud plumes in the NH between 1974 and 1984. The TP identification of this study was based on a definition similar to that applied in McGuirk et al. (1987). Only the required distance to the equator was changed to 20°N. The climatology reveals two preferred subtropical regions in the NH for TP occurrence: The (i) eastern North Pacific (120°-180°W) with 40 TPs per season on average and the (ii) eastern North Atlantic (20°-60°W) with 21 TPs on average per season. The mean TP duration is 2.7 days. Furthermore, Iskenderian (1995) observed a relative minimum in plume activity in February and March and a lack of eastern Pacific TPs during the 1982/83 El Niño season. Both results are in agreement with the observations of McGuirk et al. (1987) and Kuhnel (1989). Another notable feature, found by Iskenderian (1995), is an overall tendency for above (below) normal seasons in the eastern Pacific to be balanced by below (above) normal seasons in the Atlantic region.

1.2.3 Relationship between upper troughs and convection/TPs

Several studies have linked the propagation of upper-level troughs into low latitudes with the occurrence of deep convection in tropical and subtropical regions and vice versa (e.g., Liebmann and Hartmann 1984, Kiladis and Weickmann 1992a, 1992b, Kiladis 1998, Slingo 1998, Matthews and Kiladis 1999b, Waugh and Funatsu 2003). Most of these studies used time-averaged, composited or filtered anomalies in **o**utgoing **l**ongwave **r**adiation (OLR) as an indicator for enhanced tropical cloudiness.
Liebmann and Hartmann (1984) for example, compared NH wintertime five- and ten-day

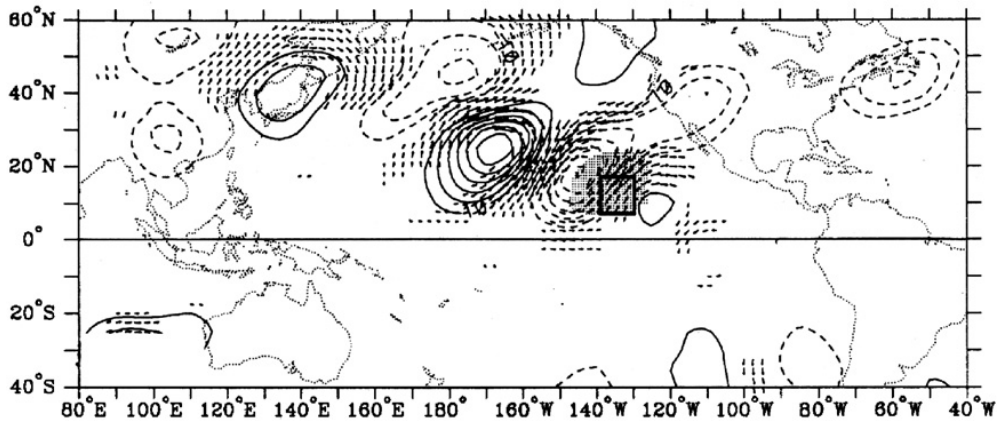

Figure 1.5: 6–14-day anomalies in OLR, 200 hPa streamfunction and locally significant wind vectors for a -1 standard deviation in OLR at the base region of 5°N–15°N, 140°W–130°W (black framed box). The contour interval is 10 x $10^5 m^2 s^{-1}$, with the zero contour omitted. The largest wind vectors are about 5 m/s. Shading outlines regions of OLR anomaly less than -6 W/m^2. The investigation period is December–February 1983/1984–1987/88. (From Kiladis and Weickmann 1992a.)

average tropical OLR anomalies with anomalies in midlatitude 500 hPa geopotential height to search for relationships between tropical and midlatitude circulation pattern. The strongest relationship was found over the Pacific (east of the date line) and the central Atlantic between a trough in the 500 hPa GPH and enhanced tropical cloudiness (10°N–15°N) to the Southeast. The trough tends to precede the signal in tropical cloudiness and displays a southwest-northeast tilt, which points to an equatorward propagation of wave energy.

Kiladis and Weickmann (1992a) examined wintertime 6-14-days filtered 200 hPa streamfunction anomalies associated with an area-averaged OLR of – 1 standard deviation at different base regions in the Tropics. The strongest signal was received for a base region located in the eastern Pacific between 140°W-130°W and 5°N-15°N. These results are presented in Fig. 1.5. The streamfunction anomalies reveal a northwest-southeast-oriented wave train with a pronounced positive tilt (i.e. southwest-northeast titled disturbances) stretching from East Asia across the North Pacific. Circulation anomalies associated with OLR anomalies at base regions in the tropical North Atlantic show similar patterns with somewhat weaker signals (Kiladis and Weickmann 1992b their Fig. 3). Lead-lag correlations reveal a southeastward propagation of the wave trains (Kiladis and Weickmann 1992b, their Fig. 2). Iskenderian (1995) constructed a composite of the 200 hPa streamfunction anomalies for 41 tropical plumes over the tropical North Pacific with origin between 120°W and 150°W (cp. Section 3.2). The anomaly pattern displays a wave train extending across the Pacific and through the plume origin region with a northwest to southeast orientation and a positive tilt similar to the results of Kiladis and Weickmann (1992a). Another approach is applied by Waugh and Funatsu (2003) based on PV intrusion events over the North Pacific (180°W-100°W), as detected in the study by Waugh and Polvani (2000) (see Sec. 3.1). Composites of 350-K PV and OLR were

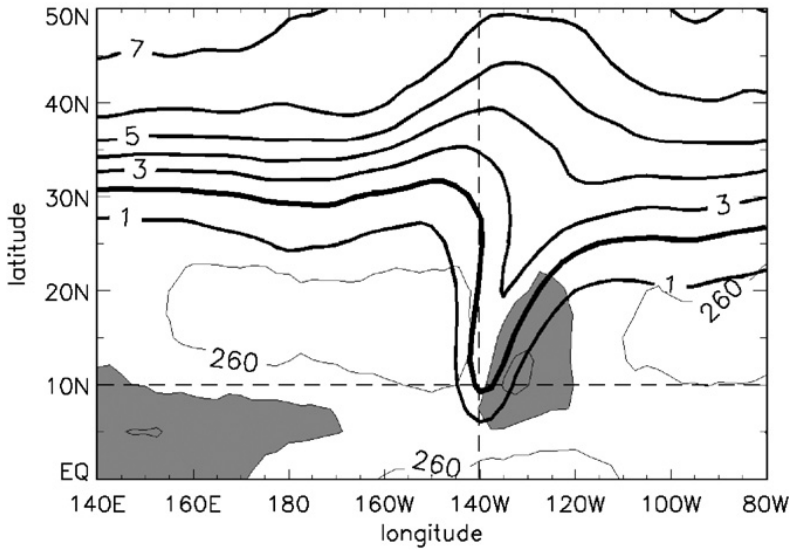

Figure 1.6: Phase-shifted composite mean 350-K PV (thick contours) and OLR south of 30°N (light contours and shading) of North Pacific events. Contour interval for PV is 1 PVU, and 20 W/m^2 for OLR (shaded region shows OLR less than 240 W/m^2). All events have been shifted to the reference longitude at 140°W. (From Waugh and Funatsu 2003.)

constructed by averaging over all intrusion events after shifting the PV tongue to the reference longitude of 140°W (see Fig. 1.6). The PV composite reveals a narrow tongue of high PV values at 140°W with an almost north-south orientation. Along the eastern edge of the PV tongue an area of low OLR values occurs that has a length of almost 2000 km and crosses 20°N, and thus resembles a tropical plume.

In summary, all studies presented in this subsection emphasize the close (statistical) linkage between Rossby wave activity, tropical convection and TP formation. However, there exist different hypothesis about the physical processes leading to this connection. According to some early studies (e.g., McGuirk et al. 1988, Kiladis 1998), convection associated with Tropical Plumes is triggered by quasi-geostrophically forced ascent ahead of the PV trough and reduced vertical stability within and below the anomaly.

In another conception, Blackwell (2000) demonstrated based on experiments with a dry barotropic shallow water model of the upper troposphere, that TP-like circulation could be initiated by convergent forcing in the eastern part of the climatological ridge over the central Pacific. It is suggested, that the convergent forcing is caused by large-scale cold advection and subsidence in association with extratropical wave train activity. In the model experiments the advection of cyclonic vorticity through the convergent winds leads to an amplification and zonal contraction of the trough downstream of the ridge, whereby subtropical air masses are accelerated toward the deep Tropics. In the deep Tropics the flow decelerates, then sharply turns cyclonically and accelerates back into the extratropics, forming an anticyclonically curved downstream STJ streak. Blackwell (2000) concludes, that moist convective processes are negligible for the generation of TP-like circulation patterns.

Another dynamical concept for tropical plume genesis is proposed by Mecikalski and Tripoli (1998) that views tropical plumes as the upper branch of a thermally direct cir-

culation driven by latent heat released along the ITCZ. Due to the fact, that in their observations the TP genesis region is relatively remote from the upper trough, they suggest in contrast to tradionally held views a rather indirect influence of the Rossby wave on plume genesis process. Further on they argue that the associated quasi-geostrophic forcing does not go down enough into the troposphere due to the small Coriolis parameter at low latitudes. In the concept of Mecikalski and Tripoli (1998) convection responds to the changes in inertial stability caused by southwesterly advection of low potential vorticity (PV) to the east of the midlatitude Rossby wave.
Finally, most studies agree on the fact, that poleward advection of convectively generated cirrus from the ITCZ by the strong winds ahead of the PV trough plays an important role in the TP generation. Nevertheless observed wind speeds at the outflow level do not always correspond to the progression rates of the TP cloud formation. This leads to the assumption that TP cloud formation is based on both development and advection (McGuirk et al. 1987, 1988).

1.2.4 Impacts on moisture fluxes and precipitation

Different studies have shown that the occurrence of troughs at low latitudes induces poleward moisture fluxes that transport tropical moisture into the subtropics (e.g., Bates et al. 2001, Waugh 2005, Ryoo et al. 2008), where they occasionally lead to extreme precipitation events in subtropical regions (e.g., Ziv 2001, Fink and Knippertz 2003, Knippertz and Martin 2005, Knippertz and Fink 2009, Meier and Knippertz 2009, **?**,). Poleward moisture fluxes in tropical regions are in contrast to the climatological mean equatorward moisture transport of the Hadley cell (Peixoto and Oort 1992). In the typically dry subtropical atmosphere these moisture fluxes are important due to the relatively large changes in the clear-sky outgoing longwave radiation.
In a case study of Knippertz and Martin (2007a) the moisture transport of an upper-level cut-off low resulting from a wave-breaking event over the subtropical North Pacific in November 2003 is analysed. Fig. 1.7 shows the geopotential height (solid lines), midlevel poleward moisture export (shading) and mixing ratio (dashed lines) from this event at 700 hPa pressure level. East of the cut-off low (centre of cut-off low located near 30°N, 123°W) an elongated, narrow band of relatively large water vapour fluxes stretches from the northern edge of the tropical moisture reservoir north-eastward into the southern USA. The mixing ratio reveals a sharp contrast between the moist air of the tropical reservoir and the transport region in the subtropics, and the dry subtropical air masses northwest of the cut-off low.
Waugh (2005) examined, for example, the impact of intrusions of high PV air into the tropical upper troposphere on subtropical humidity using satellite measurements of water vapour from two different instruments, the **A**tmospheric **I**nfrared **S**ounder (AIRS) and **M**icrowave **L**imb **S**ounder (MLS). They constructed composite-mean **r**elative **h**umidity (RH) fields for PV intrusion events over the northern Pacific, which were identified in a similar manner to Waugh and Polvani (2000) (see Chapt. 3.1) with slightly modified

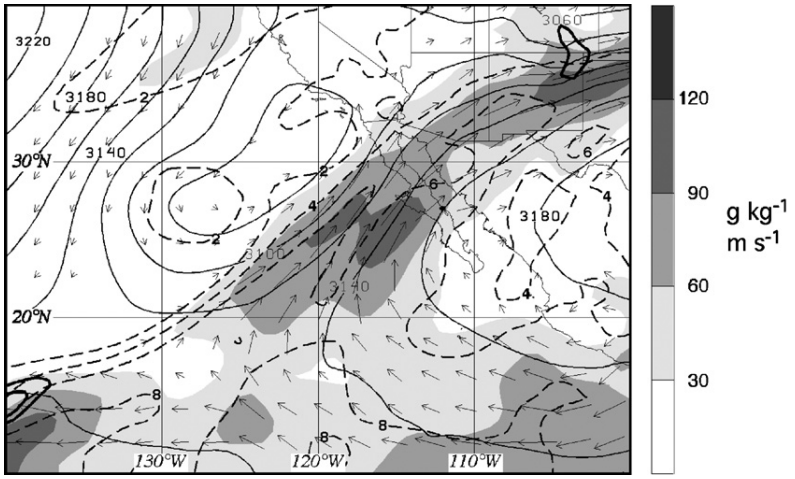

Figure 1.7: Example of a moisture conveyor belt over the eastern Pacific at 12 UTC 11 November 2003. Solid isopleths depict geopotential height every 20 gpm and dashed isopleths mixing ratio every. Vectors and shading show water vapour flux. The vertical level is 700 hPa. The employed data come from a simulation of the event using the University of Wisconsin Nonhydrostatic Modelling System. (From Knippertz 2007.)

thresholds (PV > 2.5 at 17.5°). Before averaging the RH fields the intrusion events were shifted so that all intrusions occurred at the same longitude (150°W). The composite fields for the AIRS and MLS measurements are shown in Fig. 1.8. Both data sets show large gradients in humidity in the vicinity of the intrusions, with very dry air within the intrusions and very moist air ahead (east) of the intrusion. They argue, that the combination of convection and poleward flow ahead of the PV intrusion rapidly transports lower tropospheric air into the subtropical upper troposphere. Trajectory-based water vapour simulations support their argumentation.

Ryoo et al. (2008) extended the investigations of Waugh (2005) by considering a longer time series of AIRS satellite measurements. In this study variability of subtropical humidity during winter is mainly focused on three different regions (Pacific, Atlantic and Indian Ocean). Fig. 1.9 shows the relative longitude versus height cross section of composite-mean relative humidity for intrusion systems in the North Atlantic (80°W–0°). This composite is constructed by shifting the intrusion systems to a reference longitude of 0° before averaging. The pattern reveals high RH east of the PV intrusions and low RH west and within the intrusions. Even though the high PV is confined to the upper troposphere (not shown), high RH values to the east of the trough are observed down to below 400 hPa.

In a study of Bates et al. (2001) the inter-annual variability of satellite-derived tropical **u**pper-**t**ropospheric **h**umidity (UTH) between 1979 and 1998 is analysed and compared with transient eddy activity (estimated on the basis of 200 hPa winds according to Kiladis (1998)). In agreement to the results above, they hypothesize that the vertical and horizontal motions associated with equatorward propagating Rossby waves advect moisture both vertically and horizontally, moistening the normally dry subtropics. In the central and eastern North Pacific this moistening is greatly enhanced during the ENSO cold event of 1989/90 and reduced during the ENSO warm event of 1982/83. Their investiga-

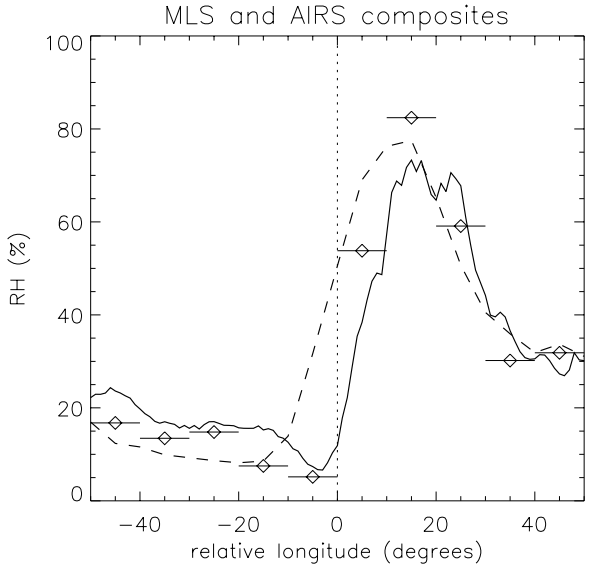

Figure 1.8: Longitudinal variation of the composite-mean RH for north Pacific intrusion events in January–February, for AIRS (solid curve) and MLS (dashed curve) measurements in 2003–2004 and 1992– 1994, respectively. Diamonds and horizontal lines show MLS composite using individual profile data rather than gridded data. Longitude is relative to longitude of the PV intrusion (vertical dotted line). (From Waugh 2005.)

tions emphasize also the relationship between variations in the mean equatorial westerly winds, in eddy activity and in the tropical UTH.

The moisture transport in association with equatorward propagating Rossby waves may lead to exceptional precipitation events away from the tropical moisture reservoir region near the ITCZ. For example, the poleward water vapour export in association with the cut-off low event in Fig. 1.7, provided the moisture for a significant precipitation event in the dry southwestern United States (Knippertz and Martin 2007a). Knippertz and Martin (2005) investigated in another study three cool season events of unusual heavy precipitation in tropical and subtropical West Africa, using observational data and high-resolution output from modelling simulations. Common characteristics of all three cases are an upper-level trough to the west of West Africa, a strong subtropical jet streak and a Tropical Plume. Furthermore, all cases show poleward moisture export from the tropical source regions similar to the case study depicted in Fig. 1.7.
Hart et al. (2010) discussed in detail three events of heavy rainfall over southern Africa. Similar to tropical-extratropical interactions in other regions, the synoptic evolution of these events was characterized by a tropical cloud band and poleward moisture fluxes along the leading edge of an upper-tropospheric westerly wave trough.
A 23-year climatology of **t**ropical **m**oisture **e**xport (TME) was constructed by Knippertz and Wernli (2010) on the basis of trajectory analysis that is applied to the ERA-40 data set. A trajectory that starts in the tropical lower troposphere and reaches a water vapour flux of at least 100 $gkg^{-1}ms^{-1}$ somewhere north of 35°N within seven days or less is defined as TME. The resulting TME climatology shows two distinct activity maxima during boreal winter (Dec.-Feb.) located over the central and eastern Pacific ("pineap-

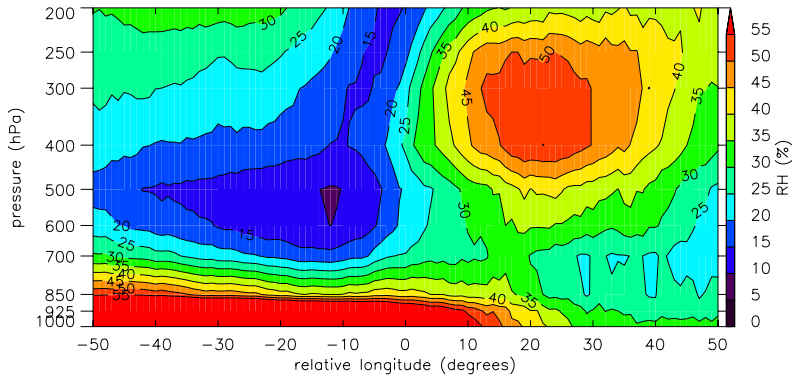

Figure 1.9: Vertical cross sections of composite RH for intrusions in the North Atlantic (80°W – 0°). Relative longitude is the longitude relative to central longitude of the PV intrusions. (From Ryoo et al. 2008.)

ple express") and over the western North Atlantic. The inter-annual TME variability is significantly influenced by ENSO in this way that during the warm phase of ENSO (El Niño) less (more) TME events are observed over the eastern North Pacific (western North Atlantic). Knippertz and Wernli (2010) explain these differences by ENSO-induced changes in the frequency of transient upper disturbances in these regions. Finally they found, that TME contributes up to 60% to climatological precipitation in the southern midlatitudes.

However, trajectory analyses by Knippertz and Martin (2007b) reveal that the midlevel moisture transport from the deep Tropics is often to slow, to generate extensive precipitation. The authors assume that only a persistent disturbance or two disturbances in short succession are able to produce significant rainfall. This observation may explain the rare occurrence of such extreme events.

In another concept, narrow bands of enhanced water vapour flux are termed atmospheric rivers (e.g., Zhu and Newell 1994, 1998, Ralph et al. 2004, Bao et al. 2006, Neiman et al. 2008) due to the great amount of water that is transported by these bands. Atmospheric rivers are responsible for most (> 90%) of the poleward water vapour transport outside of the Tropics at only about 10% of the total longitudinal length at a given latitude (Zhu and Newell 1998, Ralph et al. 2004). Atmospheric rivers are typically situated near the leading edge of polar cold fronts and are often associated with heavy rainfall events and flooding in the affected regions. Although these bands of enhanced moisture fluxes may transport an considerable amount of water vapour from the tropical moisture reservoir into the extratropics, these atmospheric rivers are rather an extratropical phenomenon.

Meier and Knippertz (2009) analysed an exceptionally heavy precipitation event in January 2002 of Cap Verde region in tropical West Africa. The rainfall was triggered by a series of two upper-level disturbances penetrating from the extratropics to the West African coast. In this study several sensitivity experiments based on modelling simulations were conducted to identify the dynamical precursors, which lead to the upper-level wave amplification and the observed precipitation rates. As a result of this study a reservoir of high PV over the North Atlantic and a PV ridge over Europe are found to be

essential precursors for the development of such a heavy rainfall event over West Africa.

1.3 Aims and outline

The main subject of this thesis is to improve the understanding of extratropical-tropical interactions related to upper-level disturbances that propagate from the extratropics into the Tropics. Embedded within this general goal the present thesis consists of two main parts, focusing on the detection, climatology and impacts (i) of upper-level troughs at low latitudes and (ii) of Tropical Plumes.
For that purpose the first step was the development of a new identification algorithm for upper-level troughs at low-latitudes (in the following often referred to as intrusions) in the ERA-40 reanalysis data set. Compared to prior studies (e.g., Waugh and Polvani 2000, Wernli and Sprenger 2007), the new algorithm analyses **v**ertically **a**veraged **P**otential **V**orticity (VAPV) fields of the upper troposphere rather than PV data on individual isentropic surfaces. A main advantage of this new data basis is that only systems with a coherent signal throughout the upper troposphere are identified, which points to rather intensive systems. In addition this procedure enables a classification of the intrusion systems by their vertical thickness (defined by the lowest vertical level of the 1.5 PVU surface within the intrusion system), which is assumed to be an indicator for the intensity of the system. Another novelty is the implementation of a simple tracking routine for the identification of intrusion episodes. A detailed description of the data sets and methodology is provided in Chapter 2 and 3 together with an illustrative example.
Applying the new algorithm to the ERA-40 reanalysis data set, a 22-year climatology of low-latitude troughs was constructed. The geographical and seasonal distributions of the identified intrusion systems are presented and compared to results from former studies in Chapter 4. This chapter also includes a sensitivity test to examine the robustness of the results. Intrusion characteristics such as life time, vertical extent and horizontal tilt are statistically evaluated in Chapter 5. The intrusion time series are analysed in terms of trends, inter-annual variabilities and their association to ENSO in Chapter 6. Based on composite studies the typical evolution of intrusion systems in the tropical upper troposphere is evaluated in Chapter 7 and their impact on water vapour fluxes is presented in Chapter 8.

In the second part of this thesis a novel climatology of Tropical Plumes is presented. This climatology is constructed with the first objective algorithm for the detection of Tropical Plumes. The development of such an algorithm allows a quick identification of TPs for a longer time period in comparison to previous TP climatologies that are all based on a subjective detection by visual inspection of satellite IR imagery. The data set and the algorithm used for TP identification are described in detail in Chapter 2 and 3. Applying the TP identification algorithm to the CLAUS brightness temperature data set, a 23-year climatology of TPs is constructed. The resulting geographical and seasonal TP distributions are presented and compared to result from former studies in Chapter 9. In

this chapter the sensitivity of the algorithm to the implementation of the LWR criterion is assessed and the robustness of the results is discussed. TP characteristics such as life time, length-to-width ratio and horizontal tilt are statistically evaluated in Chapter 10. In Chapter 11, the time series of seasonal TP frequencies are examined in terms of trends and inter-annual variabilities and their association to ENSO. Based on composite studies the circulation anomalies in the upper troposphere in relation to TP occurrence is evaluated in Chapter 12. In this chapter a brief comparison of both climatologies is presented to analyse the relationship between low-latitude trough and TP occurrence.
Finally, in Chapter 13 all results are summarized, discussed and open questions and future prospects are presented.

2 Data

2.1 ERA-40 reanalysis

In the present study investigations of upper-level troughs at low latitudes are mainly based on ERA-40 reanalysis data (Uppala et al. 2004). This data set is generated at the **E**uropean **C**entre for **M**edium-**R**ange **W**eather **F**orecasts (ECMWF) and describes the state of the atmosphere at a spectral resolution of T159 on 60 vertical levels up to 1 hPa every six hours from September 1957 to August 2002. Observational data from different sources and model data from a short-range numerical weather forecast were combined by the three dimensional variational data assimilation system (3D var) to generate the ERA-40 reanalysis data set. In this process the assimilation system and the numerical weather forcast model is unchanged throughout the entire time period to reduce inhomogeneities in the data set which are caused by variances in the analyses techniques. For long-term studies consistent time series are essential. Nevertheless inhomogeneities due to changes in instrumentation, measurement techniques or observational practices remain in the data set.
For the present investigations the required fields were interpolated onto a 1°x1° latlon grid. Only the period from January 1980 to December 2001 is considered, since the change to a more space-based observing system during this time has produced a more consistent data set, especially over tropical regions where conventional observations are rare (Bengtsson et al. 2004).

2.1.1 Ertel's Potential Vorticity

Since **p**otential **v**orticity (PV) is a frequently used term in this thesis, some background information will be given in this subsection.

In an isentropic coordinate system PV is defined by Ertel (1942) as

$$PV = (\zeta_\theta + f)\left(-g\frac{\delta\theta}{\delta p}\right) \tag{2.1}$$

where ζ_θ is the vertical component of the relative vorticity on an isentropic surface, f the Coriolis parameter (planetary vorticity) and θ the potential temperature. Potential vorticity is commonly given in PV Units ($1PVU = 10^{-6}Ks^{-1}kg^{-1}m^2$).
The climatological distribution of PV is characterized by positive values in the Northern Hemisphere, zero at (or near) the equator and negative values in the Southern Hemisphere. PV generally increases polewards and with height. In the upper troposphere, maximum values are typically below 2 PVU. For this reason the 2-PVU isosurface is often used as the dynamical tropopause. Above the tropopause PV increases rapidly due to the significant increase in static stability.
With the assumption of adiabatic and frictionless flow the PV of an air parcel is a conserved parameter. Therefore PV can be used as a tracer for movement of air parcel (Hoskins et al. 1985), which makes it a comprehensive tool to analyse e.g. synoptic-scale weather systems. The importance of PV for the present work is the fact that meridional transport of air masses in the upper troposphere leads to a positive (negative) PV anomaly as high (low) polar (equatorial) PV values advect. Furthermore, according to the invertibility principle (Eliassen and Kleinschmidt 1957, Hoskins et al. 1985) a positive PV anomaly on an isentropic surface near the tropopause will induce a cyclonic circulation. This circulation is strongest near the level of the anomaly and weakens below this level. Furthermore, the strength of the induced circulation anomalies depends on the vertical depth of the upper disturbances, that propagates equator- or poleward.
The PV calculations in this work were based on the ERA-40 three dimensional fields of temperature (T), u (U) and v (V) wind components and the two dimensional field of surface pressure (SP) (needed for the transformation onto pressure levels). At first the calculations have been accomplished on the original hybrid model levels. Finally, the PV fields in the upper troposphere were interpolated on pressure levels from 100 to 400 hPa (separated by 50 hPa) and smoothed by a 9-point interpolation with the neighbouring grid points.

Rossby wave and PV streamer

Another two frequently used terms in this thesis are “Rossby wave” and “PV streamer”, which are briefly defined here. Rossby waves are wave disturbances of the westerly flow, that propagate along the tropopause and were first described by Rossby (1940). In a PV perspective, Rossby waves are synoptic-scale perturbations on an isentropic surface near the tropopause (Hoskins et al. 1985). A Rossby wave train is a series of Rossby waves travelling nearly with the same velocity in the same direction.
The term “PV streamer” is used in the text (as an equivalent for the term PV intrusion) for an elongated and narrow intrusion of stratospheric air (with high PV values $\geq$2) de-

scending equatorward into the troposphere (Appenzeller et al. 1996). An illustrative example is given in Fig. 1.2 from a study of Tomas and Webster (1994).

2.2 CLAUS Brightness Temperature

Analysis of Tropical Plumes are based on the brightness temperature (T_b) dataset of the **C**loud **A**rchive **U**ser **S**ystem (CLAUS)[1]. This dataset is derived from 10 μm radiances (Hodges et al. 2000) measured by divers operational meteorological satellites (geostationary and polar orbiters) that participate in the **I**nternational **S**atellite **C**loud **C**limatology **P**rogramme (ISCCP)[2] and were obtained from the NASA **L**angley **A**tmospheric **S**ciences **D**ata **C**enter (LASDC)[3]. The CLAUS T_b data set currently spans a time period from July 1983 to June 2006 and is available on a global uniform latitude-longitude grid at a spatial resolution of 0.5 by 0.5 degrees and a temporal resolution of three hours.
Brightness temperature is defined as the temperature of a blackbody that emits the same intensity as measured at a given wavelength (Planck's law). The real temperature is usually somewhat higher than the measured T_b. Observed from a satellite, cold cloud top surfaces are characterised by lower T_b values compared to cloud-free land or sea surfaces. Higher cloud tops are indicated by lower temperatures. The analysis of brightness temperature is a commonly used method to separate cloudy from clear sky areas (e.g., Inoue 1987, Saunders and Kriebel 1988, Ackerman et al. 1990). A disadvantage of this method is, that information about the cloud distribution below the cloud top surface can not be obtained.

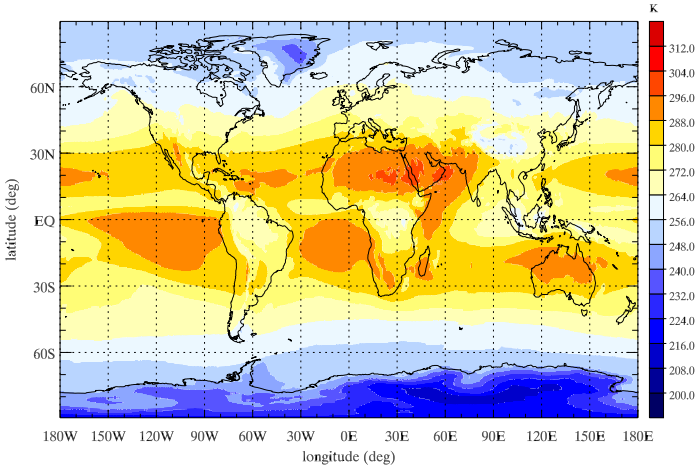

Figure 2.1: Global mean T_b [K] distribution averaged between July 1983 and June 2006 from CLAUS.

The climatological mean T_b values (averaged from July 1983 to June 2006) are globally depicted in Fig. 2.1. The T_b distribution is mainly characterized by (i) maximum values

[1] http://badc.nerc.ac.uk/data/claus/
[2] http://isccp.giss.nasa.gov
[3] http://eosweb.larc.nasa.gov/

in the subtropics (over the northern African continent/Arabian Peninsula and over the oceans related to the mean subtropical high pressure systems), (ii) a decrease from the Subtropics towards the poles and (iii) by lower values in the Tropics near the seasonal mean ITCZ. Hence, the seasonal cycle of the T_b distribution depends strongly on the inner-annual changes of the position of the mean subtropical high pressure systems and the ITCZ.

2.3 Climate state indices

Inter-annual climate variability in the time series of the detected low-latitude troughs and tropical plumes are analysed in chapter 6 and 11 with emphasis on fluctuations associated with different climate state indices. The regarded indices and their data sources are briefly described in this subsection.

El-Niño-Southern Oscillation

The **E**l **N**iño/**S**outhern **O**scillation (ENSO) is a variation of the atmosphere-ocean system in the tropical Pacific region on an interannual time scale (period: 2–7 years) with major impacts on the global weather. El Niño (La Niña), the so called warm (cold) phase of the oscillation, is associated with warmer (cooler) than normal **s**ea **s**urface **t**emperatures (SSTs) in the equatorial Pacific Ocean (e.g., Trenberth 1997). The phenomenon is described by various atmospheric and oceanic indices. A common index is the Niño3.4 index, which is the average sea surface temperature anomaly in the region 5°S to 5°N and 120°W to 170°W. Five-month running means of SST anomalies in the Niño3.4 region above/below +/- 0.4 °C for at least six consecutive months are commonly chosen to indicate El Niño/La Niña years (Trenberth 1997). The classification of ENSO phases used in this study is based on this definition and the resultant 6 El Niño and 5 La Niña winter seasons within the investigation period from 1980 and 2001 are listed in Tab. 2.1. Additionally the **S**outhern **O**scillation **I**ndex (SOI) is analysed, which describes the state of ENSO on a more large-scale and ocean-atmosphere coupled perspective. The SOI is calculated from monthly fluctuations in the air pressure difference between Tahiti and Darwin, Australia. Thereby negative (positive) values are associated with above (below) normal values of sea surface temperature in the equatorial central and eastern Pacific Ocean. Monthly SOI data is downloaded from the **C**limate **P**rediction **C**enter [4] (CPC).

North Atlantic Oscillation

The **N**orth **A**tlantic **O**scillation (NAO) is a large-scale seesaw in atmospheric mass between the subtropical high pressure system located near the Azores in the Atlantic Ocean and the sub-polar low pressure system near Iceland with significant influence on the

[4] http://www.cpc.ncep.noaa.gov/data/indices/soi

El Niño	La Niña
1982/1983	1984/1985
1986/1987	1988/1989
1987/1988	1995/1996
1991/1992	1998/1999
1994/1995	1999/2000
1997/1998	
2002/2003	

Table 2.1: Listing of El Niño and La Niña winter seasons between 1980 and 2006 as defined by the SSTs in the Niño 3.4 region and exceeding threshold from Trenberth (1997).

weather and climate in the North Atlantic region and surrounding continents including Europe (e.g., Wallace and Gutzler 1981, Barnston and Livezey 1987). The daily and monthly NAO indices used in this study are obtained from the Climate Prediction Center [5]. The daily NAO index is constructed by projecting the daily 500mb height anomalies over the Northern Hemsiphere onto the first leading mode of rotated **E**mpirical **O**rthogonal **F**unction (EOF) analysis of monthly mean 500mb height during 1950-2000 period[6]. The NAO is usually detected by differences in the normalized **m**ean **s**ea **l**evel **p**ressure (MSLP) anomalies between both centres of the pressure dipole (e.g., Hurrell 1995). However, in this study the considered NAO index is derived from 500mb geopotential height anomalies in consistence with the PNA index (see next Section 2.3) that is usually detected in the 500mb GPH fields.

Pacific/North American Pattern

The **P**acific/**N**orth **A**merican teleconnection pattern (PNA) is another prominent statistical mode of low-frequency variability in the Northern Hemisphere extratropics with four centres of action. It is characterized by height anomalies of similar sign located south of the Aleutian Islands and over the southeastern United States and opposite height anomalies located in the vicinity of Hawaii, and over the inter-montane region of North America (e.g., Wallace and Gutzler 1981). The daily and monthly PNA index obtained from CPC and used in this study is based on daily PNA indices which are computed by projecting the daily 500mb height anomlies onto the second leading mode of a rotated EOF analysis of the monthly mean 500mb height from 1950 to 2000[7].

[5] http://www.cpc.noaa.gov/products/precip/CWlink/pna/nao.shtml
[6] http://www.cpc.ncep.noaa.gov/products/precip/CWlink/pna/nao_index.html
[7] http://www.cpc.ncep.noaa.gov/products/precip/CWlink/pna/pna_index.html

Atlantic Meridional Mode

The **A**tlantic **m**eridional **m**ode (AMM) is a leading, real physical mode of coupled ocean-atmosphere variability in the tropical Atlantic (e.g., Chiang and Vimont 2004, Kossin and Vimont 2007, Vimont and Kossin 2007). Variations in the cross-equatorial SST gradient induce boundary layer winds that flow towards the anomalously warmer water and lead to a meridional displacement of the ITCZ. Meridional shifts of the ITCZ are responsible for droughts or floods in sensitive regions like the Nordeste region of Brazil or in the Sahel region of Africa; especially in boreal spring, when the AMM amplitude is maximized. There is an evidence for a positive air-sea feedback between surface winds, evaporation and off-equatorial SST anomalies to maximize their cross-equatorial gradient (Xie and Philander 1994, Chang et al. 1997). Further information about the structure and dynamics of the AMM can be found in the review article by Xie and Carton (2004)
Monthly AMM indices used in the present work are obtained from the **N**ational **O**ceanic and **A**tmospheric **A**dministration (NOAA)[8]. The AMM time series are calulated via projecting SST or the 10m wind field onto the spatial structure resulting from a **M**aximum **C**ovariance **A**nalysis (MCA) of both data sets over the relevant region (21°S-32°N, 74°W-15°E) and the time period 1950 to 2005 from the NCEP/NCAR Reanalysis[9]. Further information about the calculation method are also given in Xie and Carton (2004)

[8] http://www.esrl.noaa.gov/psd/data/timeseries/monthly/AMM/

[9] Reanalysis project from the **N**ational **C**enters for **E**nvironmental **P**rediction (NCEP) and the **N**ational **C**enter for **A**tmospheric **R**esearch (NCAR)

3 Methods

3.1 Identification of low-latitude troughs

The identification of low-latitude disturbances from the extratropics is based on **v**ertically **a**veraged **p**otential **v**orticity (VAPV) fields of the upper troposphere between 400 and 100 hPa. Due to the weak gradients in geopotential height at low latitudes PV fields are commonly used to explore tropical or subtropical disturbances (e.g., Waugh and Polvani 2000, Wernli and Sprenger 2007, cf. Chap. 1.2). However, analysing vertical averages of PV is different from prior studies which focus mainly on individual isentropic surfaces. The novel approach allows the detection of disturbances with a coherent signal throughout the upper troposphere. Furthermore, less seasonal and hemispheric variation in the data basis enable better comparisons between different seasons and the two hemispheres. This fact is evident in Fig. 3.1 which shows absolute values of the winter and summer zonal mean VAPV averaged over the whole investigation period, together with the

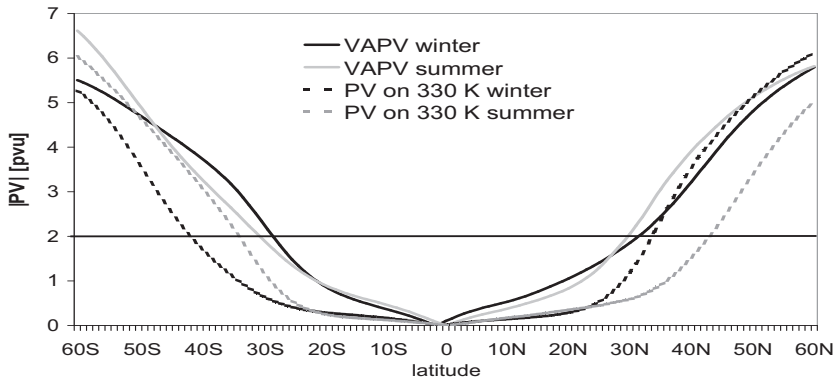

Figure 3.1: Absolute values of mean zonal VAPV [PVU] (PV vertically averaged between 400 and 100 hPa) and PV [PVU] at 330-K averaged over the period from 1980 to 2001. The line at 2 PVU represents the dynamical tropopause.

corresponding PV values on the 330-K isentropic surface (located between 450 and 250 hPa in the Tropics). The variations between the summer and winter climatology in the vicinity of the subtropical tropopause (2-PVU isosurface) are less pronounced for VAPV than for PV on the 330-K isentropic surface.
The identification procedure is illustrated in Fig. 3.2 and explained on the basis of trough events in the subtropical Northern Hemisphere. The algorithm detects contiguous regions between the equator and 25°N (see Fig. 3.2) with

1. VAPV $\geq$ 2 PVU
2. the southern-most point located south of 17°N and
3. the horizontal area covering at least 15 grid points.

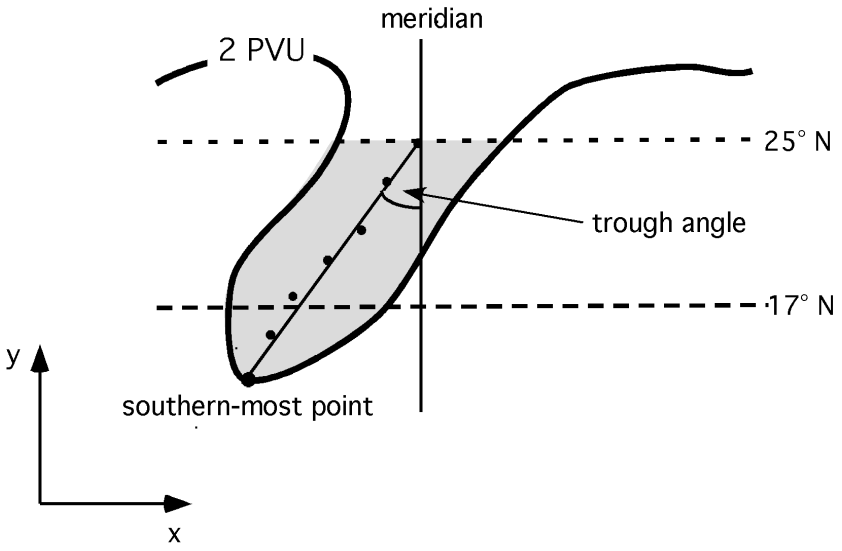

Figure 3.2: Schematic illustration of an intrusion system in the Northern Hemisphere (gray shaded area). For details see text.

The detected regions are defined as an **intrusion event**. In this thesis the term 'intrusion event' corresponds to an upper-level trough at low latitudes but refers especially to events detected at a certain analysis time by the introduced identification algorithm. Intrusion events in the Southern Hemisphere (SH) are detected accordingly with adjusted thresholds, i.e. regions between the equator and 25°S with VAPV $\leq$ -2 PVU and the northern-most point north of 17°S are in the SH defined as intrusion event.
In the following further details about the choice of the identification criteria are given:

- The $\pm$ 2 PVU VAPV contour is chosen as a threshold for the detection of low-latitude disturbances following the widely used definition for the dynamical tropopause (see Chap. 2.1.1). Due to the fact, that stratospheric air is generally characterized by PV values of above 2 PVU, it can be assumed that the air masses within the PV structure have their origin in the extratropical stratosphere (Appenzeller et al. 1996, Wernli and Sprenger 2007).

- The second criteria is implemented due to the fact that disturbances at low latitudes are of main interest here. The crossing latitude of 17°N was chosen to receive a large enough statistical ensemble of intrusion systems with a clear signal of tropical-extratropical interactions that is given e.g. for intrusion systems linked to the generation of a Tropical Plume. Hence, the threshold of 17°N provided the best results for a high frequency of intrusion systems associated with a Tropical Plume. Higher latitudes lead to a larger ensemble of intrusion systems but TP formation in relation to these systems is reduced. In Section 4.2 results of trough identification with another crossing latitude are illustrated to examine the robustness of the method.
- The last criterion is chosen to exclude small scale features that do not imply significant extratropical-tropical interactions.

The detection routine is able to distinguish between upper-level troughs with a connection to the subtropical high-PV reservoir and cut-off systems with a closed 2-PVU contour equatorward of 25°N. However, the routine is not able to decide whether the PV anomaly is of stratospheric origin or produced by latent heat release due to condensation (e.g., Hoskins et al. 1985) or frictional processes near high mountains (e.g., Thorpe et al. 1993). But it is assumed that diabatically produced PV anomalies are negligible in the upper troposphere. Finally it has to be mentioned that due to the lack of any specific shape criterion not only "classical" troughs are detected. However, these sometimes rather ill-defined looking features at least point to some kind of flow disturbance in the upper tropical troposphere.

The output of the identification routine are six hourly integer fields for the entire investigation period. Grid points within an intrusion event are set to values greater than zero and remaining grid points are set to zero. Furthermore, the intrusion events are numbered in dependence on the date and order of detection. For the climatological evaluation, these six hourly fields are averaged (intrusion event grid point values are first set to one) into fields of relative seasonal intrusion occurrence. In another output file additional information on the intrusion events, such as size, horizontal tilt and different characteristic points (e.g., southern-most point, central point) are stored and are evaluated later in this thesis.

Tracking algorithm

Another novelty is the implementation of a tracking algorithm. All intrusion systems are tracked based on spatial overlap at consecutive analysis times. This rather simple approach is possible due to the generally slow propagation of the troughs and a high temporal resolution of 6 hours. If a intrusion event is identified and tracked for at least two consecutive analysis times, the respective period is defined as an **intrusion episode**. We allow one analysis time without a detected event during an episode, if the event reappears in the following analysis time. This happens when the southern-most point of the

trough moves slightly north and south of 17°N. The identification of intrusion episodes provides information about the lifetime and the translation velocity of the detected low-latitude troughs. Less than 2% of all intrusion events are not part of an intrusion episode.

Vertical extent

Extending previous work, the vertical depth of an intrusion event is assessed based on the pressure averaged over the ten grid points within an intrusion system where the 1.5-PVU surface is lowest. It is assumed that the vertical thickness increases with a decrease of the lowest pressure level of the 1.5-PVU surface (in other words the PV anomaly caused by the trough reaches farther down). Note, that due to the omission of PV data in the lower troposphere (see 2.1.1) the 1.5-PVU surface can be detected only down to 400hPa. Hence, a calculated vertical depth of 400 hPa means that the 1.5-PVU surface within the intrusion system reaches down to 400 hPa or even lower. The intrusion episodes are classified depending on the maximum vertical extension during their lifetime.
Dynamical processes such as moisture transports related to intrusion systems behave differently depending on the vertical extension of the PV anomaly (cp. Chap. 8).

Horizontal tilt

The horizontal tilt of an intrusion event is determined by the angle between the trough axis and the meridian (Fig. 3.2). The axis is defined as the linear regression line of the centre points of all latitudes within the intrusion system using kilometers as the metric. The tilt is positive for a SW–NE orientated intrusion as in Fig. 3.2 and negative for a SE–NW orientation. In the SH the denotation is reversed. The tilt of the trough axis influences the transport of angular momentum (e.g., Peixoto and Oort 1992 their Fig. 11.6) in a sense that a positive tilt causes a poleward transport. We expect this procedure to give slightly more robust results than the method by Martius et al. (2007) who determines a PV streamer orientation by simply connecting the northernmost and southern-most centre point.

3.2 Identification of tropical plumes

For the identification of Tropical Plumes a novel algorithm is developed that basically follows the TP definition of McGuirk (1987, see also Sec. 1.3). The algorithm is an extended version of a TP identification routine developed in collaboration with Esther Hohberger and Peter Knippertz and firstly introduced in the diploma thesis of Hohberger (2008). For the present thesis the algorithm was extended by a further criteria that considers the shape of a Tropical Plume.
By applying the identification routine to brightness temperature (T_b) anomalies calculated from the long-term monthly mean T_b of the CLAUS data set (cf. Sec. 2.2), **Tropical Plume** events are defined as contiguous regions with

1. T_b anomaly values $\leq$ -20 K
2. maximum extension $\geq$ 2000 km
3. crossing 15°N (15°S) in the NH (SH)

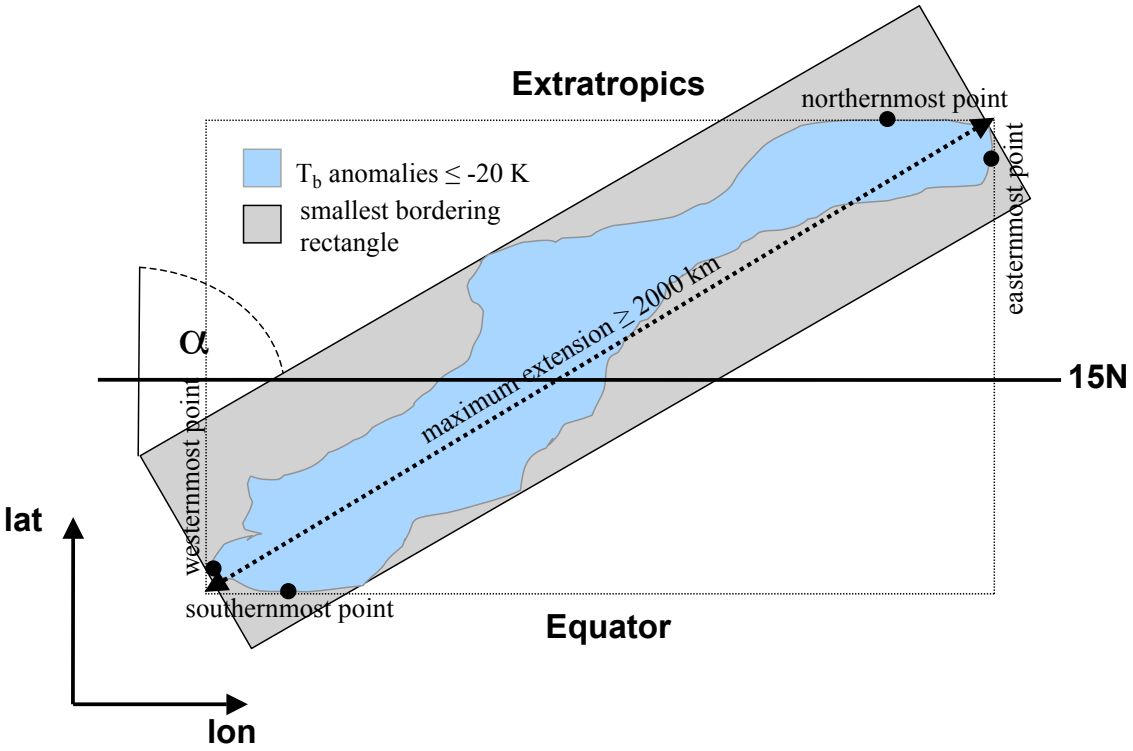

Figure 3.3: Schematic illustration of the Tropical Plume identification procedure for the Northern Hemisphere. For more details see text.

The TP identification procedure is illustrated in Fig. 3.3 for TPs in the Northern Hemisphere. In this thesis the term 'TP event' refers especially to a cloud structure that is detected by the algorithm at a certain analysis time. In the following the four requirements for TP events are explained in detail:

- As mentioned in Chap. 2.2, cold T_b values are an indicator for high cloud tops. The advantage of using anomalies is to foster the identification of transient systems, i.e. cloud systems in regions with climatologically low cloudiness (e.g. Northwest Africa region). The T_b anomaly threshold of -20 K was chosen in comparison to subjectively identified TPs during a short test period. TP frequencies decrease markedly with decreasing T_b anomaly thresholds.
- The maximum extension of a TP event is defined as the length of diagonal of the rectangle that goes through the southern-, northern-, western- and eastern-most

point of the TP as seen in Fig. 3.3 (unfilled rectangle). A minimum length of 2000 km is chosen to detect at least synoptic scale cloud systems.

- Furthermore cloud bands have to cross 15°N/S, which leads to cloud systems at low latitudes with a significant tropical-extratropical interaction.

- Tropical Plumes are generally described as elongated cloud bands, but none of the previous criteria accounts for this attribute. The **l**ength-to-**w**idth **r**atio (LWR) is introduced as a parameter for the elongatedness of a cloud structure. The LWR of a TP is assessed in two steps: First, rectangles with different tilting angles are drawn tightly around the TP. Second, the length-to-width ratio of the smallest rectangle (see Fig. 3.3, grey filled rectangle) that borders a cloud system is computed. To make this point clear, Fig. 3.4 shows a strongly elongated TP event over

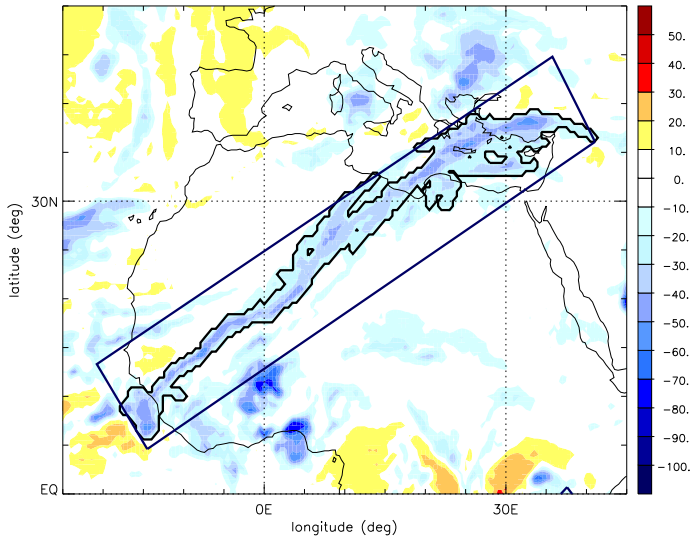

Figure 3.4: Brightness temperature anomalies [K] of the North Atlantic/Northwest African region for 00 UTC 19 November 1985. Detected TP is marked with a black line. The smallest rectangle bordering the TP is presented (also black line) line

Northwestern Africa on 19, November 1985. The smallest surrounding rectangle is drawn around the TP whose LWR value is 6.25.
The LWR criterion is applied to TP episodes (further information about the definition of a TP episode see next subsection) rather than to individual detected cloud bands. This is due to the fact that the shape of a TP changes during its life time. The elongated shape is only achieved at a mature state. Therefore this criterion is implemented in the following way: In a first step, the detection routine searches for all cloud bands that fulfill criteria 1 to 3. In another step, TP episodes are defined and the maximum LWR value is assessed.
A LWR value of 3 is arbitrarily chosen as threshold for the TP identification in respect to produce a large enough ensemble of TP events with a certain elongated shape. Larger LWR thresholds would emphasize the elongatedness of a Tropical

Plumes, but the number of detected TPs decreases rapidly with increasing LWR value (further details in Chap. 9.2).

The described method is not able to distinguish between mesoscale or larger convective systems or cloud bands that are produced mainly by advective or frontal processes (see discussion in Knippertz 2007). But due to the fact, that convective systems often have a rather circular shape, the LWR criterion should reduce the number of convective cloud systems (see also Chap. 9.2).
The horizontal tilt of a TP event is defined by the tilting angle α between the smallest surrounding rectangle and the equator (see also Fig. 3.3). Contrary to the tilting angle of intrusion systems, a west-east (south-north) aligned TP is characterized by a tilting angle of α=0° (90°). Furthermore, a southwest-northeast orientated TP is positively and a northwest-southeast negatively tilted.

TP tracking

The TP events are tracked based on spatial overlap at consecutive analysis times in a similar way to the intrusion events. It has to be mentioned that for the TP tracking procedure, all cloud structures that meet criteria 1 to 3 of the TP identification algorithm are regarded. If such a cloud structure can be tracked at least for two consecutive analysis times and the maximum LWR value is 3 or more (LWR criterion), the respective period is defined as a **TP episode**. The maximum LWR value of a TP episode is here considered due to the fact that the TP shape changes during its life time. TP formation starts often with a small cloud formation near the equator (cf., Knippertz 2005) and only at the mature stage the TP will have the typical elongated shape.
Similar to the definition of an intrusion episode, we allow one analysis time without a detected system during an episode, if the system reappears in the following analysis time. This happens if the cloud regime is for example not contiguous but fragmented at one analysis time. The identification of TP episodes provides information about the lifetime which is evaluated in Chap. 10.1.

3.3 An illustrative example

In this section one intrusion episode over the North Atlantic is exemplary discussed. Figure 3.5 shows the VAPV field and 200 hPa isotachs for different analysis times between 10 and 13 December 2001. The VAPV field for 00 UTC 10 December exhibits a ridge-trough structure with low values over the western North Atlantic and high values off the northwest African coast (Fig. 3.5a). Around the northern edge of the ridge the PV gradient is enhanced accompanied by a strong jet stream. This feature is a typical precursor of low-latitude troughs as described by Knippertz and Martin (2007b). In the following hours the ridge amplifies and expands over the central Atlantic between 40° and 30°W while the trough stretches southward and is detected by the identification al-

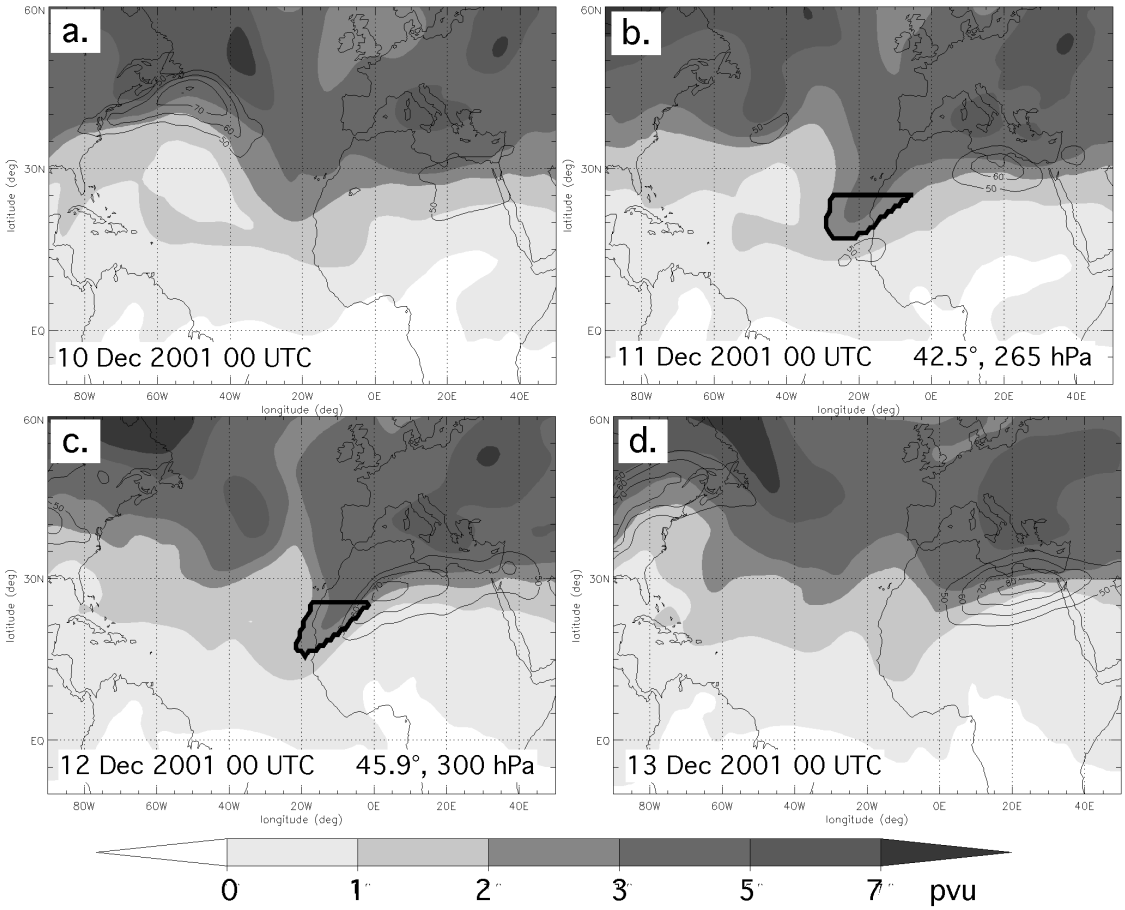

Figure 3.5: VAPV (shaded) and isotachs at 200 hPa (thin black contours every 10 m/s starting with 50 m/s) for (a) 00 UTC 10 December, (b) 00 UTC 11 December, (c) 00 UTC 12 December and (d) 00 UTC 13 December 2001. Detected intrusion systems are marked with thick black lines in (b) and (c). The numbers in the bottom right corners are the estimated horizontal tilt and vertical depth. .

gorithm for the first time at 00 UTC 11 December (Fig. 3.5b). A thick black line in Fig 3.5b marks the intrusion area just off the African coast. The horizontal tilt is estimated as 42.5° and the vertical depth is 260 hPa. One day later the trough has narrowed and moved eastward by about 5 degrees (Fig. 3.5c). The system has become deeper and the horizontal tilt has increased by a few degrees. A band of high wind speeds and enhanced PV gradients has formed along the eastern edge of the trough and further downstream over northern Africa (Fig. 3.5c). The formation of a subtropical jet streak is a typical feature accompanying low-latitude troughs in this region (Ziv 2001; Knippertz 2005). At 06 UTC the trough is identified for the last time and then decays quickly (Fig. 3.5d), while the upper level winds remain strong for a few more analysis times. Due to the slow movement the tracking routine joins the identified systems to an intrusion episode with a lifetime of 30 hours (00 UTC 11 to 06 UTC 12 December). The temporal evolution and other characteristics shown in Fig. 3.5 are typical of wintertime intrusion episodes over the North Atlantic.

In Fig 3.6 T_b anomalies and the identified TP events for the same period and region are

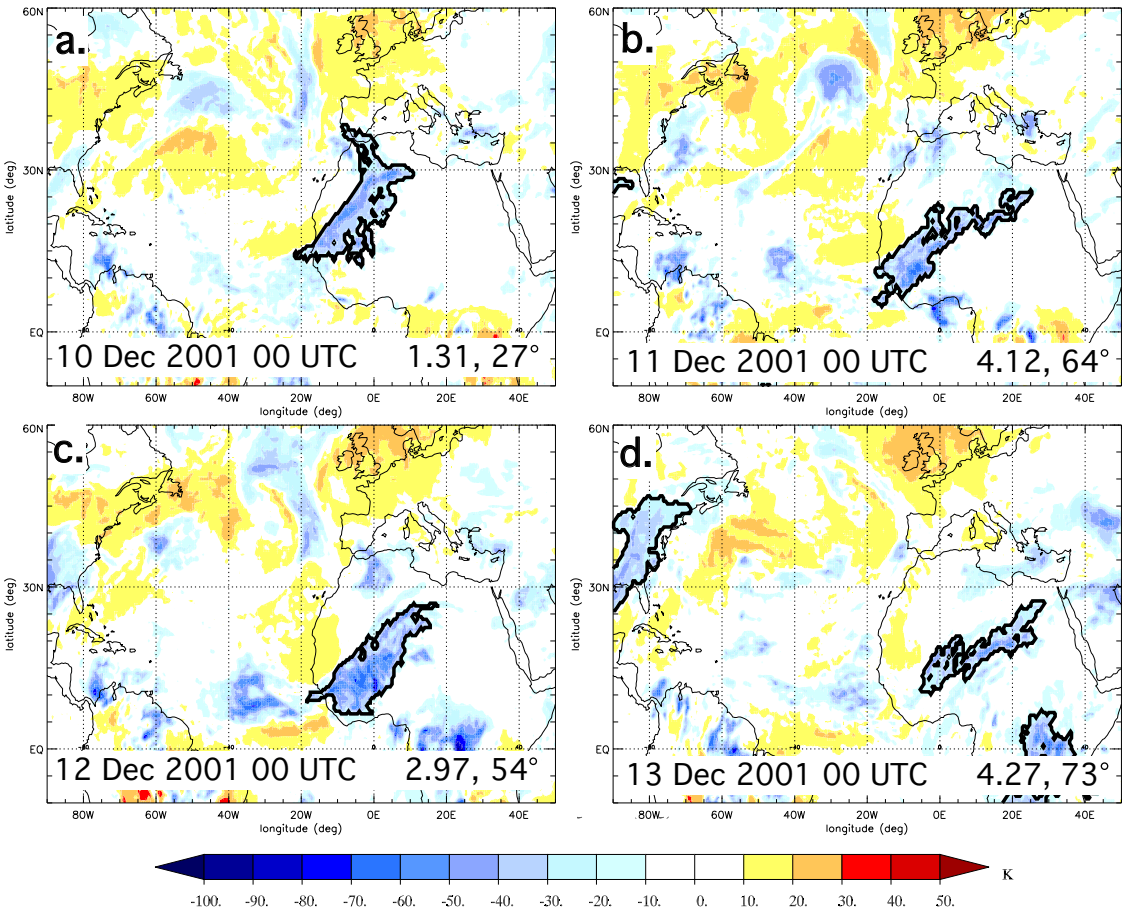

Figure 3.6: Brightness temperature anomalies [K] for (a) 00 UTC 10 December, (b) 00 UTC 11 December, (c) 00 UTC 12 December and (d) 00 UTC 13 December 2001. Detected Tropical Plumes are marked with thick black lines in (b) and (c). The numbers in the bottom right corners are the estimated horizontal tilt and the LWR value (see Sec. 3.2). .

depicted. In comparison to the PV, the T_b anomaly fields are of smaller scale and exhibit stronger day-to-day fluctuations. Every presented field exhibits a cloud structure over northwestern Africa that meets the criteria for the TP identification. All these cloud structures are accompanied by positive T_b anomalies to the west located below an upper-level trough (see Fig. 3.5), which point to dryer, cloudless air masses. This dry/moist dipole in connection to TP formation has been described by e.g. McGuirk and Ulsh (1990) and Blackwell (2000). All the detected TP events over North Africa in Fig. 3.6 are part of a long-living TP episode (almost 6 days) that was firstly identified at 12 UTC 7 Dec. and disappeared after 06 UTC 13 Dec. It's appearance changes strongly during its lifetime (see e.g. LWR value and tilting angle) and is more fragmented in comparison to the intrusion episode. For example in the beginning (07 Dec. 2001, not shown), the TP episode was located over the North Atlantic (40°W-20°W) and reached from the Tropics for into the midlatitudes (from 10°N up to 70°N). Such an elongated cloud band strongly suggests tropical-extratropical interactions. At later dates (cf. Fig. 3.6) the observed TP episode is located farther east and is rather confined to the Tropics and subtropics. The strong alterations in shape and the long lifetime of this TP episode are caused by several

low-latitude troughs that traverse successively the subtropical North Atlantic region and consistently lead to cloud genesis. Not all of these troughs are also detected as intrusion event by the above-mentioned identification routine. For example at 00 UTC 10 Dec. (see Fig. 3.6a) the trough over the Northeast Atlantic misses the criteria for an intrusion event. A distinctive feature of this TP event at this analysis time is the cyclonic roll up at the northeastern end of the TP, which has been termed a comma cloud structure and is often associated with a low pressure beneath (e.g., Thepenir and Cruette 1981, Fink and Knippertz 2003).

On the following days the detected TP can be associated with the identified intrusion episode described above and seen in Fig. 3.5. The TP runs along the eastern flank of the intrusion and moves eastward ahead of the trough.

Although the described TP episode is quite exceptional due to its long lifetime, it shows the typical features of TP evolution over the North Atlantic/North Africa in respect to its shape, tilting angle, LWR value and location relative to the trough. As expected, this example shows that the intrusion episode is connected to TP formation. But both phenomena do not occur exactly at the same time. Generally it is observed that troughs propagate into the Tropics before TP genesis, while the TP episode persists longer (see Fig. 3.6d).

Finally, hydrological processes in relation to the detected trough are briefly discussed. For that reason in Fig. 3.7b and 3.7d moisture flux anomalies at 00 UTC 11 December averaged over two vertical layers in the lower (between 1000 and 800 hPa) and in the middle (between 750 and 500 hPa) troposphere are depicted. The anomalies are calculated from the long-time monthly mean and the meridional component is shaded in Fig. 3.7. In both vertical layers a narrow band of positive anomalies has formed near the eastern flank of the PV trough, that points to a poleward transport of water vapour out of the Tropics into the subtropics and even further into the midlatitudes. These anomalies are strongest pronounced in the lower troposphere rather north of the detected intrusion event in an area over the North Atlantic between the coast of Morocco and the southwestern coast of the Iberian Peninsula. Below the western edge of the trough negative moisture flux anomalies occur, that are also strongest in the lower troposphere and north of the detected trough. These negative fluxes coincide with positive T_b anomalies pointing to enhanced outgoing long-wave radiation through less clouds. In relation to the trough, that is located further upstream over the North Atlantic, a similar pattern of positive and negative anomalies in the meridional moisture flux has formed. In the region below the detected TP (east of the PV trough) of this date (see Fig. 3.6b) slightly positive moisture flux anomalies (magnitudes are much lower) are observed that are stronger in the upper vertical layer.

Within the time period discussed above, strongest rainfall was observed on 11, December in the evening from 18 to 21 UTC with a maximum of 45 mm in 3 hours over some parts of the Moroccan coast (where the moist air crosses at first over land masses) as seen in Fig. 3.7d. The rainfall data was obtained from the **T**ropical **R**ainfall **M**easuring

(a) Meteosat IR image (12 Dec. 00 UTC)

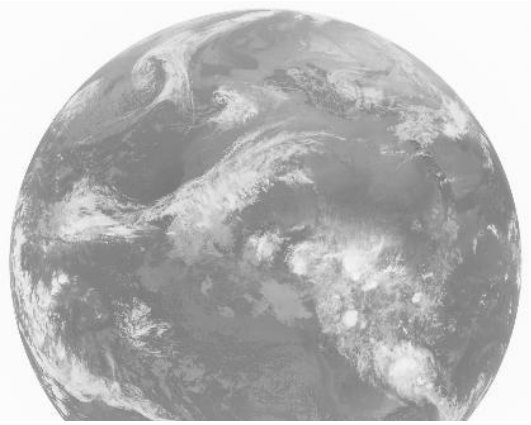

(b) QV anomaly: 1000–800hPa (11 Dec. 00 UTC)

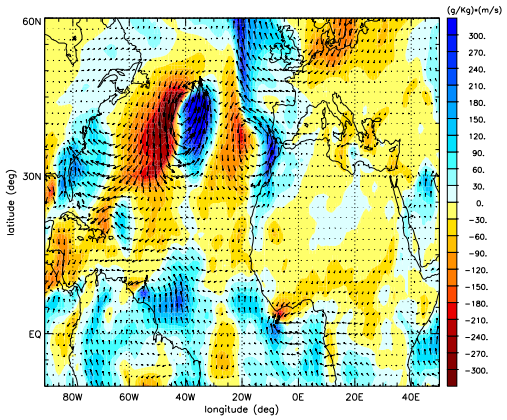

(c) Precipitation (11 Dec. 18-21 UTC)

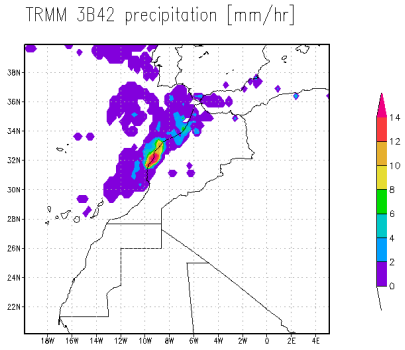

(d) QV anomaly: 750–500 hPa (11 Dec. 00 UTC)

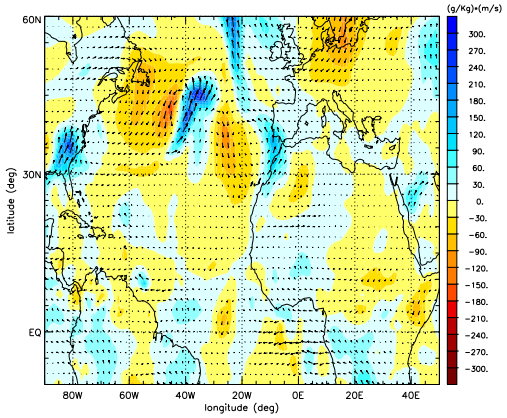

Figure 3.7: Meteosat IR satellite image at 00 UTC 12 December 2001 (a). Moisture flux anomalies [(g/kg)*(m/s)] (vertical component shaded) for 00 UTC 11 December averaged between 1000 and 800 hPa (b) and between 750 and 500 hPa (d). TRMM 3B42 precipitation [mm/hr] on 11 December between 18 and 21 UTC (c).

Mission[1] (TRMM) homepage. The observed rainfall and moisture flux anomalies in relation to the PV intrusion detected over the North Atlantic are generally in accordance with results from previous studies that has been described in Chap. 1.2.4.

3.4 Centered composite analysis

Based on the identified low-latitude troughs, centred composite analysis of several meteorological parameters were performed to analyse (i) the evolution of intrusion and TP events in the upper tropospheric circulation (Chap. 7 and 12) and (ii) the impact of the intrusion events on water vapour fluxes (Chap. 8). The so-called centred composite analysis takes into account not only the times, but also the locations of the identified events. That means (for the construction of a composite mean) the considered meteorological fields are centred on a reference longitude according to the location of the intrusion event

[1] http://$gdata1.sci.gsfc.nasa.gov/daac-bin/G3/gui.cgi?instance_id = TRMM_3 - Hourly$

before averages are calculated. In this way the spatial smoothing is reduced compared to the 'uncentred' composite analysis and the significance of the variations is enhanced. These composites are constructed in three steps, which are described here exemplary for variations in the vertical averaged PV (VAPV) associated with the occurrence of intrusion episodes and are illustrated in Fig. 3.8.

0. Data basis are the VAPV fields of all intrusion episodes identified between 1980 and 2001 in a certain region (cf. Fig. 3.8a).

1. Anomalies of VAPV fields with respect to the long-term monthly mean are calculated (Fig. 3.8b).

2. VAPV anomaly fields are shifted east- or westward until the central points of the intrusion events are located on a reference longitude of 0° (Figs. 3.8b (arrow) and 3.8c).

3. Centred VAPV fields are averaged.

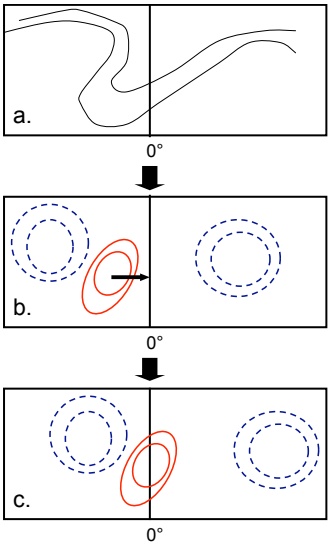

Figure 3.8: Schematic illustration of the preparation of centred composites.

Composite analysis are also performed for 1-day periods up to 5 days prior to the first and 3 days after the last occurrence date of the intrusion episode. As mentioned before the method is applied to further meteorological fields such as the moisture transport, sea level pressure or precipitation.
Centred composites on the basis of the Tropical Plumes episodes are performed accordingly to analyse their influence on the general circulation.

Significance test via Monte-Carlo-Simulation

The statistical significance of the centred composites is examined via a Monte Carlo calculation described by Moore et al. (2008). The method is based on a comparison of the composite fields with 300 composites constructed with randomly selected episodes. More precisely, for each intrusion episode, which is included in the composite calculation, a time period of the same duration is selected. The selected time periods are constrained to occur: i) within plus or minus 10 calendar days of the actual intrusion episode but ii) in a different year to exclude the intrusion episode itself in the comparison. After the selection the analysis fields are also east-west shifted according to the location of the corresponding intrusion episode and equal to the preparation of the centred composites. Finally all fields are averaged to construct a 'random' composite.

Once the 'random' composites are created the robustness of the centred composites is tested on a grid point basis: If the real data value at a grid point is greater/less (depending on the sign of the anomaly) than more than 293 (97.5% of 300 to achieve a two-sided significance level of 95%) of the 'random' data values at the same grid point, the real composite data value is considered to be statistically significant at or above the 95% confidence level.

3.5 Mann-Kendall Test

The **M**ann-**K**endall (MK) test is a non-parametric test for trend detection in time series data without any distribution requirements (Mann 1945, Kendall 1975). A main feature of the MK test is that the relative magnitudes of the data is compared instead of the data values themselves. The MK test is based on the statistic S, which is defined for a time series $(X_k, k = 1,2,...,n)$ as

$$S = \sum_{k=1}^{n-1} \sum_{j=k+1}^{n} sign(x_j - x_k)$$

with:

$$sign(x_j - x_k) = \begin{cases} 1 & : \quad x_j - x_k > 0 \\ 0 & : \quad x_j - x_k = 0 \\ -1 & : \quad x_j - x_k < 0 \end{cases}$$

For time series with data values randomly ordered (no trend exists) S is expected to be zero. Highly positive (negative) S values point to an increasing (decreasing) trend in the data set. To evaluated the statistical significance of the trend (probability of S) further computational steps have to applied. In the next step the variance of S, VAR(S), is calculated by the following equation:

$$VAR(S) = 1/18 \left[n(n-1)(2n+5) - \sum_{p=1}^{g} t_p(t_p-1)(2t_p+5) \right]$$

where n is the number of data points, g is the number of tied groups (a tied group is a set of sample data having the same value), and t_p is the number of data points in the pth group. Furthermore, the normalized test statistic Z is calculated as follows:

$$Z = \begin{cases} \frac{S-1}{[VAR(S)]^{1/2}} & : \quad S > 0 \\ 0 & : \quad S = 0 \\ \frac{S+1}{[VAR(S)]^{1/2}} & : \quad x_j - x_k < 0 \end{cases}$$

Finally the probability associated with this normalized test statistic Z is computed. The

probability density function for a normal distribution is given by the following equation:

$$f(z) = \frac{1}{\sqrt{2\pi}} e^{\frac{z^2}{2}}$$

The trend is called decreasing (increasing) if Z is negative (positive) and the computed probability is greater than the level of significance. If the computed probability is less than the level of significance, there is no trend.
The MK test is applied in this work to evaluate long-term trends in the seasonal intrusion and TP frequencies in Chap. 6 and 11.

Part I

Low-Latitude Troughs

4 Climatology

4.1 Geographical and seasonal distribution

The climatological distribution of the intrusion event frequency (f_{is}) for the period 1980–2001 is depicted inFig. 4.1. f_{is} is the percentage of analysis times during the investigation period at which a respective grid point is part of an intrusion system. Note that in both hemispheres nearly one-fifth of all detected systems are cut offs.Fig. 4.1 reveals that intrusion systems occur almost exclusively over the Pacific and Atlantic Oceans in both hemispheres. During boreal winter the f_{is} maxima are located over the eastern parts of the ocean basins with the exception of the South Atlantic, where intrusions are comparably rare. The absolute maximum of f_{is} of $\sim 12\%$ is found over the eastern subtropical North Atlantic followed by the eastern South Pacific. In boreal summer, the geographical distribution pattern is rather similar, but the magnitude is strongly reduced, in particular over the North Atlantic and South Pacific with less than 4% (Fig. 4.1b). However, over the North Pacific f_{is} increases to more than 10% and the maximum shifts towards the centre of the basin. This maximum corresponds well with the strong RWB activity near the subtropical high pressure systems as documented by Postel and Hitchman (1999). A similar east-west shift of intrusion occurrence (although strongly reduced frequencies) is observed over the North Atlantic region. These summer troughs are commonly referred to as **t**ropical **u**pper **t**ropospheric **t**roughs (TUTT) (e.g., Ferreira and Schubert 1999) and are even more apparent in intrusion frequency plots based on three-month means (seeFig. A.1 in the appendix).

During both seasons most of the f_{is} maxima have a positive horizontal tilt in accordance with the majority of the individual systems as discussed in Sec. 5.3 below.

An alternative way to describe the geographical distribution of low latitude troughs is to compare regional intrusion frequencies. For this purpose each intrusion system is assigned to one 90°-longitude wide region (black boxes in 4.1) according to the loca-

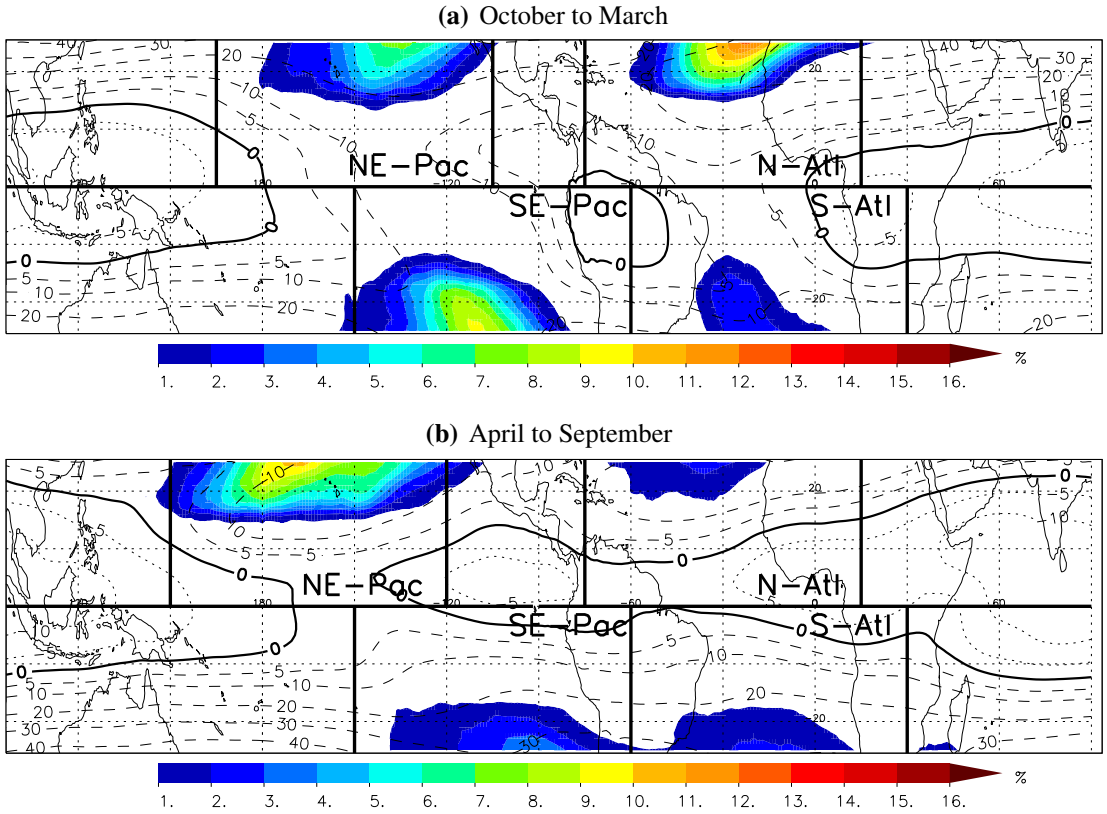

Figure 4.1: Mean intrusion frequency [%] (shaded) and mean zonal wind at 200 hPa [m/s] (dashed contours for westerlies and dotted contours for easterlies with the zero contour in bold) for (a) NH winter (b) NH summer for the period 1980–2001. The regions used for further investigations are indicated by black boxes.

tion of its southern-most point. Since the entire Indian Ocean and the Southwest Pacific are practically void of intrusions, the following investigations focus on the North Atlantic (N-Atl: 15°E–75°W), Northeast Pacific (NE-Pac: 105°W–165°E for NH winter, 120°W–150°E for NH summer), Southeast Pacific (SE-Pac: 150°W–60°W) and South Atlantic (S-Atl: 60°W–30°E) regions that together contain more than 90% of all identified systems. In the North Pacific a region with seasonally variable boundaries is chosen to capture the bulk of intrusion systems by a 90°-longitude wide region despite of the east-west shift of the intrusion maximum between the seasons. The intrusion frequencies of the selected regions, together with the ones for the entire NH and SH, are presented inFig. 4.2. During boreal winter (black bars inFig. 4.2), an intrusion system is detected on average at nearly every second analysis time somewhere in both hemispheres. On the regional scale the maximum intrusion frequency of 27.6% is observed in the SE-Pac region, followed by the NE-Pac (23.1%) and the N-Atl (20.5%). This reflects the larger spatial extent of the two Pacific maxima compared to the North Atlantic (Fig. 4.1). During boreal summer the occurrence of intrusion systems in the NH (47.4%) is approximately as high as the winter frequency but largely dominated by the Northeast Pacific (grey bars in; see also 4.1b). In the SH the intrusion activity (24.3%) is only half of the boreal winter frequency due to a strong reduction in the SE-Pac and a more

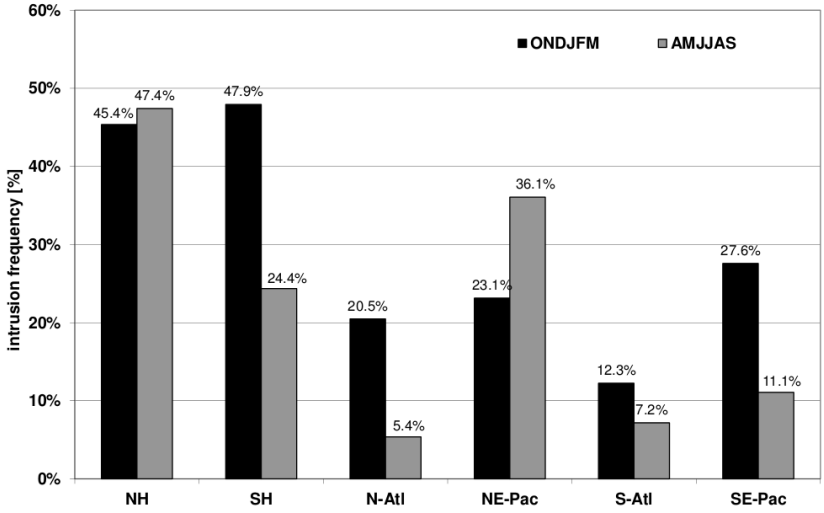

Figure 4.2: Boreal winter (black) and summer (grey) mean intrusion frequencies [%] per region for the period 1980–2001. Regions are defined inFig. 4.1a.

moderate reduction over the S-Atl. It is remarkable that the SH activity is strongest during austral summer when the storm track activity in the midlatitudes is weaker and shifted polewards. This points to a strong control of the intrusion frequency by tropical processes. In fact,Fig. 4.1 shows that the 200 hPa winds in the Tropics are westerly over the regions of interest in austral summer allowing the equatorward penetration of Rossby waves, while they are mainly easterly in austral winter, when the wave activity in the SH extratropics is higher. Such a close relation between the activity of low-latitude disturbances and the strength of the westerly ducts has been previously documented by various authors (e.g., Kiladis and Weickmann 1997, Waugh and Polvani 2000, see also Chap. 1.2). On the other side, austral summer is the time when the SPCZ is most active (Vincent 1994), which might suggest an influence of the SPCZ on intrusion development over the South Pacific.

Further information about the seasonal cycle are provided by the mean monthly intrusion frequencies inFig. 4.3. All regions except for the North Pacific show similar behaviour with maximum intrusion frequencies in December or January and relatively low magnitudes from April to September. In contrast over the North Pacific the intrusion frequency increases during NH summer up to more than 60% in June. A secondary maximum in the North Pacific region of nearly 30% is found in December. The reasons why the North Pacific is active in boreal summer despite the weak westerly ducts will be discussed later in this work.

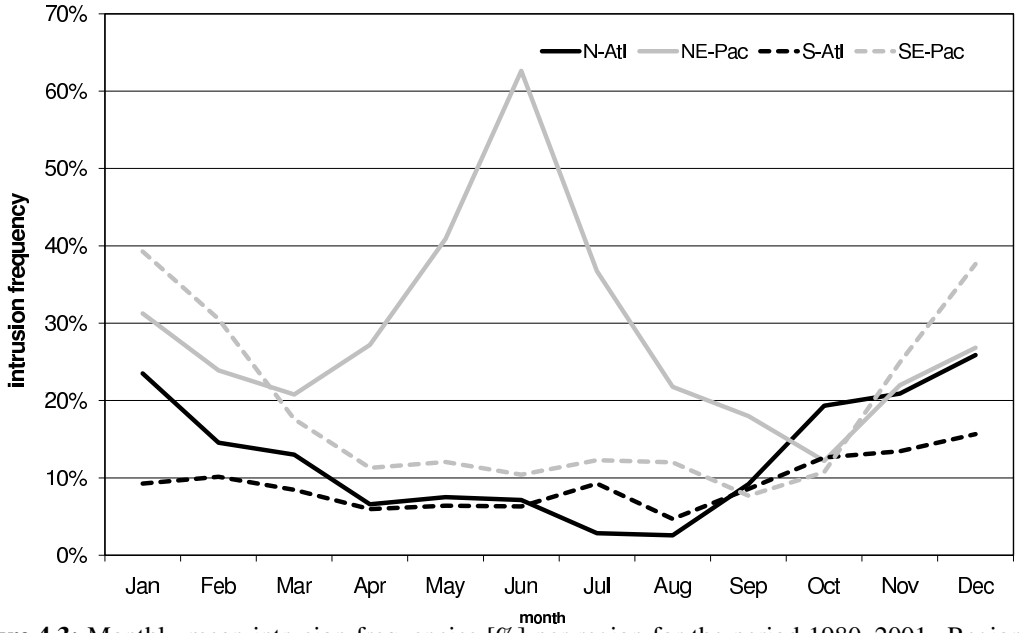

Figure 4.3: Monthly mean intrusion frequencies [%] per region for the period 1980–2001. Regions are defined inFig. 4.1a.

Discussion

Comparison with the intrusion climatology of Waugh and Polvani (2000) (see Chap. 3.1) shows a good agreement with respect to spatial and seasonal variations in intrusion occurrence. However, some differences are found: In the South Atlantic region for instance the number of intrusion events significantly exceeds the number of North Atlantic events in the study of Waugh and Polvani (2000).

Further more the pronounced peak of North Pacific intrusion frequency in NH summer is not reflected by their climatology. However, such a NH summer maximum is presented in the Rossby wave breaking (RWB) climatologies presented by Postel and Hitchman (1999) and Abatzoglou and Magnusdottir (2006b) and in the Potential Vorticity streamer climatology by Wernli and Sprenger (2007) and Martius et al. (2007). RWB identification algorithm focus on large-scale and irreversible overturning of PV contours, which are detected mostly at the northern summer subtropical tropopause near the date line and about 60° W. Due to the similarity of the frequency maxima in the central North Pacific between the intrusion and RWB climatologies it can be assumed that the intrusion events detected there represent actually RWB events that are relatively large and strongly tilted (see also Chap. 5.3).

In the remaining regions the seasonal cycle of intrusion event occurrence is opposite to the RWB and PV streamer climatology especially for the Northern Hemisphere. This indicates that wave breaking events, which reach far into the deep Tropics are more frequent in winter (when equatorial westerlies are prevalent), although the NH summer subtropical tropopause reveals more wave breaking than the winter tropopause.

Waugh and Polvani (2000) note, that northern and southern intrusions often occur simultaneously more or less in the same longitudinal sector. Different simple statistical

tests were applied to the intrusion event data set of this thesis. But none of them gave evidence for such a synchronized trough occurrence. Nevertheless, it is possible that wave disturbance simultaneously develops for instance in the North and South Atlantic but not both disturbances are detected by the identification routine as an intrusion event (i.e. one disturbance does not reach equatorward of 17°N/S). This argumentation is confirmed later in Chap. 7 with composite studies of PV anomalies that reveal in association with intrusion detection a slight signal also in the opposite hemisphere.
Finally, it has to be mentioned that the results presented in this and in the following chapter (Chap. 4.1 and 5) have been documented already in a paper by Froehlich and Knippertz (2008).

4.2 A sensitivity study

To examine the robustness of the results, another intrusion climatology was generated that focuses on larger PV anomalies farther away from the equator. For this sensitivity experiment the VAPV threshold is increased from 2 to 3 PVU and latitudinal thresholds are shifted by 5 degrees to 22°N and 30°N in the NH. The identification thresholds in the SH are modified accordingly. The geographical distribution of the intrusion fre-

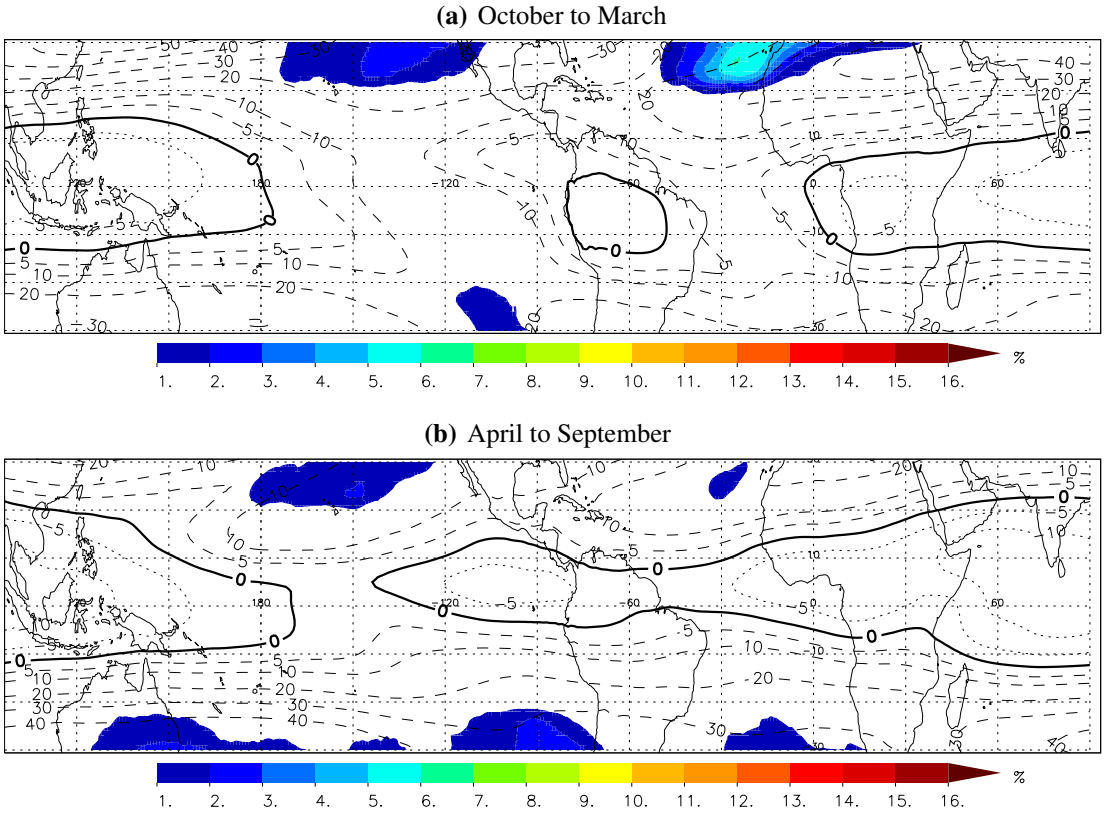

Figure 4.4: Mean intrusion frequency [%] (shaded) detected with a modified identification algorithm using ± 3 PVU between 22°N and 22° and mean zonal wind at 200 hPa [m/s] (dashed contours for westerlies and dotted contours for easterlies with the zero contour in bold) for (a) NH winter and (b) NH summer for the period 1980 and 2001.

quency qualitatively resembles the original climatology, but total numbers are somewhat lower (seeFig. 4.4). Intrusion systems are mainly detected over the eastern Pacific and Atlantic Oceans with an absolute f_{is} maximum of less than 6% observed over the North Atlantic. Analysis based on the selected regions (see Fig. 4.1) inFig. 4.5 show a intrusion frequency maximum of 18.2% in the N-Atl. It should be noted that with the modified thresholds about 25% of all intrusion systems occur over Australia and the Southwest Pacific Ocean (not shown inFig. 4.5). Another evident difference is the stronger seasonality with a clear hemispheric winter maximum in both hemispheres and in all regions but the North Pacific. This points to a stronger impact of the midlatitude storm track activity on the systems identified with the modified algorithm as compared to their 'more tropical' counterparts discussed in Chap. 4.1. Further investigations show that only approx. 40% of the intrusion systems correspond to (overlap with) one of the original systems. For example, the intrusion episode shown inFig. 3.5 is identified by both methods. This analysis demonstrates that intrusion climatologies are sensitive to the choice of the identification thresholds and presumably to other details of the detection algorithm as well. However, the geographical distribution of the most active regions over the Pacific and Atlantic Oceans appears to be a robust feature of most methods.

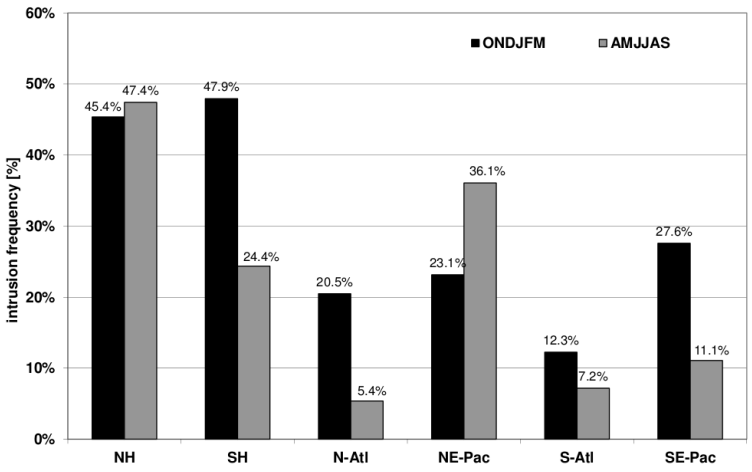

Figure 4.5: Boreal winter (black) and summer (grey) mean intrusion frequencies [%] detected with a modified identification algorithm using $\pm$ 3 PVU between 22°N and 22° per region for the period 1980–2001. Regions are defined inFig. 4.1a.

5 Trough characteristics

5.1 Life time

In the following section the intrusion episodes, detected by the original identification algorithm described in Section 3.1, are analyzed with respect to geographical and seasonal variations in their occurrence and lifetime. The mean number of intrusion episodes per season and their mean lifetime are displayed inFig. 5.1 for the regions defined in Chap. 4. Recall that an intrusion episode is assigned to a region according to the location of the southern-most point at the first time of appearance and that the minimum lifetime of an intrusion episode is 6 hours.
Not surprisingly the geographical pattern of intrusion episode appearance shows similar characteristics as the frequency distribution of the intrusion systems. In boreal winter, on average between 15 and 20 episodes are detected per season in the N-Atl, NE-Pac and SE-Pac (black bars in 5.1). In the SE-Pac region the numbers of intrusion episodes is much smaller with 8 episodes per season.
The intrusion episodes in the NH last on average approx. 2 days with only 4% of all episodes persisting longer than 5 days. In the SH the mean lifetime is somewhat higher with around 3 days and nearly 10% lasting longer than 5 days. Five events were found that last even longer than 2 weeks. Such a long persistence might be related to the quasi-permanent convergence zones found in these regions at this time of the year (Kodama 1993).
In the boreal summer, the mean lifetime in the SH dramatically decreases (grey-filled circles inFig. 5.1) with only 1% of all episodes lasting longer than 5 days. This results in only slightly reduced numbers of episodes in contrast to the strong seasonality in intrusion system frequency (Fig. 4.1). Presumably SH intrusions during this time of the year are related to short-lived, fast-moving storm track disturbances. Over the North Pacific intrusion episodes are more persistent during boreal summer, however, the seasonal

differences in the mean intrusion lifetime are smaller than in the SH. Over the N-Atl seasonal variations are contrary with shorter lifetimes in summer. The percentage of episodes lasting longer than 5 days in the entire NH doubles from winter to summer to 8%.

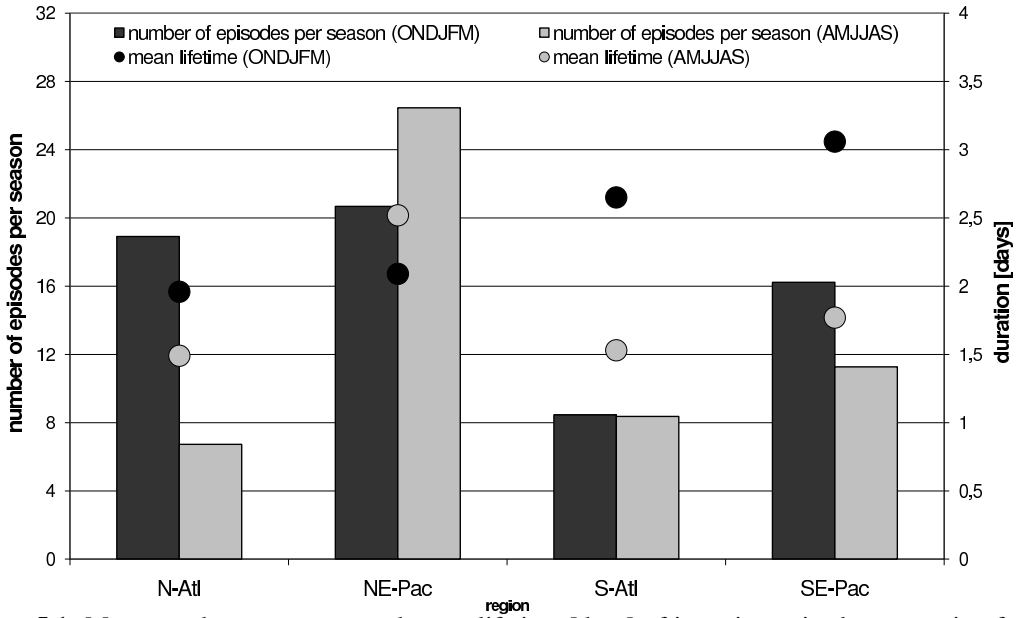

Figure 5.1: Mean number per season and mean lifetime [days] of intrusion episodes per region for NH winter (black) and summer (grey) during the period 1980 – 2001. Regions are defined in Fig. 4.1a.

5.2 Vertical depth

In this section the vertical depth of the intrusion systems is statistically evaluated. Recall, the vertical depth is defined by the lowest pressure level of the 1.5 PVU surface within an intrusion system (see Chap. 3.1 for further information). All intrusion systems in each hemisphere and in each season are divided into six 50-hPa bins between 100 hPa and 400 hPa according to their vertical depth and then normalized with the respective total numbers (Fig. 5.2). Note, due to the omission of PV data below 400 hPa, vertical depth of 400 hPa means that the 1.5-PVU surface within the intrusion system reaches down to 400 hPa or beneath.

In the NH the intrusion depths during summer and winter approximately follow a normal distribution with a shift between the two seasons of about 50 hPa (Figs. 5.2a and 5.2b). Most frequent are intrusion systems reaching down to 250–300 hPa in winter and to 200–250 hPa in summer. In winter 14.0% (11.9%) of all NE-Pac (N-Atl) systems reach below 350 hPa and directly influence the middle tropical troposphere.

The distributions in the SH (Figs. 5.2c and 5.2d) show a seasonal shift similar to their NH counterparts, but with a general tendency to greater depth. 21.8% (18.8%) of the SE-Pac (S-Atl) intrusion systems during austral winter belong to the category with the

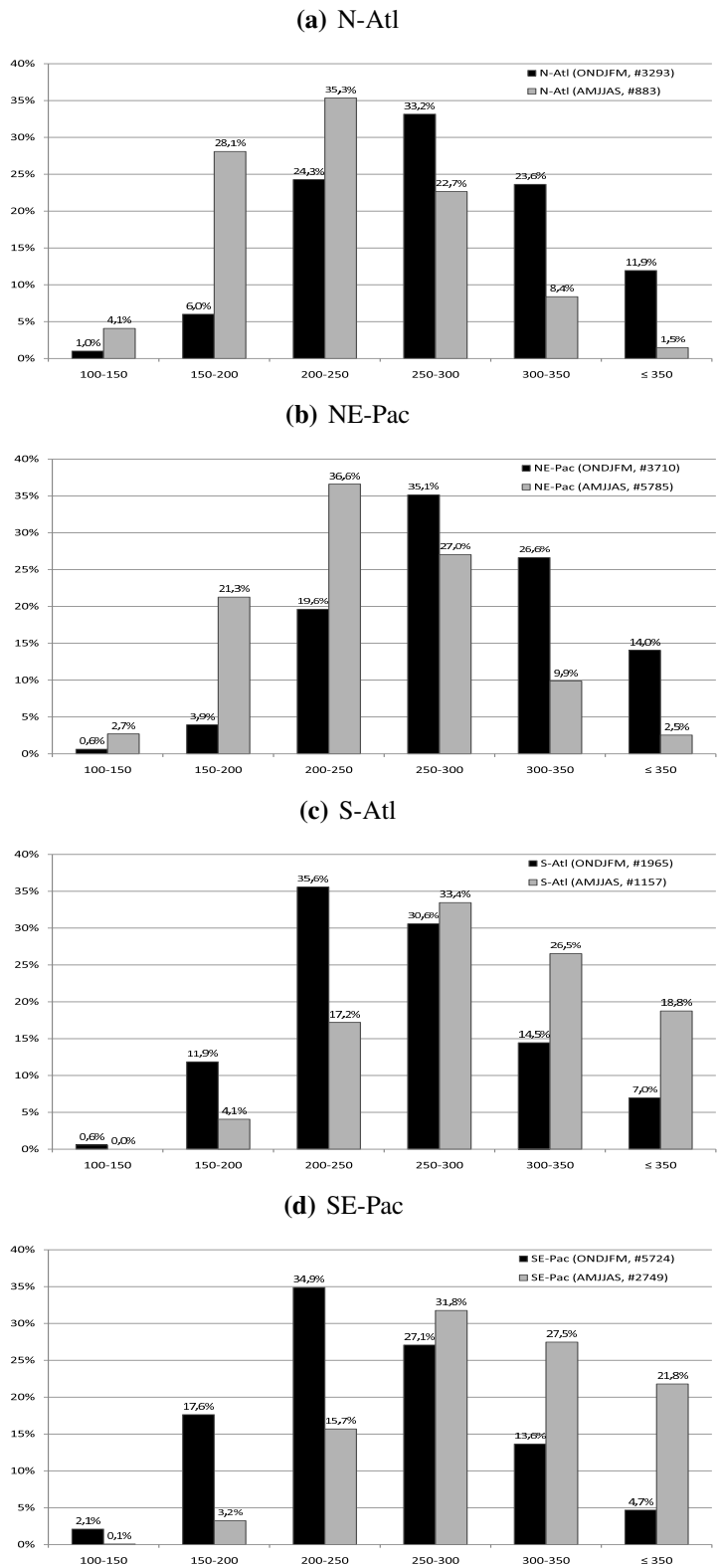

Figure 5.2: Normalized distributions of intrusion vertical depth for the (a) N-Atl, (b) NE-Pac, (c) S-Atl and (d) SE-Pac region. The black (grey) bars show boreal winter (summer) frequencies of the period 1980–2001. The total numbers for each season and region are given in brackets. Regions are defined inFig. 4.1a.

maximum vertical depth. This suggests that only very intense systems can penetrate into the Tropics during a season when the westerly ducts are weakest (seeFig. 4.1). Such developments presumably require a particularly explosive development in the extratropical storm track.
The number of detected intrusion episodes classified by their maximum vertical depth during its life time are listed in Tab. 5.1. While in the NE-Pac (N-Atl) region in winter about 20% (25%) of all intrusion episodes reach at least once below 350 hPa, in summer it is only 7% (2%). In the SH the seasonal behavior is respective. During austral winter nearly one-third of all episodes belong to the group with the maximum vertical extension and in austral summer the numbers are halved.

	all		150–200		200–250		250–300		300–350		350–400	
N-Atl	416	148	7	32	71	46	106	46	130	19	102	4
NE-Pac	455	582	7	73	37	155	118	188	144	119	148	40
S-Atl	186	184	8	1	40	18	69	43	39	62	29	60
SE-Pac	357	248	38	5	94	26	118	59	61	77	43	81

Table 5.1: Number of intrusion episodes per maximum vertical depth detected during boreal winter (white boxes) and summer (grey boxes) between 1980 and 2001 in the selected regions. Regions are defined inFig. 4.1a.

5.3 Horizontal tilt

The normalized distribution of intrusion horizontal tilt shows that globally nearly 90% of the systems are positively tilted (Fig. 5.3). Most frequent during all seasons and in all regions are tilts between 0 and 45° with respect to the meridian ($\sim$ 60% of all intrusion systems), i.e. a SW-NE (NW-SE) orientated intrusion axis in the NH (SH). In boreal winter NE-Atl intrusions are generally more tilted than NE-Pac events. The NE-Atl exhibits the greatest percentage of intrusions with angles of more than 45°. The distribution of intrusion horizontal tilt is in both SH regions quite similar. In all regions the climatology reveals a seasonal shift from boreal winter to summer towards less tilted or even negatively tilted intrusion systems. Except for the NE-Pac region where in summer nearly 40% of all intrusion systems reveal tilts of more than 45°. This is consistent with the strong RWB breaking maximum found by Postel and Hitchman (1999) in this region during this time of year. SH intrusions during austral summer show the least positive tilt. These are also the episodes with the longest lifetimes (5.1). The modifications of the algorithm tested in Section 4.2 do not substantially change the statistical distribution of trough orientations (not shown).

(a) N-Atl

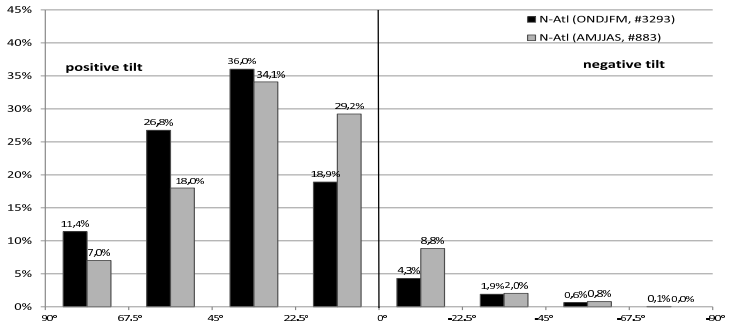

(b) NE-Pac

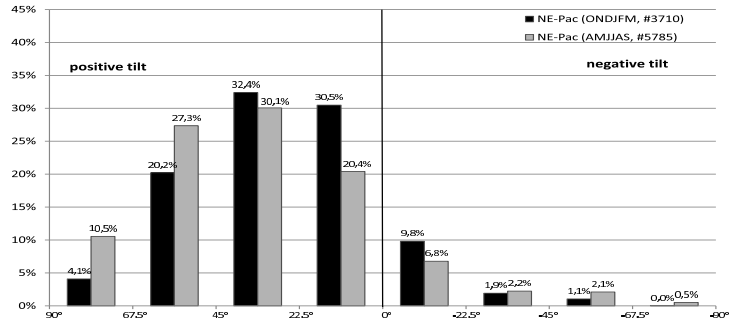

(c) S-Atl

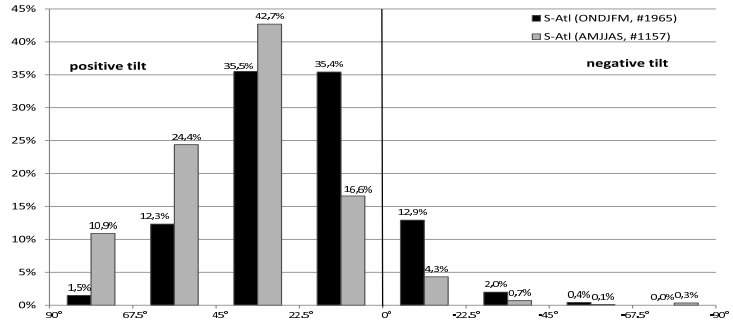

(d) SE-Pac

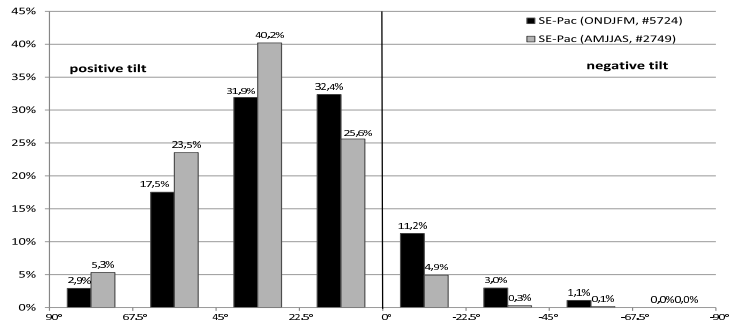

Figure 5.3: Normalized distributions of intrusion horizontal tilt for the (a) N-Atl, (b) NE-Pac, (c) S-Atl and (d) SE-Pac region. The black (grey) bars show boreal winter (summer) intrusion frequencies of the period 1980–2001. The total numbers for each season and region are given in brackets. Regions are defined inFig. 4.1a.

6 Trends and inter-annual variability

In the following section the regional time series of seasonal intrusion frequencies, displayed in Fig. 6.1, are analysed with respect to inter-annual variations and long-term trends during the investigation period from 1980 to 2001. In all regions the seasonal intrusion occurrences are characterized by large year-to-year fluctuations, which are generally more pronounced in boreal winter. However, largest variations are observed in NE-Pac summer (Fig. 6.1b), where intrusion frequencies range from 10% in the summer of 1997 to almost 70% in the summer of 2000 (standard deviation of nearly 15%). Variations in winter in the NE-Pac are barely smaller with a minimum in intrusion frequency of 5% in the winter of 1997/98 and a maximum of more then 50% in the winter of 1999/2000. N-Atl intrusion frequencies in winter vary from 10% to 30% with one outstanding maximum of 40% in the Winter 1982/83 (Fig. 6.1a). In boreal summer intrusion frequencies typically do not exceed 10% in this region. While in the S-ATl region intrusion frequencies stay generally below 20% in summer and winter, there is one outstanding maximum of more than 40% in the boreal winter of 1982/83 (Fig. 6.1c), equal to the N-Atl time series. Fluctuations in the SE-Pac intrusion frequency in austral summer are comparable with the NE-Pac boreal winter fluctuations with a minimum of less than 5% in the winter of 1997/98 and a maximum of more than 50% in the winters of 1985/86 and 1989/90 (Fig. 6.1d).

Temporal trends in the regional intrusion numbers are examined in two ways: First, linear trend lines of all time series were computed via regression analysis (black and grey dashed lines in Fig. 6.1) and second, a Mann-Kendall test was applied to receive information about the statistical significance of these trends (for further information see Chap. 3.5): In the NH, there is a slight downward (upward) trend in intrusion occurrence in the Atlantic (Pacific) region; however, none of these tendencies are statistically significant. In both regions in the SH, the time series reveal a more pronounced downward linear trend in the number of intrusion events in winter and in summer as the NH time

series,

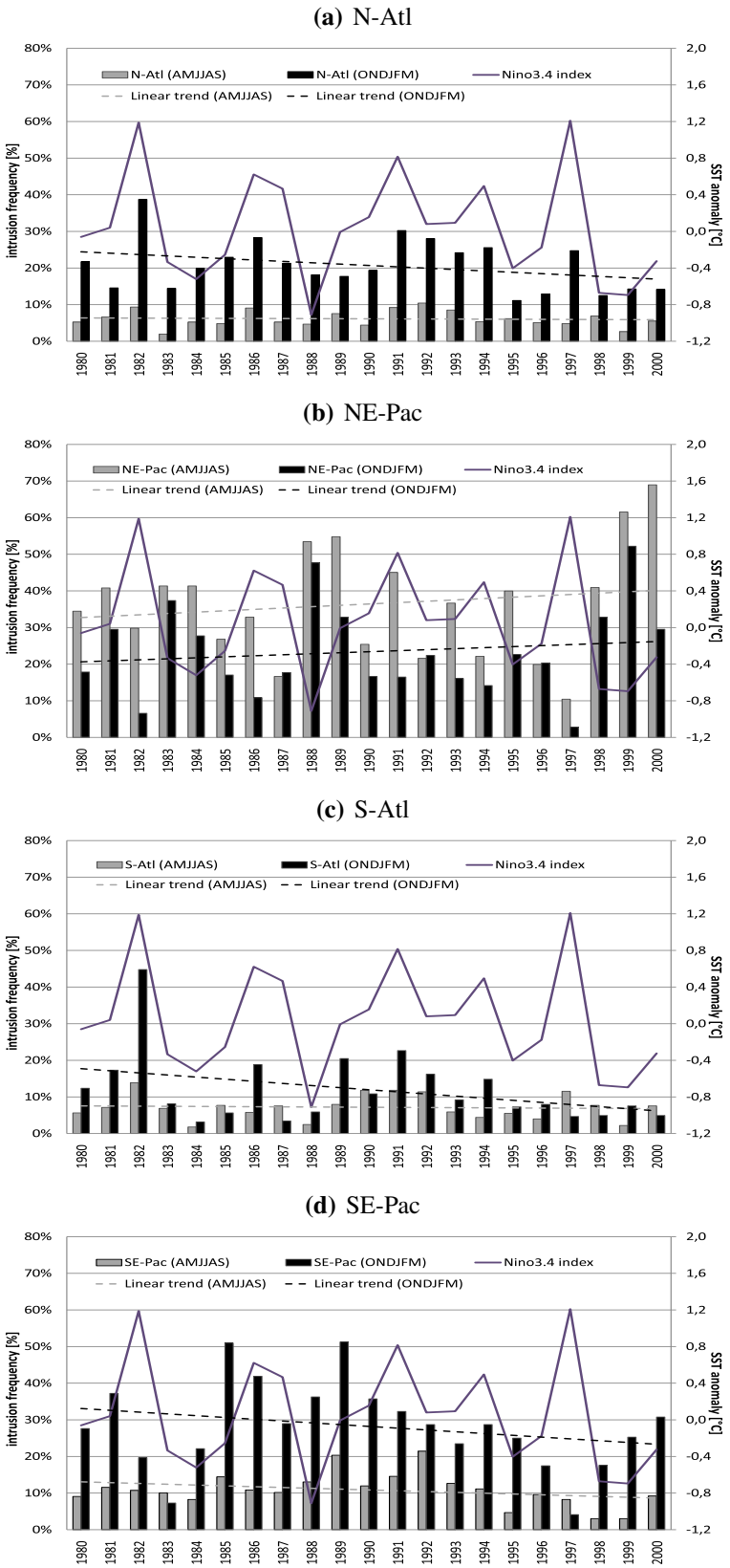

Figure 6.1: Seasonal mean intrusion frequencies in [%] for the (a) N-Atl, (b) NE-Pac, (c) S-Atl and (d) SE-Pac region. Black (grey) bars show boreal winter (summer) frequencies between 1980 and 2000/01. "1980" corresponds to the 1980/81 winter mean. Dashed black (grey) lines are the corresponding linear trend lines of the winter (summer) intrusion time series. The purple line displays the boreal winter mean of the Niño3.4 index in [°C]. Regions are defined in Fig. 4.1a.

but only regarding the SH as a whole yields a statistically significant (on a 90% level) long-term downward trend in austral summer.
Correlation coefficients, calculated from the time series of seasonal intrusion frequencies between different regions (Tab. 6.1), indicate for the N-Atl a positive relation with the S-Atl and a negative with the NE-Pac. Both correlations are statistically significant on a 99.9% level. In summer, the correlation coefficients are much smaller (results not shown). Calculations of the statistical relationship between the summer and subsequent winter intrusion frequencies within the same region (labelled with * in Tab. 6.1) point to a statistically significant positive autocorrelation in both regions of the NH. Lag correlations between boreal winter and the following summer frequencies are strongly reduced, e.g., in the N-Atl region the correlation coefficient decreases from 0.61 to 0.13 (not shown), which is due to the seasonal cycle of ENSO as described in the next section.

	N-Atl	NE-Pac	S-Atl	SE-Pac
N-Atl	**0.61***	**-0.65**	**0.69**	0.07
NE-Pac		**0.74***	-0.35	0.1
S-Atl			0.54*	0.15
SE-Pac				0.53*

Table 6.1: Correlation coefficients between the time series of winter intrusion frequencies in different regions (see Fig. 6.1) between 1980/81 and 2000/01 (21 winters). The correlation coefficients labelled with * correspond to the autocorrelation between the summer (e.g., 1980) and the subsequent winter (e.g., 1980/81) intrusion frequencies within the same region. Statistically significant (99% level) correlation coefficients are bold. Regions are defined in Fig. 4.1a.

6.1 Association with ENSO

In this section year-to-year fluctuations in intrusion occurrence are examined with respect to ENSO-related variability. For that reason in all plots of Fig. 6.1 the mean boreal winter Niño3.4 index (purple line) is additionally drawn as an indicator for the different phases (resp. "strength") of ENSO (for further information see Chap. 2.3). A comparison of the time series of intrusion frequencies with ENSO reveals, most notably in the N-Atl region, a positive and in the NE-Pac a negative relationship. Apparently, the intrusion maxima and minima often occur during exceptionally strong El Niño or La Niña years. This assumption is quantitatively confirmed by a correlation analyses, that was applied to compare the regional time series of intrusion occurrence with the two ENSO indices the Niño3.4 and the Southern Oscillation index (SOI, see Chap. 2.3). The resulting correlation coefficients are presented in Table 6.2 and point to a statistically significant relationship at the 99.9% level in three regions (N-Atl, NE-Pac and S-Atl).
Regarding first the SST-based Niño3.4 index, the strongest relationship exhibits the NE-Pac with a correlation coefficient of -0.83 implying an increase (decrease) of intrusion events during the cold (warm) phase of ENSO. According to this correlation 70% of

winter-to-winter variance in intrusion occurrence in the NE-Pac region is controlled by ENSO. In the whole Atlantic the relationship is of opposite sign with positive correlation coefficients of 0.77 in the N-Atl and of 0.59 in the S-Atl pointing to more intrusion events during El Niño winters (warmer SSTs in the equatorial Central Pacific).
The correlation coefficients, calculated with the atmosphere-based SO index, exhibit a slightly stronger relationship in all regions (except for the SE-Pac). The calculations for the N-Atl region show highest correlation at all between intrusion activity and ENSO with a negative correlation coefficient of -0.86, which is unexpectedly large considering the great distance between the two centres of action (equatorial Central Pacific <-> tropical Northeast Atlantic). Furthermore, this correlation implies that in the N-Atl region nearly 74% of year-to-year fluctuations in intrusion activity is controlled by the SO activity.
In contrast, in the SE-Pac region an association with ENSO is barely detectable. Correlations in summer are generally strongly reduced in both hemispheres (see Table A.1 in the Appendix).
The great percentage of variance that explained by ENSO in the N-Atl, S-Atl and NE-Pac regions in boreal winter is assumed to be the main reason for the correlations between the regional intrusion time series presented in Tab. 6.1. The seasonal cycle of ENSO (starting in spring with a peak at the end of the year) provides an explanation for the significant autocorrelations between the summer and subsequent winter intrusion frequencies especially in the Northern Hemisphere. It also explains why correlations are strongly reduced comparing the winter and subsequent summer frequencies in this region.
As a next step these results are compared with the grid point-based differences in intrusion frequencies between the two phases of ENSO (El Niño minus La Niña) in Fig. 6.2. Note that due to the very small sample size (6 El Niño and 5 La Niña winter) no significance test was carried out for these calculations. The corresponding mean intrusion climatologies of the 6 El Niño and of the 5 La Niña winter are plotted in Fig. A.2 in the Appendix. Similar to the results above, Fig. 6.2 reveals higher intrusion frequencies over the North and South Atlantic and lower frequencies over the Northeast Pacific during El Niño winter. In the Southeast Pacific, Fig. 6.2 exhibits an eastward shift of the main region of intrusion occurrence during El Niño winter (although, as mentioned above, the absolute numbers do not seem to depend on ENSO). The SPCZ shows a similar shift to

	N-Atl	NE-Pac	S-Atl	SE-Pac
Niño3.4	**0.77**	**-0.83**	**0.59**	-0.12
SOI	**-0.86**	**0.78**	**-0.7**	0.12

Table 6.2: Correlation coefficients between regional intrusion frequencies (cp. Fig. 6.1) and the ENSO indices Niño3.4 and SOI for boreal winter seasons from 1980/81 until 2000/01 (21 winters). Statistically significant (99% level) correlation coefficients are bold. Regions are defined in Fig. 4.1a.

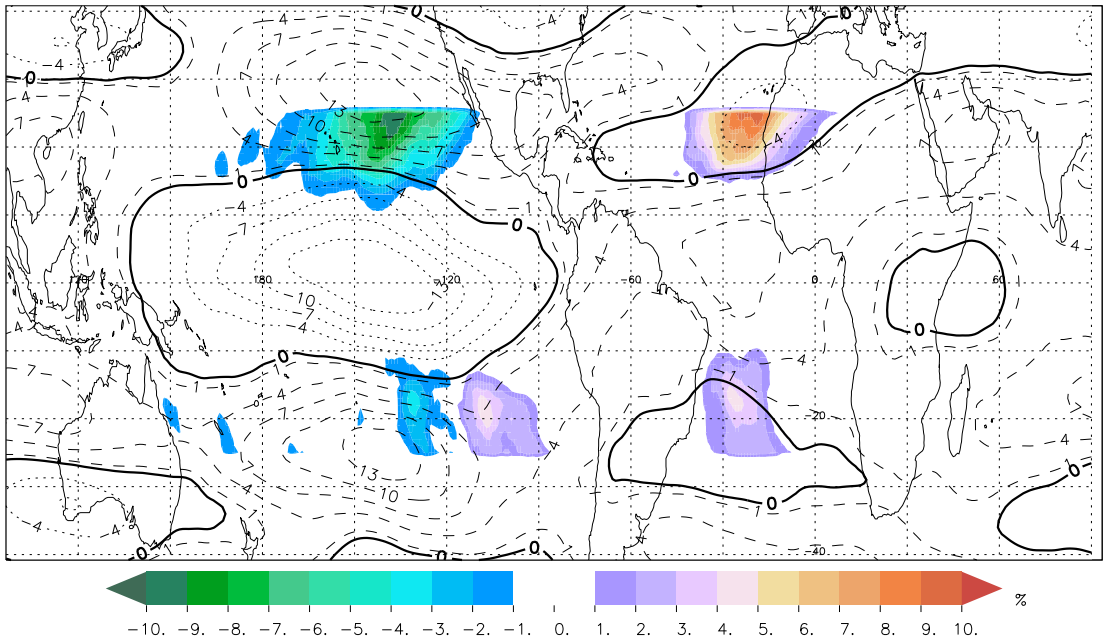

Figure 6.2: Differences in the mean intrusion frequency [%, percentage points] (shaded) and in the mean zonal wind at 200 hPa [m/s] between El Niño minus La Niña winter from 1980 until 2001. For ENSO winter classification see Sec. 2.1.

the east in the warm phase of ENSO (Vincent 1994)
In Fig. 6.3 the mean numbers of intrusion episodes and life times are presented for the two different ENSO winter phases (no test of significance). This diagram reveals, that the life time of the intrusion episodes is affected by ENSO as well. In both Atlantic and in the NE-Pac regions changes in intrusion episode numbers are accompanied with equal-signed changes in the mean intrusion life times. This relationship is contrary in the SE-Pac, where slightly less (more) intrusion episodes with longer (shorter) life times are detected during El Niño (La Niña) although the seasonal intrusion frequencies were not significantly correlated with ENSO. An other interesting point in Fig. 6.3 is that in the NE-Pac the number of intrusion episodes during La Niña winters is on average more than twice as high as during El Niño winter (with even longer life times).

Discussion

The influence of ENSO on the equatorward propagation of extratropical disturbances in the central and eastern North Pacific has been linked consistently in several studies to ENSO-related variations (i) in the extension of the „westerly duct“ over the equatorial Pacific and (ii) in the strength and longitudinal extent of the North Pacific jet stream (e.g., Held et al. 1989, Ambrizzi et al. 1995, Matthews and Kiladis 1999a, Waugh and Polvani 2000, Abatzoglou and Magnusdottir 2006b). During the warm phase of ENSO (El Niño) the region of high SSTs and related deep convective activity in the western equatorial Pacific is shifted eastward to the central and eastern Pacific. This leads to a

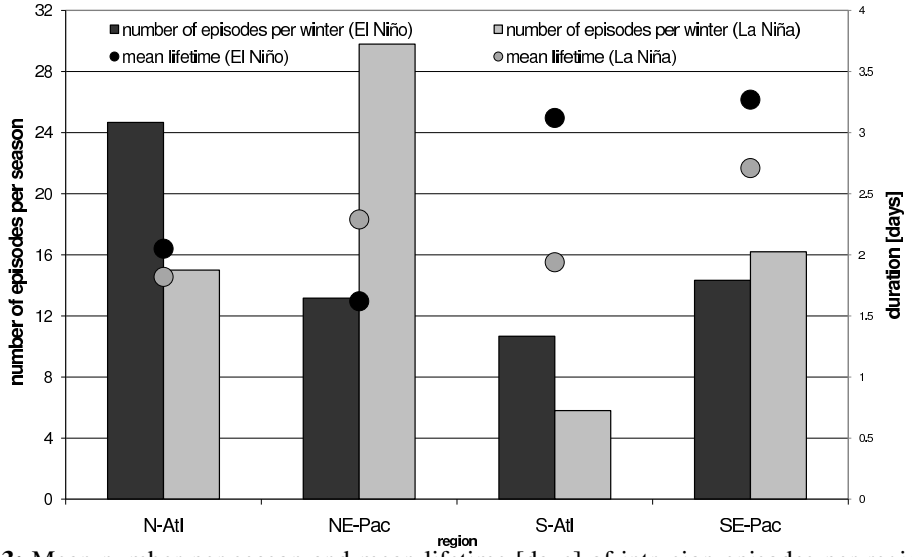

Figure 6.3: Mean number per season and mean lifetime [days] of intrusion episodes per region for NH winter (black) and summer (grey) during the period 1980 – 2001. Regions are defined in Fig. 4.1a.

change in the seasonal mean atmospheric circulation pattern, with a weakening of the upper-tropospheric mean „westerly duct“ over the tropical eastern Pacific and an equatorward shift and eastward extension of the Pacific jet stream across the central North Pacific (see differences in the mean 200 hPa wind field in Fig. 6.2). In this situation the extended subtropical jet stream acts as an near-continuous wave guide, which along wave activity preferentially propagates across the whole northern Pacific. Together with the weakening of the „westerly duct”, this finally leads to a reduction of equatorward propagation of transient disturbances over the north-eastern tropical Pacific and is in agreement with the findings of the present study (see Table 6.2 and Fig. 6.2). During the cold phase of ENSO, La Niña, the situation over the North Pacific is reversed and causes more frequent intrusions into the tropical upper troposphere over the Northeast Pacific.
Similar ENSO-related variations (but with opposite sign) are observed in the mean zonal upper wind field over the North Atlantic-European sector are observed (e.g., May and Bengtsson 1998, Brönnimann 2007, Li and Lau 2011). During El Niño these variations are characterized by (i) a reduction and equatorward shift of the subtropical jet stream over the North Atlantic and (ii) an extension of the Atlantic westerly duct (see also Fig. 6.2). Both effects support a development of disturbances at low latitudes in consistence with our observations. During La Niña the change in the mean circulation, causes less intrusions over the tropical Atlantic.
The increasing evidence that ENSO induces symmetric anomalies in the subtropical flow of both hemispheres (e.g., Arkin 1982, Seager et al. 2003, L'Heureux and Thompson 2006) implies similar changes in the mean upper wind field over the subtropical South Atlantic as in the N-Atl region (see Fig. 6.2) and explains at least partly the inter-annual variations in relation to ENSO in the S-Atl. However, in the SE-Pac ENSO-related variations are quite different to the NE-Pac region, which is assumed to be related to changes in the South Pacific subtropical jet stream and to the shift of the SPCZ.

Although ENSO-induced changes in the mean upper wind field qualitatively explain the alterations in the intrusion frequencies, it can be assumed that other parameters such as additional additional Rossby wave sources and latent heating upstream or blockings downstream, might play an important role in modulating PV intrusion development (see next chapter). Such relationships are not well established yet and need further investigations.

For the sake of completeness, correlations between intrusion frequencies and other climate state indices such as NAO, PNA and AMM were calculated on the same inter-annual time scale (see Table A.1 in the Appendix). The strongest statistically significant correlations of 0.67 yields the correlation between the Atlantic Meridional Mode SST index and N-Atl intrusion numbers. None of the calculations with the NAO and PNA indices yield a significant correlation coefficient, which is assumed to be due to the rather sub-monthly to synoptic time scale of these phenomena. However, a correlation of 0.4 is found between the winter mean of the NAO index and intrusion frequencies in the N-Atl region. In the next chapter it is described how the occurrence of intrusions affects the NAO index.

7 Composited evolution of PV intrusions

With a view on the physical processes leading to the genesis of PV intrusions, composite analysis (see Chap. 3.4) of the vertical averaged PV (VAPV) before, during and after the existence of an intrusion system are investigated and described in this chapter. The analysis is based on the most vertically extended intrusion episodes with PV values higher than 1.5 PVU below 350 hPa south of 25°N at least once during its lifetime (see for definition of vertical depth Chap. 3.1). These disturbances exhibit the strongest signal in the upper PV field. This fact becomes obvious with the help of Fig. A.3 in the Appendix, which shows composites of VAPV anomalies based on intrusion episodes in the N-Atl with different vertical extensions. In summary, Fig. A.3 illustrates that the anomalies in the VAPV field increase with the vertical extent of the intrusions, although the shape, tilt and extension of the PV streamer demonstrate only minor differences. Similar results are achieved analysing disturbances in other regions and/or in association with other meteorological parameters (i.e. SLP, wind, water vapour flux).
In the following intrusion development is analysed separately for the four main intrusion activity regions. Note that the regional VAPV composites are based on the respective hemispheric winter intrusion systems.

North Atlantic

In the first subsection the evolution of PV intrusions into the tropical North Atlantic during boreal winter is investigated on the basis of Fig. 7.1, which shows composite maps of the VAPV anomalies from 5 days before until 3 days after intrusion occurrence and the corresponding anomalous wind vectors at 200 hPa. Already five days ahead (see Fig. 7.1a) of the first intrusion detection, significant PV structures, which remain and even intensify in the following days, can be distinguished in large parts of the NH. Relative to the reference longitude of 0° (position of later intrusion system) we find

- a PV anomaly structure (A) between 150° and 60° W in the storm track region representing a Rossby wave train over the north-eastern Pacific and western North America,
- positive PV anomalies (B) to the Northwest corresponding to a large PV reservoir,
- a negative PV anomaly (C) to the Northeast which might reflect a blocking situation over Europe and
- a small positive anomaly (D) at lower latitudes close to where the streamer is detected four days later.

Note that the "real" geographical position of the PV structures mentioned above is roughly derived from the location of the frequency maximum in the North Atlantic in Fig. 4.1a. The interpretation of atmospheric blocking as a negative PV anomaly in the upper troposphere that is persistent over a certain time period (e.g. 5-day period) is a common method previously applied in e.g. a study of Schwierz et al. (2004). However, due to the lack of sufficient information about the persistence of the negative PV anomaly over Europe, we can only speculate that this PV ridge represents a blocking event.
From day -5 to -3 (see Fig. 7.1b) the Rossby wave train (A) intensifies and moves eastward, while the PV anomaly dipole (B+C) over the North Atlantic and over Europe remains quite stationary. The positive PV anomaly D shows only minor changes except for a slight spatial extension. Another negative PV anomaly (E) forms to the Southeast of the approaching Rossby wave train, that explosively amplifies in the following days and corresponds to a amplified ridge over the North Atlantic mid latitudes. In former studies (e.g., Massacand et al. 2001; Knippertz and Martin 2007b) it was argued that the rapid ridge amplification and breaking over the North Atlantic can be forced by local diabatic upper PV reduction and plays an important role for the subsequent streamer formation farther east.
On day -1 (Fig. 7.1c) the negative PV anomaly E is well developed. It is assumed that E helps to advect air with high PV values from the PV reservoir B toward low latitudes, which causes a quick intensification of the PV anomaly D. Related to this anomaly D the mean PV field reveals a streamer like structure for the first time. The Rossby wave train A together with the PV anomalies E and D now forms a pronounced wave train that reaches from North America to the eastern tropical Atlantic. This wave train is northwest-southeast orientated with positively (i.e. southwest-northeast) tilted waves, which indicates equatorward energy dispersion and poleward westerly momentum flux. A similar wave train in association with convective anomalies over the eastern tropical North Atlantic was found by Kiladis and Weickmann (1997, their Fig. 6c). The upper wind field exhibits at this day strong anomalies confined to the PV anomalies E and D. The wind vectors show the typical PV-induced anomalous anticyclonic (cyclonic) circulation around the negative (positive) PV anomaly structure, which will remain until day 0.

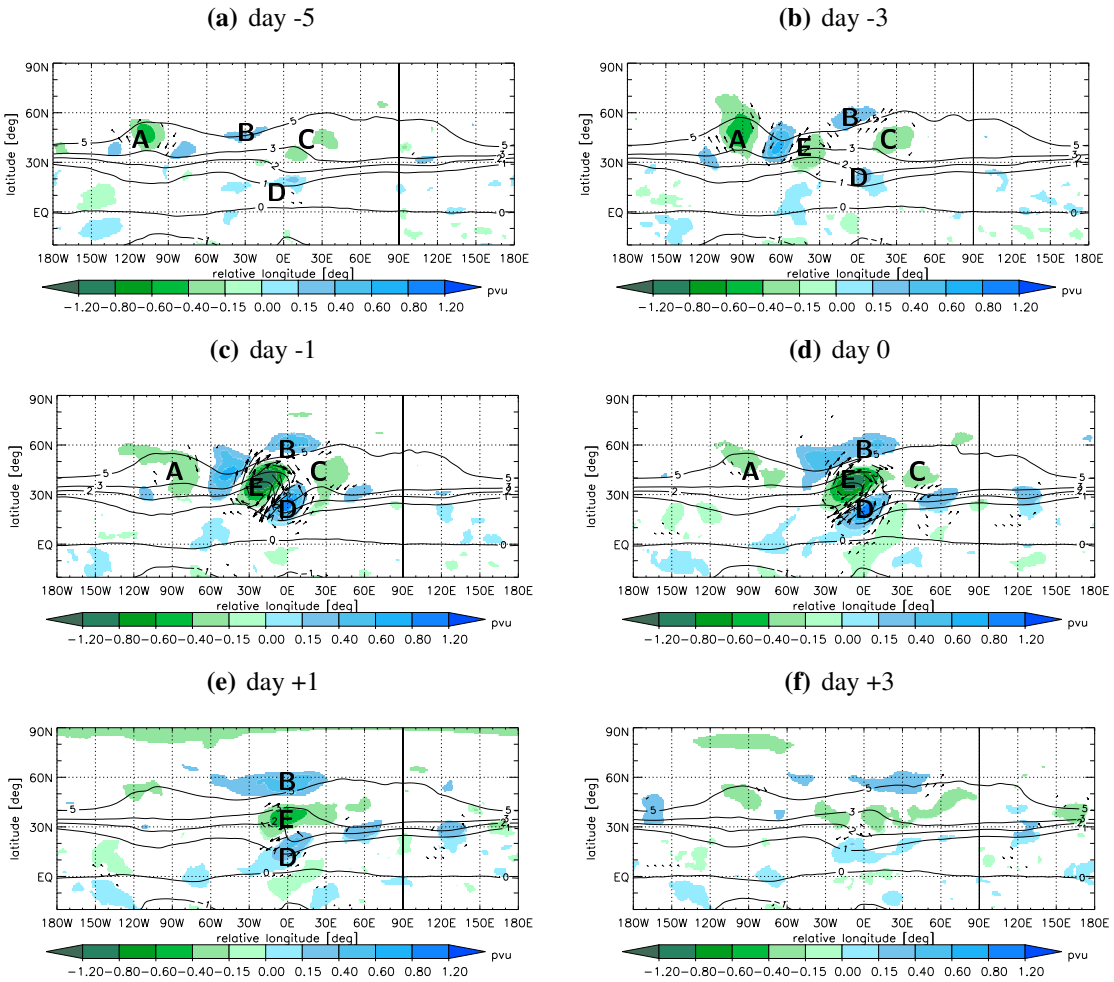

Figure 7.1: Composite of statistically significant (95% level) VAPV anomalies (shaded) and VAPV values (lines) [PVU] averaged for (a) five days, (b) three days, (c) one day before, (d) during (e) one day and (f) three days after the occurence of intense intrusion episodes in the N-Atl region from October to March between 1980-2001 (#102). For definitions of regions see Fig. 4.1a.

On day 0 (Fig. 7.1d) the Rossby wave train over the Northern Atlantic is nearly north-south orientated, which leads to a reversal of the meridional PV gradient similar to the common definition of Rossby wave breaking (RWB) events in e.g. Abatzoglou and Magnusdottir (2006a, their Fig. 2). The PV anomaly signal south of the intrusion suggests wave dispersion across the equator into the Southern Hemisphere, in consistence with results of Webster and Holton (1982). The PV structures east of the PV intrusion indicate that another small portion of wave energy is proceeding eastward over Europe along the subtropical jet stream (Hoskins and Ambrizzi 1993).

The corresponding composite of anomalies in sea level pressure (SLP) at day 0 in Fig. 7.2b is dominated by a dipole structure similar to the North Atlantic Oscillation pattern (in association with the upper PV anomaly dipole B+E). Hence, it indicates that the lower troposphere is also influenced by this kind of intrusions over the N-Atl, although the SLP field directly underneath the intrusion system exhibits no significant anomalies. At day +1 after the intrusion (see Fig. 7.1e) the VAPV anomaly field displays a meridional aligned tripole structure in the NH. The northern two centres reflect again a positive

NAO phase as described in previous studies (i.e. Benedict et al. 2004, Abatzoglou and Magnusdottir 2006a, Woollings et al. 2008, Strong and Magnusdottir 2008). The investigation of Benedict et al. (2004) for example suggests that anticyclonic wave breaking over North America and the North Atlantic is essential for the growth and maintenance of the positive NAO phase. A composite of the daily mean NAO index (see Chap. 2.3) in association with intense intrusion systems in the N-Atl region in Fig. 7.2a supports this hypothesis: From six days prior until intrusion appearance, the NAO index increases quickly and nearly linearly. Thereafter the NAO index decreases much slower and remains above 0.4 until day 5 after the intrusion. Statistically significant (on 95% sign. level) indices are noted from one day before until five days after the intrusion occurrence. The behaviour of the NAO index in Fig. 7.2a is similar (but not equal) to the findings of Abatzoglou and Magnusdottir (2006a, their Fig. 7), who analysed the NAO index in connection with different kinds of Rossby wave breaking (RWB) events.
Three days after the intrusion, the tripole pattern, although weakened, is still present in the VAPV anomaly field (Fig. 7.1f) in accordance with the NAO index at this day in Fig. 7.2a.

(a) daily NAO index

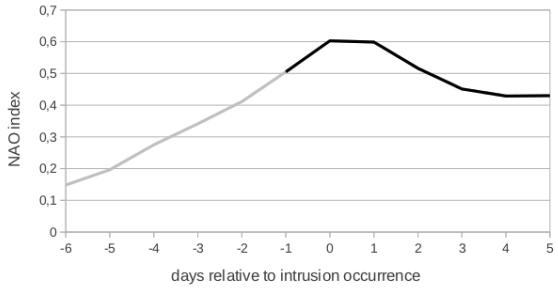

(b) SLP at day 0

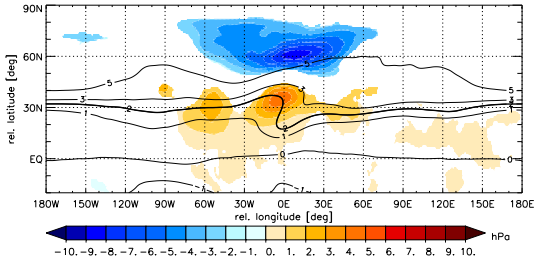

Figure 7.2: (a) Composite lead-lag daily mean NAO index for the most intense intrusions in the tropical North Atlantic. Black lines highlight the statistical significant (95% level) NAO indices. (b) Composite of statistically significant (95% level) SLP anomalies (shaded) [hPa] and VAPV values (lines) [PVU] averaged during the occurrence of most intense intrusion episodes in the N-Atl region between 1980–2001 from Oct. to March (#102).

Northeast Pacific

In this subsection the development of PV intrusions that propagate into the tropical Northeastern Pacific region is analysed. The main features in the VAPV composite five days prior to the first intrusion detection (see Fig. 7.3a) are a PV anomaly formation (A) located between 180° and 90°W corresponding to a northwest-southeast orientated Rossby wave train, which stretches from eastern Europe to Western Asia, and a positive PV anomaly (B) at 30°W, from which eventually the intrusion system will emerge.
From day -5 to -3 (Fig. 7.3b) the Rossby wave train A intensifies and propagates eastward while at its eastern end a new negative PV anomaly (C) appears. The anomaly B is slightly amplified and south-eastward shifted. At its north-eastern flank another

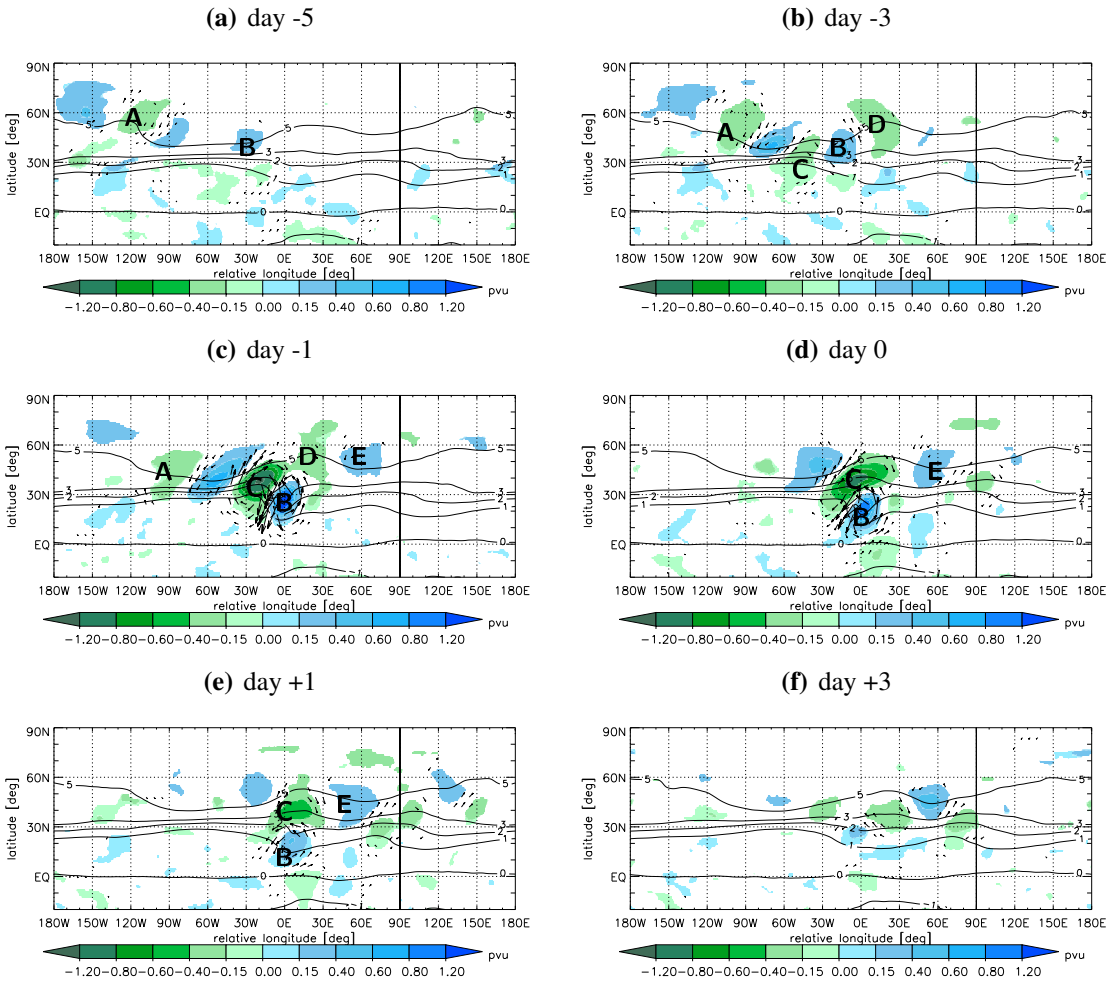

Figure 7.3: As in Fig. 7.1 except for intrusion episodes in the NE-Pac region (#148).

negative PV anomaly (D) develops, that might indicate a blocking situation over North-west America. All PV structures together form a continuous wave train, which gets reflected at 30° W on the latitude with maximum meridional PV gradients (resp. on the jet stream).

From day -3 to -1 (see Fig. 7.3c) the PV structures B and C become more pronounced. While C moves slightly to the Northeast and develops a northeast-southwest tilt, B extents to the Southeast. During the intrusion development the PV anomalies B and C seem to move anticyclonically around each other, while the dipole as a whole propagates slowly eastward. At day -1 another positive PV anomaly (E) forms east of the potential blocking over north-western America (D), possibly corresponding to a lee trough of the Rocky Mountains (i.e., Steenburgh and Mass 1994). This PV anomaly is quite persistent; even four days later it is similarly shaped detectable at the same position (Fig. 7.3f). It is related to anomalously low surface pressure, as seen in the SLP anomaly composite in Fig. 7.4.

From day -1 to day 0 (Fig. 7.3d) the PV anomaly B exhibits a streamer-like shape with a very slight positive tilt and expands further to the South into the tropical Northeast Pacific. The PV anomaly signal south of the intrusion suggests wave dispersion across the

equator into the SH similar to the results of Kiladis and Weickmann (1992b, their Figs. 2 and 7). The SLP composite at day 0 in Fig. 7.4 shows a pressure dipole in association with the anomalies C and the most eastern positive PV anomaly of the wave train A. In contrast to the N-Atl intrusions, this dipole is more northwest-southeast orientated. Also in contrast to the N-Atl, the SLP field directly underneath the intrusion systems in the NE-Pac reveals a negative anomaly, pointing to lower surface pressure as usual. This observation is in agreement with investigations by the author, focusing on the occurrence of cyclones in relationship with intrusion systems, based on a climatology of Wernli and Schwierz (2006). These investigations display an increase in cyclone frequency below the top of the PV streamer over the Northeast Pacific (not shown).

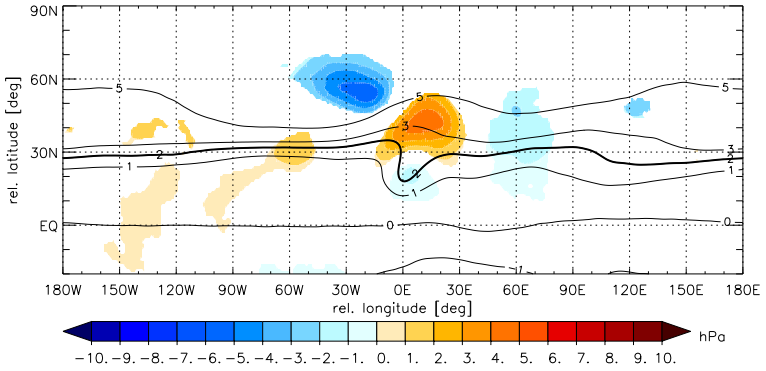

Figure 7.4: As in Fig. 7.2b except for intrusion episodes in the NE-Pac region (#148).

South Atlantic and Southeast Pacific

In this subsection the development of intrusion systems in the S-Atl and SE-Pac are described together due to the similarities in both regions. Already three days prior to the intrusion detection (Figs. 7.5a and b) a pronounced negative PV anomaly (A) is observed at low latitudes and near the reference longitude, which is eventually going to form the intrusion system. East of this anomaly a pronounced Rossby wave train (B) occurs quite similar in both regions, even though B develops for the S-Atl intrusions and over the Southern Pacific for SE-Pac intrusions. This PV structure is detection apparent in the SH mid latitudes between 30° and 120°W already five days prior to intrusion (not shown). This Rossby wave train includes a strong positive PV anomaly at its eastern end pointing to a pronounced ridge directly upstream of the later PV intrusion, similar to the observations in the North Atlantic and Pacific.
From day -3 to day 0 (see Figs. 7.5c and d) parts of the Rossby wave train B and the negative PV anomaly A intensify and propagate eastward. The resultant wave train (B and A) is northwest-southeast orientated and negatively tilted, indicating equatorward wave dispersion and a southward momentum fluxes. Another distinct positive PV anomaly (C) forms to the Southeast of the identified streamer, indicating cross equatorial wave dispersion along a great circle (e.g., Hoskins and Karoly 1981). At day +1 (see Fig. 7.5e and f) the Rossby wave train B degenerates, while the PV streamer is still apparent in

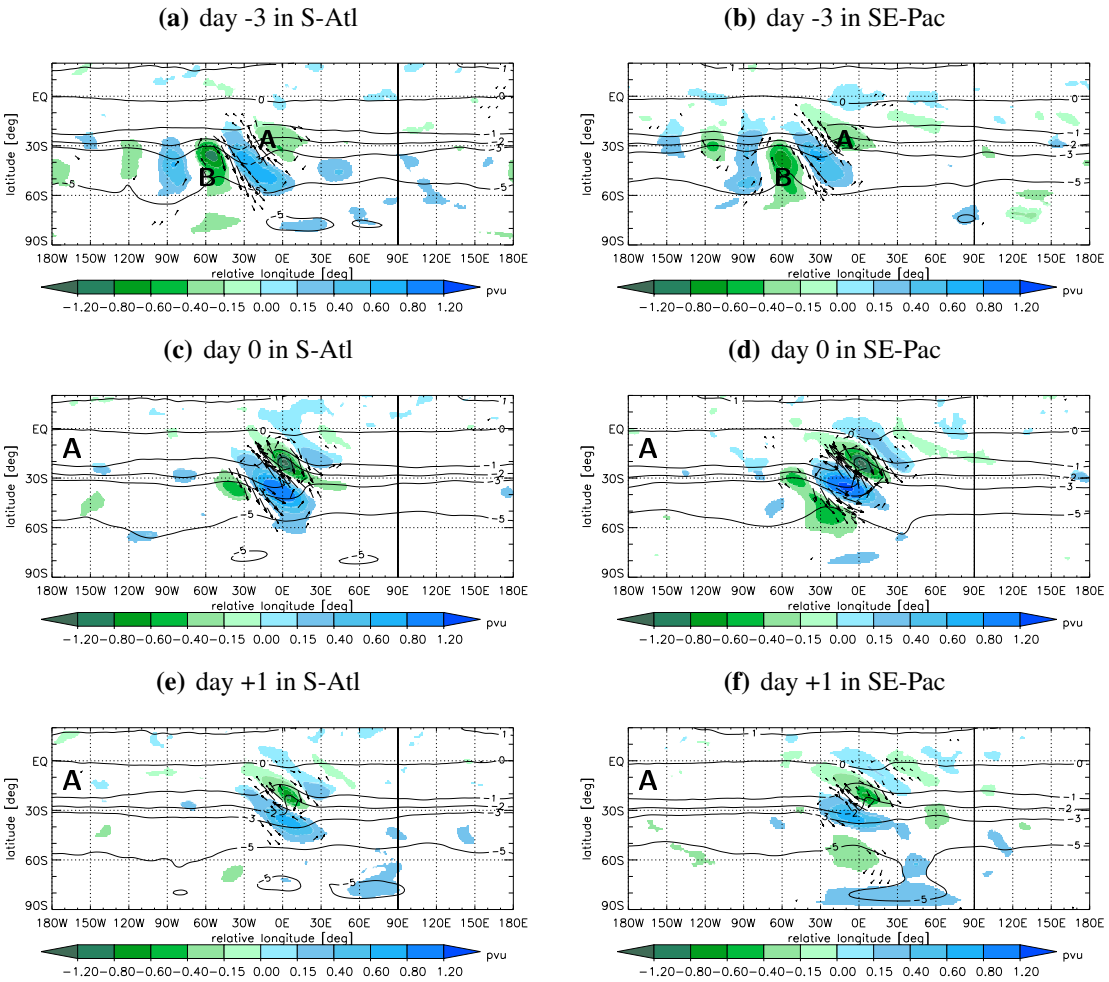

Figure 7.5: As in Fig. 7.1 except for intrusion episodes during austral winter in the SE-Pac and S-Atl regions (#81 and #60). Composites from three days before (a) & (b), during (c) & (d) and one day after (e) & (f) are presented.

the VAPV field.

Discussion

In this subsection the main similarities and differences between the different regions in the VAPV anomaly field associated with intrusion development are summarized and possible physical processes, which may lead to intrusion development, are briefly discussed. In all regions the upper circulation five days before intrusion detection shows in all region an eastward propagating Rossby wave train located between 30° and 180°W (relative to the reference longitude) in the extratropics (depending on the region of investigation), which is largely in agreement with results of several previous studies (e.g., Liebmann and Hartmann 1984, Kiladis and Weickmann 1992b, Tomas and Webster 1994, Slingo 1998). While this wave train approaches the reference longitude of 0° in the following days, it intensifies, turns equatorward and end a negative (positive) and a positive (negative) PV anomaly form in the NH (SH) at its eastern. Both PV anomalies rapidly

intensify, develop a positive (negative) tilt in the NH (SH) and move further equatorward into the Tropics where the positive (negative) PV anomaly in the NH (SH) forms the PV streamer at day 0. In all regions a small initial disturbance in the upper PV field is noticeable already five days ahead of detection, from which the later intrusion system emerges.
However, there are a few striking, primarily inter-hemispheric differences in intrusion development: For example the observed wave train (especially at day +1) is in both regions of the NH almost north-south orientated but rather southwest-northeast orientated in the SH regions. Further differences mainly arise downstream of the PV streamer: While in the SH most of the wave dispersion proceeds across the equator, in the NH a portion of the wave energy disperses to the east, along the region with maximum meridional PV gradients. The negative PV anomaly detected to the Northeast of the reference longitude in the N-Atl and NE-Pac regions, which might correspond to blocking situations, is not found in the SH regions.

With the help of composite analysis the typical evolution upstream of a PV intrusion was described. However this analysis to separate the influence of single factors in a fully non-linear context which are ultimately responsible for the development of intense PV intrusions into the Tropics. For that purpose Meier and Knippertz (2009) simulated a case study of a very pronounced PV intrusion over the tropical Northeastern Atlantic in January 2002 using the global model of the German Weather Service. Several sensitivity experiments were conducted by eliminating single PV features via PV inversion technique for balanced initial conditions. The results of their studies indicate that a PV ridge over Europe (C) followed by a reservoir of high PV over the North Atlantic (B) are most important for the intrusion formation. A combination of the statistical and sensitivity studies points to a high relevance of the PV dipole over the North Atlantic and Europe out to five days ahead of the event. These findings indicate a relatively high predictability of PV intrusions. In additional experiments Meier and Knippertz (2009) showed with suppressed latent heating over the North Atlantic that diabatic PV reduction east of the Rossby wave train have smaller impacts contrary to former expectations of Massacand et al. (2001) and Knippertz and Martin (2007b)).
However, these results can not be directly applied to intrusion development in the other regions due to the absence of the relevant PV features such as the PV reservoir to the Northwest and the PV ridge to the Northeast of the PV streamer. Therefore further numerical studies are needed to extract the main processes that are responsible for wave amplification in these regions.

8 Impact on moisture transport

In this chapter moisture flux anomalies in relation to intrusion occurrence are assessed via composite analysis as described in Chap. 3.4. Due to the fact that the moisture content in the atmosphere decreases with height and from the equator to the pole only the most intense intrusion episodes are considered for the construction of these composite (cf. Chap. 3.1 and 5.2), as their circulation presumably reaches deep enough in the troposphere and far enough equatorward to benefit from the tropical moisture reservoir (cf. Knippertz 2007). Significant (95% level) moisture flux anomalies (meridional component is shaded) in relation to intrusion occurrence in the selected regions during the respective winter season are depicted in Figs. 8.1 and 8.2 averaged over two vertical layers in the lower (between 1000 and 800 hPa) and middle (between 750 and 500 hPa) troposphere. The meridional (zonal) moisture flux is the product of the meridional (zonal) wind and the specific humidity and anomalies are calculated from the long-term monthly mean moisture flux. The climatological upper PV trough, centred at the reference longitude of 0°, is indicated by the 2 PVU-contour of the mean vertically (between 400 and 100 hPa) averaged PV field (black bold line).

The moisture flux anomalies between 750 and 500 hPa in relation to N-Atl intrusion systems (Fig. 8.1a) display a positive anomaly close to the eastern flank of the PV trough between the equator and about 30°N that points to a transport of water vapour out of the Tropics into the Subtropics. Below the western flank of the trough a negative anomaly suggests a southward transport of dry air into the Tropics. Further to the West a similar west-east dipole of positive and negative moisture flux anomalies forms in relation to the trough that has developed further upstream over the North Atlantic. This trough is clearly seen in the corresponding composite of upper circulation anomalies, depicted in Fig. 7.1d, as a positive anomaly to the Northeast of the detected intrusion.

The signal in the moisture flux anomalies induced by upper PV troughs is similar in all regions and both vertical layers. The anomalies are generally stronger pronounced in the

(a) N-Atl: 750 to 500 hPa

(b) NE-Pac: 750 to 500 hPa

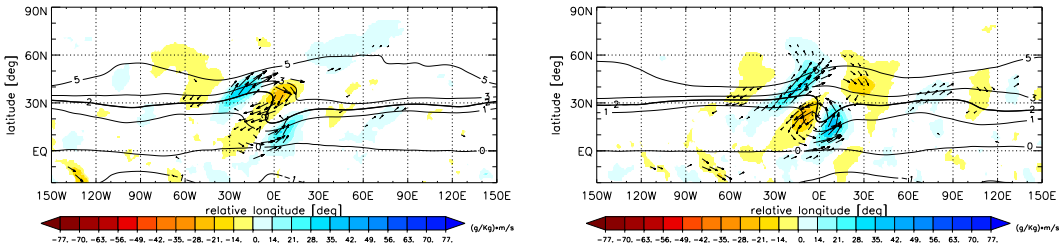

(c) N-Atl: 1000 to 800 hPa

(d) NE-Pac:750 to 500 hPa

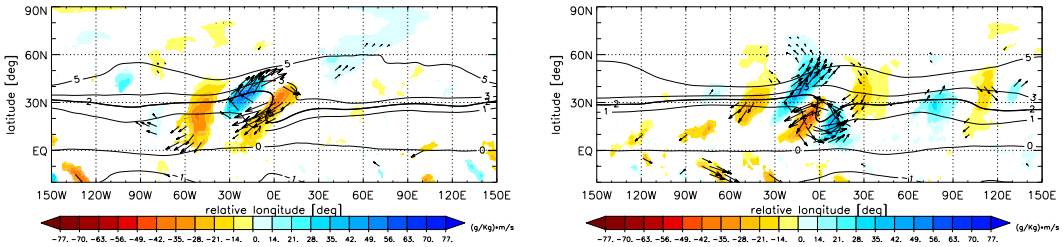

Figure 8.1: Composite of statistically significant (95% level) meridional moisture flux anomalies (shaded) [(g/kg)*(m/s)] and significant moisture flux anomalies as vectors averaged during the occurence of most intense intrusion episodes in the N-Atl region between 1980-2001 from October to March (#102). VAPV mean values [PVU] are drawn as lines. For definitions of regions see Fig. 4.1

lower troposphere due to the highest content of water vapour in this layer. One exception is found ahead of the N-Atl intrusions (see Fig. 8.1c), where in the lower troposphere the poleward transport is negligible. These findings are assumed to be due to the geographical position of the majority of the N-Atl troughs, whose eastern flank is often located over the African continent, where evaporation is small. For NE-Pac intrusions another negative moisture flux anomaly to the northeast of the PV streamer forms (Fig. 8.1d) that is related to the lee trough of the Rock Mountain as seen in the corresponding composite of the SLP anomalies in Fig. 7.4.

Moisture flux anomalies in relation to intrusion systems in the SH during austral winter are similarly structured (see Fig. 8.2). In the SH negative anomalies of the meridional moisture flux point to a poleward (southward) transport of moisture out of the Tropics into the southern Subtropics as seen ahead of the trough in Fig. 8.2c and d. Similar to the N-Atl intrusions, this signal is in both SH regions only minor in the lower troposphere which might be also due to the geographical conditions in the vicinity of the PV streamer. However, the poleward moisture transport in relation to the trough further upstream is more pronounced in both SH regions compared to NH intrusions. According to their geographical location they can be related to the precipitation and cloud bands of the SPCZ/SPAZ (Kodama 1992,1993). A negative moisture flux anomaly, which appears about 60° East of the S-Atl intrusions, is related to an area of low surface pressure over Southern Africa (see Fig. A.4 in the Appendix) and coincides with the “Rainfall area” over south-eastern Africa (Kodama 1993).

(a) S-Atl: 750 to 500 hPa

(b) SE-Pac: 750 to 500 hPa

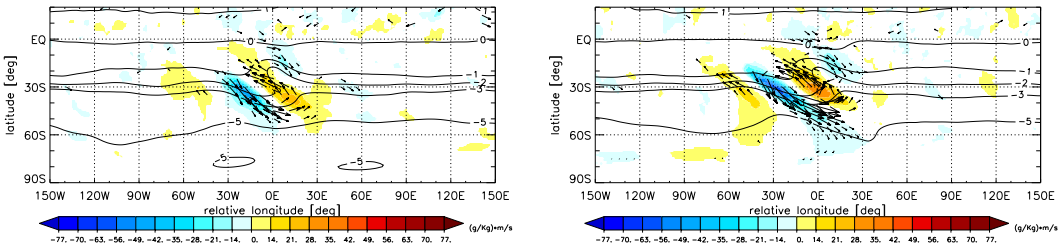

(c) S-Atl: 1000 to 800 hPa

(d) SE-Pac:750 to 500 hPa

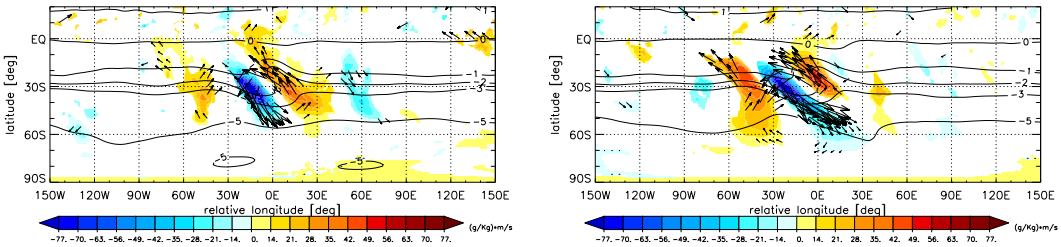

Figure 8.2: As in Fig. 8.1 except for intrusion episodes during austral winter (April to Sept.) in the SE-Pac and S-Atl region (#81 and #60) and an **inverted colorbar**.

In both layers and all regions, the moisture flux anomalies observed west of the positive anomaly ahead of the trough are found to be more strongly developed from one to three days prior to intrusion detection (for N-Atl intrusions see Fig. A.5 in the Appendix), which is in accordance with the circulation anomalies in the upper troposphere presented by composites of the PV anomalies (for N-Atl intrusions see Fig. 7.1). In the N-Atl region even 5 days ahead of the event a significant positive signal in the moisture flux is found, which remains nearly stationary until day 0 and is related to the Rossby wave train (A) over the north-eastern Pacific in Fig. 7.1a. In the NE-Pac a positive anomaly occurs already five days ahead of intrusion detection (not shown) in relation to the positive PV anomaly B (see Fig. 7.3a) which later forms the intrusion system.
Finally, Fig. 8.3 demonstrates exemplary for the NE-pac region that the strength of the signal in the moisture flux anomalies increases for PV intrusions of large vertical extension. This supports the argument of Knippertz (2007) that only disturbances that reach deep enough in the troposphere can initiate considerable poleward water vapor flux.

Discussion

The results in this chapter are in accordance with several former studies relating the occurrence of low-latitude troughs with poleward moisture fluxes ahead of these disturbances (e.g., Bates et al. 2001, Fink and Knippertz 2003, Waugh 2005, Ryoo et al. 2008, Knippertz and Fink 2009, Knippertz and Wernli 2010 and see Sec. 1.2.4). A poleward transport of water vapour in this region is in contrast to the mean equatorward transport of atmospheric water vapour within the Hadley cell (Peixoto and Oort 1992). These narrow (esp. in individual case studies) bands of moisture fluxes out of

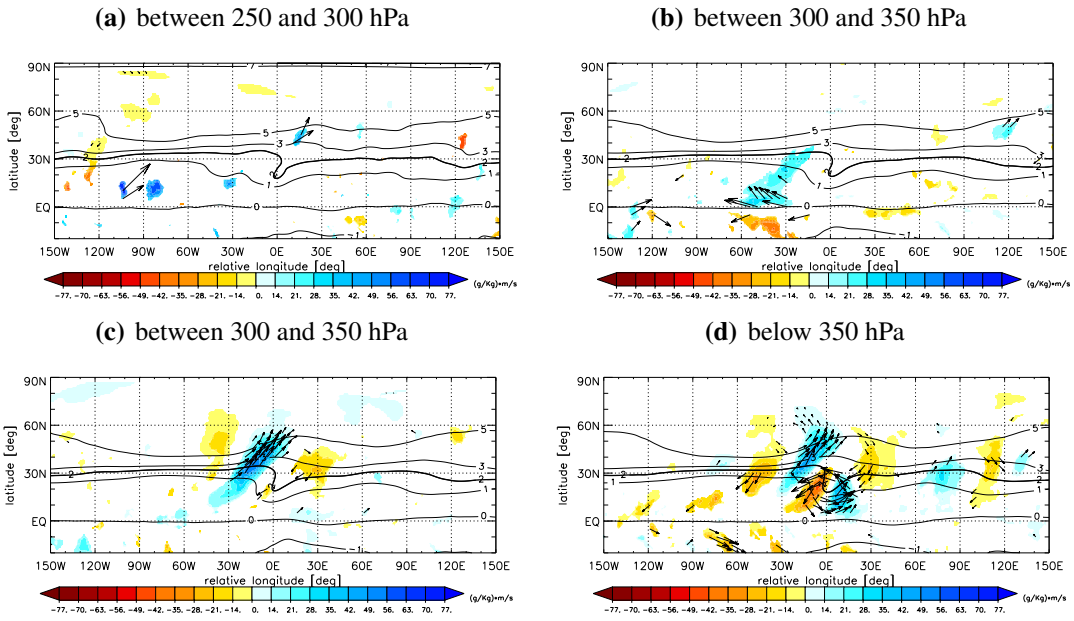

Figure 8.3: As in Fig. 8.1 except for NE-Pac intrusion episodes with the lowest vertical level (lowest level of 1.5PVU-surface within the intrusion system) between (a) 200 and 250 hPa (b) 250 and 300 hPa (c) 300 and 350 hPa and (d) below 350 hPa.

the Tropics are reminiscent of the conceptual model of the "warm conveyer belt" (e.g. Browning 1990). However, in contrast to this concept the situations discussed here are not characterized by a sharp thermal front and moist air in these bands is preferentially transported in a quasi-horizontal direction. Therefore, Bao et al. (2006) and Knippertz and Martin (2007a) termed these narrow bands of poleward water vapour fluxes "moist conveyor belts". In another concept these narrow bands of enhanced water vapour flux are termed atmospheric rivers (e.g., Zhu and Newell 1994, 1998, Ralph et al. 2004, Bao et al. 2006, Neiman et al. 2008) due to the great amount of water that is transported by these bands. Atmospheric rivers are typically situated near the leading edge of polar cold fronts and are often associated with heavy rainfall events and flooding in the affected regions. Although these rivers may transport an considerable amount of water vapour from the tropical moisture reservoir into the extratropics these rivers are rather an extratropical phenomenon.

The positive anomaly in the meridional moisture flux further upstream to the Northwest of the detected trough is related to transient wave disturbances in the storm track region and, hence, it is more in line with the conceptual model of the "warm conveyor belt" (e.g., Eckhardt et al. 2004).

Finally, there are studies that describe the transport of dry air masses from the mid latitudes into the Subtropics and Tropics associated with equatorward moving PV troughs (e.g., Yoneyama and Parsons 1999, Cau et al. 2005, Cau et al. 2007, Allen et al. 2009). These studies generally emphasize the convective-inhibiting properties and the resultant implications on the global radiation budget. In a study of Brown and Zhang (1997) these situations are proposed to induce droughts in the Tropics through the decreasing deep convective activity.

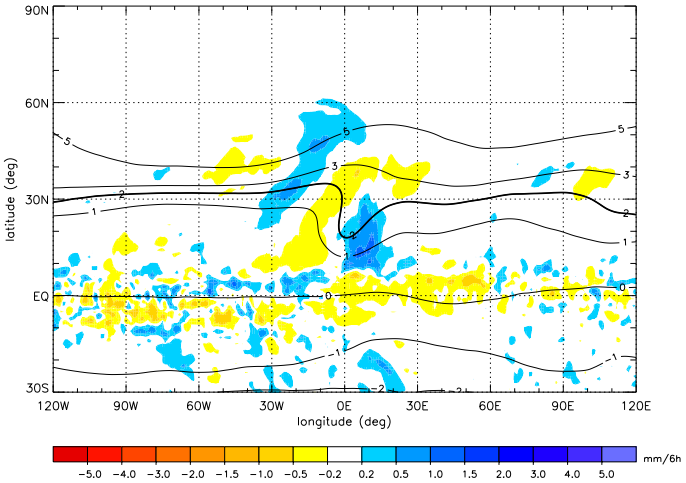

Figure 8.4: Composite of the precipitation anomalies [mm/6h] and VAPV values (lines) [PVU] for the most intense intrusion episodes in the NE-Pac from 1980 to 2001 in winter. Precipitation data is from ERA-40 with missing data from 1987 to 1989.

In several case studies it has been shown that extreme precipitation events over south-western North America, West Africa and in other semi-arid subtropical regions such as the Middle East and Australia are often caused by an export of moisture out of the Tropics in relation to upper troughs at low latitudes (e.g., Wright 1997, Ziv 2001, Knippertz and Martin 2005, Knippertz and Martin 2007a, 2007b, Rubin et al. 2007, Knippertz and Wernli 2010). For example in the case study of Knippertz and Martin (2007a) the "moist conveyer belt" of a cut-off low was related to exceptional precipitation over the dry south-western United States.

A look at a composite of the precipitation anomalies (and convective precipitation from ERA-40) for NE-Pac intrusions (Fig. 8.4) reveals enhanced precipitation in an area between 10 and 30°N near the eastern part of the trough and reduced precipitation behind the trough (anomalies are not tested for statistically significance). Hence, this supports the results of the previous case studies (e.g., Knippertz and Martin 2007a) in a climatological perspective.

However, based on the results of a trajectory analysis, Knippertz and Martin (2007a) suggest that midlevel moisture fluxes are generally too slow to transport enough moisture into the Subtropics for substantial precipitation. Their argument is also supported by the rareness of such precipitation events. Hence, Knippertz and Martin (2007b) assume that extreme precipitation events in the Subtropics are often the result of a persistent disturbance or of two disturbances in short succession. Further investigations in this context are needed. The intrusion climatology, developed in this work, can provide a basis for such studies in the future.

Part II

Tropical Plumes

9 Climatology

9.1 Geographical and seasonal distribution

In the second part of the present thesis a 23-year climatology of Tropical Plumes is analysed, which was constructed by applying a novel identification routine to the CLAUS brightness temperature (T_b) data set (for further information see Chap. 2.2 and 3.2). The resulting seasonal TP frequencies f_{TP}, depicted in Fig. 9.1, are based on the percentage of analysis times at which a respective grid point is part of a TP event during the investigation period (July 1983–June 2006). Recall, that only TP events are taken into account, that are part of a TP episode with a maximum length-to-width ratio (LWR) of 3 or more (see also Chap. 3.2).

The global distribution of TP frequencies in Fig. 9.1 reveals several well-defined areas of preferred TP formation, which are mostly located over oceanic regions. In boreal winter (Fig. 9.1a) the absolute f_{TP} maximum of 12% is found over the south-western Pacific followed by f_{TP} maxima of nearly 9% over the North and South Atlantic region and by f_{TP} maxima of nearly 7% over the north-eastern Pacific and over northern Australia. Further local f_{TP} maxima over the southern Indian Ocean, western North Pacific, Bay of Bengal and over southern Africa are characterized by frequencies below 6%. It is remarkable that in the NH the regions with highest TP frequencies (North Atlantic and Northeast Pacific) are located west of the landmasses (that means over the eastern ocean basins), while the opposite is true in the SH (Southwest Pacific and South Atlantic).

In boreal summer (Fig. 9.1b), the geographical distribution pattern in the SH is quite similar, although the magnitudes are strongly reduced. In the NH, seasonal changes are more pronounced: While over the North Atlantic and the Northeast Pacific TP occurrence is reduced and shifted westwards, f_{TP} increase over the western North Pacific and over India and the Bay of Bengal.

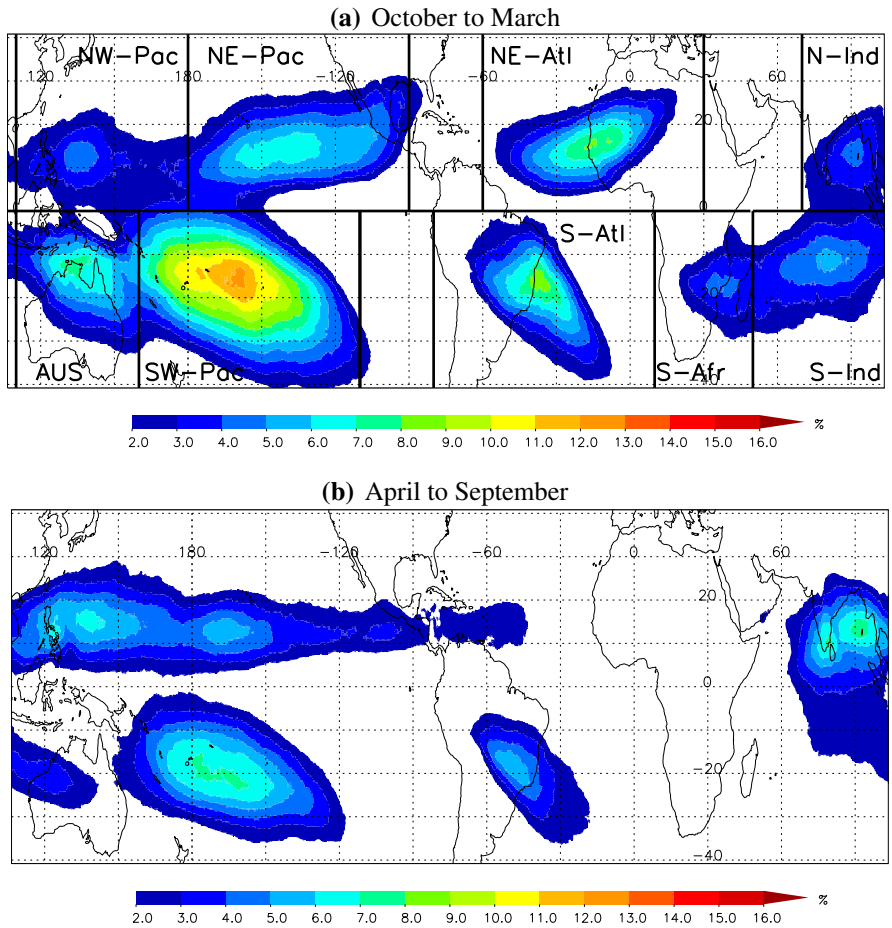

Figure 9.1: Mean Tropical Plume frequency [%] (shaded) for (a) NH winter and (b) summer during the investigation period July 1983 – June 2006. The regions used for further investigations are indicated by black boxes.

For the following investigations nine regions of high TP activity are subjectively defined on the basis of the winter climatology (Fig. 9.1a). The four regions in the NH and the five regions in the SH are: The northern Indian Ocean (N-Ind: 70°E-110°E), Northwest Pacific (NW-Pac: 110°E–180°E), Northeast Pacific (NE-Pac: 180°W–90°W), Northeast Atlantic (NE-Atl: 60°W–30°E), southern Indian Ocean (S-Ind: 50°E–110°E), Australian (Austr: 110°E–160°E), Southwest Pacific (SW-Pac: 160°E–110°W), South Atlantic (S-Atl:80°W–10°E), southern African (S-Afr: 10°E–50°E) region. For calculating regional TP frequencies each TP is assigned to one of these regions according to its southern-most point. TP events that extent over the equator (about 17% of all TP events) are added to the hemisphere in which most of their cold cloud is detected. Note that the longitudinal extent of the selected regions differ. However, the regions with the highest TP frequencies (NE-Pac, NE-Atl, SW-Pac and S-Atl) are all based on 90°-longitudinal wide boxes. The nine TP activity regions are selected on the basis of the winter TP climatology due to the fact that TP development in relation to intrusions of extratropical air masses into low latitudes is rather a winter phenomenon (see Chap. 1.2.2) and main focus of this thesis. The regional classification captures about 98% of the detected TP events in the SH in

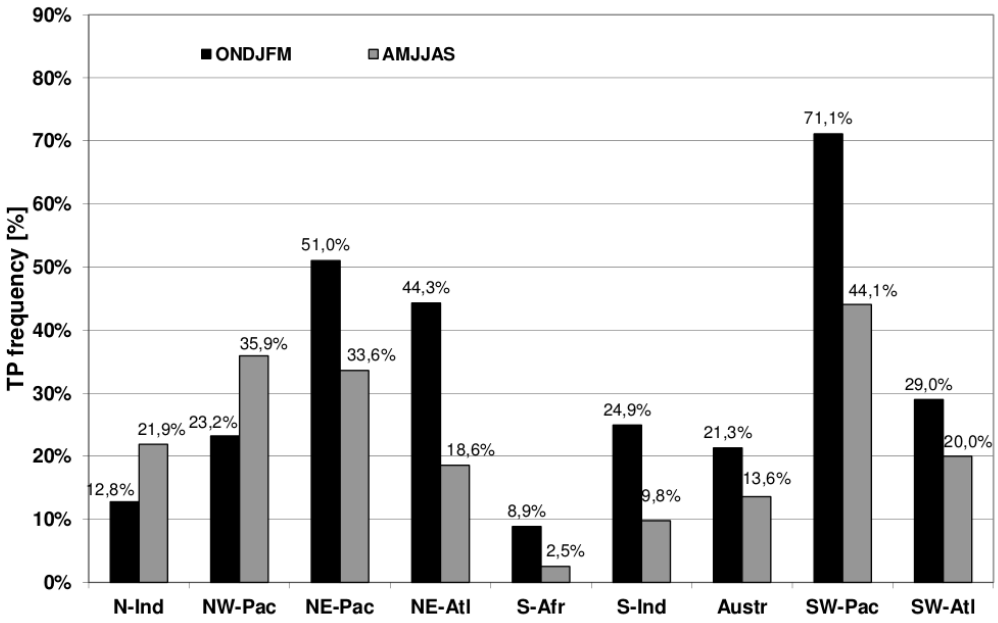

Figure 9.2: Boreal winter (black) and summer (grey) mean TP frequencies [%] per region for the period July 1983 – June 2006. Regions are defined in Fig. 9.1a.

summer as well as in winter. However, in the NH during winter (summer) only 92% (85%) of the TP events develop in one of the selected regions. Most of the events, which do not occur in these regions, are detected over the Caribbean Sea (in summer) and over the north-western Indian Ocean.
On average nearly three (two) TP events are detected at each analysis time in boreal winter (summer) worldwide. While in northern winter the TP frequency in the SH (161%) lies above that of the NH (143%), it is reversed in summer with TP frequencies of 128% in the NH and of 92% in the SH.
Similar to the grid-point based analysis, the TP frequencies of the selected regions, presented in Fig. 9.2, are generally higher in boreal winter except for the N-Ind and NW-Pac regions. Maximum TP frequencies during boreal winter are found in the SW-Pac (71.1%) followed by the NE-Pac (51.0%) and by the N-Atl (44.3%). The different total numbers reflect the larger extent of the North Pacific maxima compared to both Atlantic regions.

The monthly mean TP frequencies presented in Fig. 9.3 reveal roughly three major seasonal cycles: the first showing frequency maxima in the intermediate seasons (NE-Atl, NE-Pac and S-Atl), the second with maxima between October and March (SW-Pac, S-Afr, Austr and S-Ind) and the third with maxima occurring in summer (NW-Pac and N-Ind). Furthermore, the TP frequencies in the regions with maxima in the intermediate seasons (i.e. NE-Atl, NE-Pac and S-Atl) remain quite high after the peak in fall throughout the whole winter season.

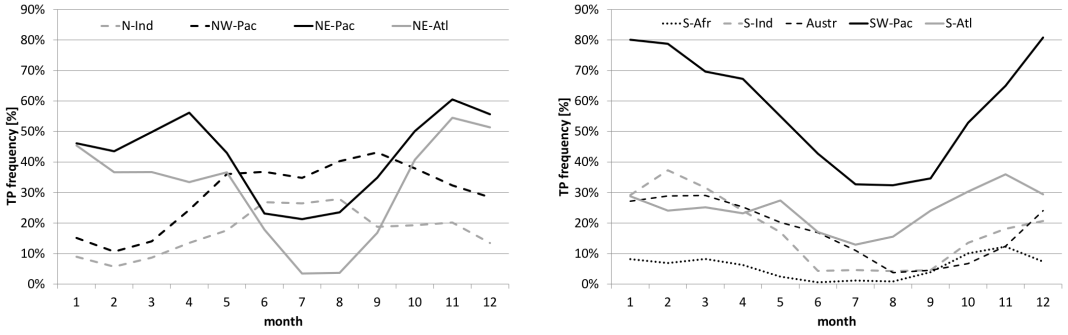

Figure 9.3: Monthly mean TP frequencies [%] for the selected regions in the (a) NH and (b) SH averaged between July 1980 – June 2001. Regions are defined in Fig. 9.1a.

Discussion

With respect to the geographical and seasonal distribution of TP frequencies, the presented climatology reflects well the results documented in previous studies (e.g., Thepenir and Cruette 1981, McGuirk et al. 1987, Kuhnel 1989, Iskenderian 1995), although TP identification in the past generally was based on a visual inspection of IR satellite imagery. Most of these former studies analysed TP occurrences in the Northern Hemisphere during winter, where high TP activity was commonly detected over the central and eastern North Pacific and North Atlantic (e.g., Iskenderian 1995) in agreement with the results above (Fig. 9.1). McGuirk et al. (1987) constructed a 3-year climatology of cloud bands over the central and eastern North Pacific from November to April and found maxima of cloud band activity in November and April and a relative minimum from February to March. These findings are in agreement with the seasonal cycle of TP frequencies in the NE-Pac presented in Fig. 9.3a.
The most comprehensive study was done by Kuhnel (1989) who constructed the first global 5-year climatology of tropical-extratropical cloud bands. On a global scale, he defined 14 regions of high TP activity (seven in each hemisphere, see also Fig. 1.4), which are also characterized by local f_{TP} maxima in the present TP climatology either in summer or winter (cp. Fig. 9.1). Most of these regions overlap with the nine high TP activity regions defined in this work. Similar to the results above the climatology of Kuhnel (1989) is dominated by high TP frequencies over the Southwest Pacific and over southern America/Atlantic. The global, yearly mean TP frequency obtained by Kuhnel (1989) lies with 220% below the TP frequency of 260% in the present climatology, which is assumed to be due to the coarser temporal resolution of the analysed IR imageries (once per day) and to some missing data.

With a view on the processes that lead to transient convection in the Tropics, Kiladis and Weickmann (1997) distinguish between tropical convection in regions with mean easterly and westerly wind in the upper troposphere over the equator (for information about the mean zonal wind see Fig. 4.1). It is argued that in regions close to the "westerly ducts" TP formation is primarily activated by equatorward propagating troughs from the extratropics (see also Chapt. 1.2.3). This occurs over the eastern North Pacific and

Atlantic regions during northern winter, and over the South Pacific and South America/Atlantic region during southern summer.
However, the f_{TP} maxima over the South Pacific and the South Atlantic, related to the quasi-stationary cloud bands of the South Pacific/Atlantic (SPCZ and SACZ) during austral summer (e.g., Kodama 1992, 1993, Vincent 1994), are according to McGuirk (1987, p. 789) considered a different meteorological phenomenon compared to the short-lived, transient TPs of the cool season. The same is true for the f_{TP} maximum over the western North Pacific in boreal summer, which is the result of a similar quasi-stationary cloud band along the Baiu/Mei-yu front (Kodama 1992, 1993) and for the f_{TP} maximum related to the rainfall area over Southeast Africa.
In regions with mean upper easterlies over the equator tropical convection often coincides with a displacement of the ITCZ into the subtropics (Kuhnel 1989) as a consequence of monsoon related heating anomalies (e.g., over India, the Bay of Bengal and the Southern Indian ocean).
In the present climatology, differences in the relationship with the mean upper equatorial winds become obvious in the spatial structure of the f_{TP} maxima in Fig. 9.1: For example in the "westerly duct"-related regions over the Northeast Pacific and Atlantic during winter the f_{TP} maxima are southwest-northeast orientated. This is in accordance with the majority of the individual systems (see Sect. 10.3 below) and, hence, it reflects the elongated shape of the cloud bands detected in these regions. The f_{TP} maxima in regions with mean equatorial easterly winds are generally circularly shaped (cp. NW-Pac and N-Ind regions in Fig. 9.1) pointing to higher proportion of tropical disturbances.

Finally a brief comparison of the boreal winter TP and intrusion climatology (see Fig. 4.1a and 9.1a) reveals that high intrusion frequencies occur west of the TP maxima in the Northeast Pacific and Atlantic and east of the TP maxima in the Southern Pacific and Atlantic. This observation supports the idea that TP development in the Northern Pacific and Atlantic is related to extratropical disturbances at low latitudes. However, over the Southern Pacific and Atlantic the detected intrusions cannot directly be related to cloud band development due to the different positions of both phenomena. Furthermore, in the remaining regions (mainly regions with upper-level mean easterlies over the equator) no relevant trough occurrence, which could lead to TP development, is detected at all.

9.2 Sensitivity to length-to-width ratio criterion

In this subsection the sensitivity of the TP identification algorithm to the new **l**ength-to-**w**idth **r**atio (LWR) criterion is assessed. Recall, that the LWR value is the length-to-width ratio of the smallest rectangle surrounding a cloud band at a certain analysis time (for further information see 3.2). It is a measurement for the "elongatedness" of a cloud structure with higher LWR values pointing to more elongated cloud bands. The LWR criterion is one of the four requirements for TP identification and demands a maximum LWR value of 3 or more during a TP episode. The intention of implementing this cri-

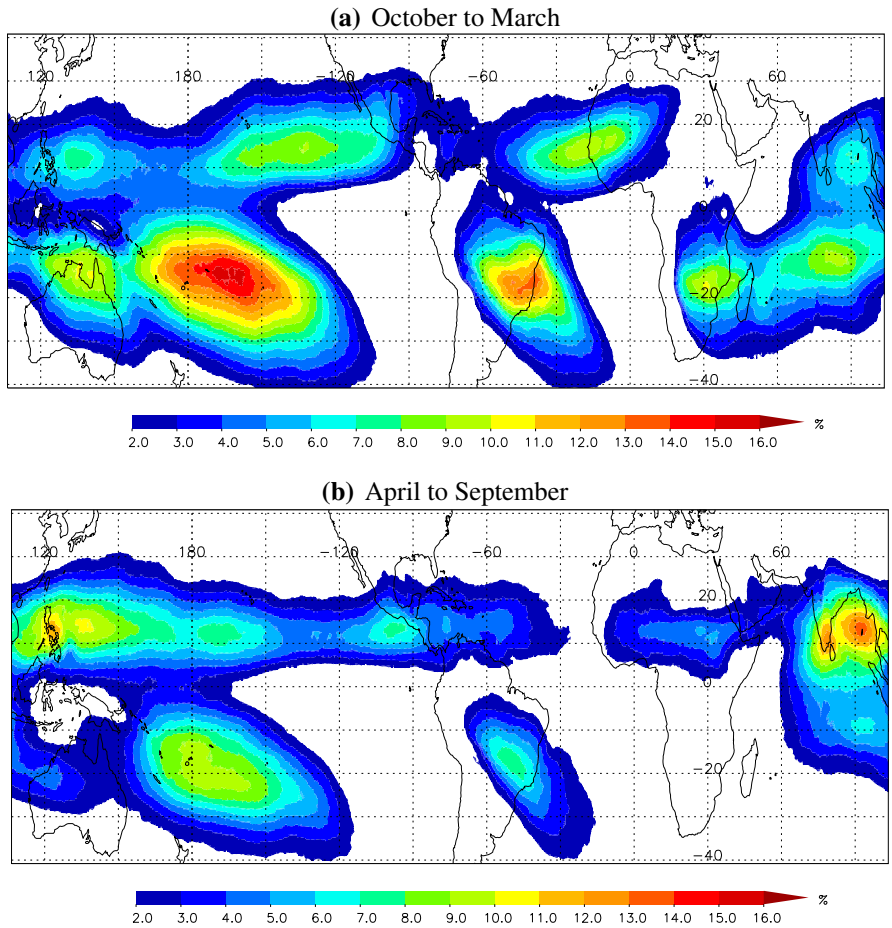

Figure 9.4: Mean TP frequency [%] during (a) NH winter and (b) summer for the period Jul. 1983–Jun. 2006. The TPs were detected without applying the LWR criterion i.e. the maximum LWR value of a TP episode is 1 or more.

terion was to reduce the detection of circularly shaped cloud structures such as tropical disturbances.

In the following the influence of the implementation of the LWR criterion on the geographical TP distribution is assessed by comparing the TP climatology constructed without LWR requirements with the original TP climatology (based on TPs that are part of an episode with a maximum LWR value of 3 or more) presented in the previous section. At the first view, the TP climatology without LWR criterion, presented in Fig. 9.4, qualitatively resembles the original TP climatology in Fig. 9.1, but TP frequencies are generally higher with f_{TP} maxima over the South Pacific and America/Atlantic region of more than 13% during austral summer followed by f_{TP} maxima of more than 10% over northern Australia and south-eastern Africa. The same is true for the regional TP frequencies presented in Fig. 9.5a (cp. Fig. 9.2). More detailed information about the differences between both climatologies are received by analysing the regional fraction of the originally detected TPs to TPs that are detected without the LWR criterion (Fig. 9.5b). As expected, the implementation of the LWR criterion causes a general decrease in TP numbers worldwide, which is more pronounced during summer in most of

the regions. Globally about 65% (59%) of the detected cloud bands satisfy the LWR criterion in boreal winter (summer). The greatest differences between both TP climatologies are observed in the S-Afr region: Only about 30% of the detected cloud bands in austral summer are part of a TP episode with a maximum LWR value of 3 or more. The highest fraction of these TPs exhibit the NE-Atl and SW-Pac regions with more than 70% in boreal winter.

(a) TP freqencies with LWR ≥ 1

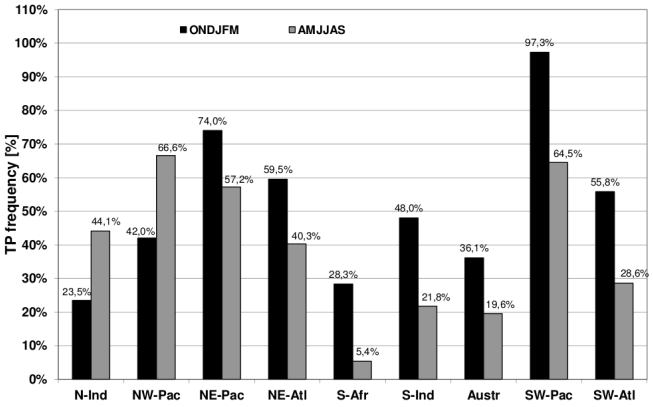

(b) Fraction of TPs with LWR ≥ 3

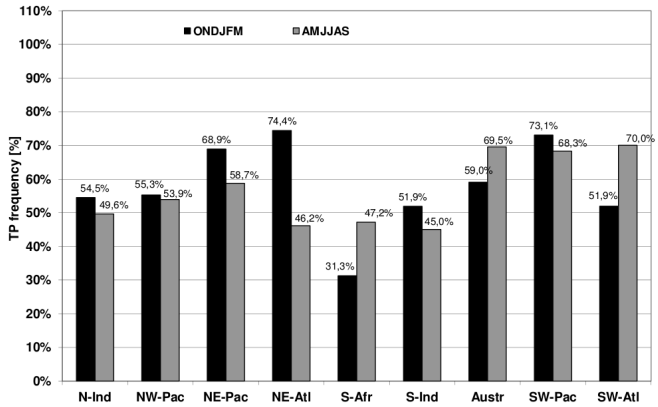

Figure 9.5: (a) Boreal winter (black) and summer (grey) mean TP frequencies [%] per region for the period 1983–2006. (b) Regional fraction of TP events with side length ration greater equal of 3 in all TP events detected without LWR requirements. Regions are defined in Fig. 9.1a.

On the basis of Fig. 9.5, it has been shown that the inclusion of the LWR criterion in the TP identification algorithm leads to modifications in the geographical TP distribution with a stronger reduction of TP frequencies in regions where circularly shaped cloud structures are predominant and a weaker reduction of well-elongated TP events that occur preferentially in regions related to the westerly duct such as the NE-Atl, NE-Pac or SW-Pac regions. Tests with higher LWR criteria emphasize these changes in the TP distribution even more. TP detection with a LWR criterion of 5 or more leads to a distribution with an absolute maximum of TP frequencies in the NE-Atl region (not shown). Changes in the other TP identification thresholds (e.g., T_b anomaly, minimum size, max-

imum extension, crossing latitude) generally produce TP climatologies with similar geographical and seasonal distributions but with different magnitudes in the total TP numbers. For example, a reduction in the T_b anomaly threshold is accompanied with lower TP frequencies and a shift of the crossing latitude e.g. to the north, leads to a northward shift of the main TP activity regions (results are not shown).
Nevertheless, this analysis demonstrates that the geographical distribution of the most active TP regions is a robust feature despite of the sensitivity of the TP identification to the choice of the individual thresholds and to other details of the detection algorithm.

10 TP characteristics

10.1 Life time

In the following section Tropical Plume episodes, detected by the original identification algorithm as described in Section 3.2, are analysed with respect to geographical and seasonal variations in their occurrence and lifetime. Recall, that the definition of TP episodes is based on a spatial overlap of at least two TP events at consecutive analysis times. This implies that the minimum lifetime of a TP episode is three hours. On a global scale 94% of all detected TP events are part of a TP episode before applying the LWR criterion. 38% (35%) of these TP episodes satisfy the LWR criterion during northern winter (summer). These episodes are considered in this section.
In Fig. 10.1 the mean TP number per season and the mean lifetime of the TP episodes with maximum LWR values of 3 or more, are presented for the nine high TP activity regions, defined in Chapt. 9.1. Each TP episode is assigned to one of the regions according to the location of its southern-most point at the first detection time. The geographical distribution of the TP episodes qualitatively resembles the frequency distribution of the TP events in Fig. 9.2. In boreal winter, TP episodes are most frequent in the SW-Pac region with 57 episodes on average per winter (black bars in Fig. 10.1). In the S-Atl, NE-Pac and NE-Atl region the mean numbers of TP episodes per winter lie between 42 and 47. In the remaining regions less than 30 episodes per winter are detected. During summer the geographical distribution of TP episodes is quite similar although absolute numbers are much reduced except for the N-Ind and NW-Pac region.
The definition of TP episodes is in accordance with prior studies, which often consider cloud bands from the beginning to the end as one cloud system (e.g., McGuirk et al. 1987; Iskenderian 1995). Therefore the definition of TP episodes allows a comparison of absolute numbers with these previous studies: McGuirk et al. (1987) analysed the TP activity over the eastern North Pacific between 180° E and 90° W of three winter

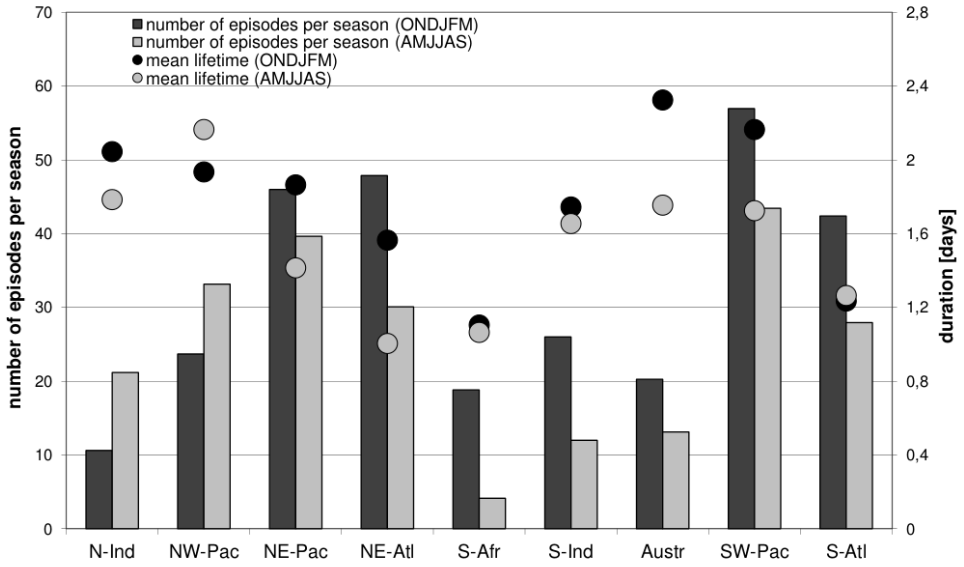

Figure 10.1: Mean number per season and mean lifetime [days] of TP episodes per region for NH winter (black) and summer (grey) averaged from Winter 1983/84 to Winter 2005/06 (23 winter and 22 summer). Regions are defined in Fig. 9.1a.

seasons (November to April). They detected on average 48 cloud plumes per winter in a good agreement with the present study (NE-Pac: #46). In a 10-year period Iskenderian (1995) observed on average 106 cloud plumes per winter season (October to May) in the NH, which is only about 70% of the number of TP episodes (#144) detected in the NH in this study. On a regional scale Iskenderian (1995) observed about 40 cloud plumes per winter in the eastern Pacific more or less in accordance with the present climatology. The differences to the results of Iskenderian (1995) are assumed to be due to the coarser temporal resolution of the data basis used in this study (twice daily IR imagery).

In the following, the duration of the TP episodes is evaluated with the help of Fig. 10.1 (black and grey dots). On a global scale the mean life time of all TP episodes detected year-round is 1.64 days. On average TP episodes are more persistent in the northern winter than in summer and in the SH than in the NH. The maximum TP duration of nearly two and a half days is found in the Australian region during austral summer. In this region more than 4% of all episodes persist 10 days or longer and there are even 6 TP episodes that last longer than 20 days. The second winter maximum exhibits the SW-Pac region with a mean life time of about 2.2 days and with more than 3% of all TP episodes lasting longer than 10 days. In the NH the mean life times vary between 1.5 and 2 days during boreal winter. And only 0.8% (#26) of all episodes exhibit durations of 10 days or more.

During boreal summer the mean life time of the TP episodes is in most of the regions reduced, except for the S-Afr and NW-Pac regions. In the latter a detected cloud band persists 2.2 days on average and more than 3% last longer than 10 days.

The mean duration of the cloud bands estimated in McGuirk et al. (1987) in the North

Pacific sector is 2.6 days similar to the results of Iskenderian (1995). It is somewhat longer than the mean life time of the TP episodes in the NE-Pac assessed in this study (2 days). This is presumable due to the differences in detecting the first appearance of a cloud band. McGuirk et al. (1987) define the time of beginning as "the first evidence of poleward progression of the cloud mass which later develops into a moisture burst", that means that a cloud band is already detected before it satisfies the actual TP definition. This is in contrast to the objective TP identification procedure applied in this work. Furthermore, while in the study of McGuirk et al. (1987) most of the cloud bands last 2 to 4 days, in the present climatology nearly 50% of all detected TP episodes exhibit durations of one day and shorter. It is worth noting that, the fraction of long-living TP episodes increases with higher maximum LWR values of the TP episode (not shown).

10.2 Length-to-width ratio

In this subsection the length-to-width ratio is statistically evaluated for TP events detected before applying the LWR criterion (the respective climatology is presented in Chap. 9.2). Hence, the LWR value is regarded as a measurement for the elongatedness of an individual TP event rather than as a identification criterion. The influence of the implementation of the LWR criterion in the identification routine on the TP climatology has been discussed in the previous chapter (Chap. 9.2).
For the following evaluations all TP events in each hemisphere and in each season are divided into 6 classes according to their LWR value and then normalized with the respective total numbers. The resulting normalized distribution of TP side length ratios, presented in Fig. 10.2, shows that in both hemispheres TP frequencies decrease with increasing LWR values. In the NH about 47% of all TP events are characterized by LWR values of less than 2 during boreal winter and only about 20% show LWR values of 3 or more (see Fig. 10.2a). In summer the TP distribution in the NH shifts slightly towards lower LWR values, which means that less elongated TP events are detected during this time of year. On a regional basis the LWR distributions differ slightly between the selected regions (Fig. A.6 in the Appendix). The NE-Atl region in winter reveals with the greatest proportion of TP events with LWR values greater equal 3 (30%), which points to a higher number of cloud bands with a pronounced elongated shape in this region and is in accordance with the results discussed in Sec. 9.2. This region also shows with the greatest percentage of TPs with LWR values of 5 and more (4%). In the SH in austral summer 48% of all TP events are characterized by LWR values lower than 2 and about 15% show LWR values of greater-equal 3 (Fig. 10.2b). Furthermore, the distribution of TP events in the SH exhibits a slight seasonal shift towards higher LWR values in austral winter similar to the NH. On a regional scale a similar seasonal shift is observed in the S-Afr, Austr and S-Atl region (see Fig. A.6). The latter region in austral winter reveals the greatest proportion of TP events with LWR values of 3 or more (>30%) similar to the NE-Atl region. The lowest proportion of well-elongated TP events is found in the S-Ind region.

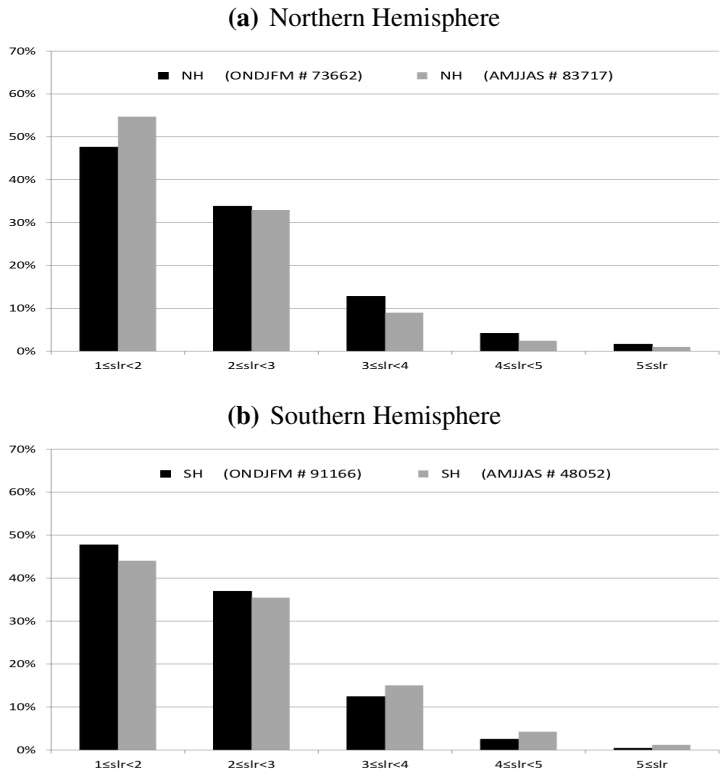

Figure 10.2: Normalized distributions of TP side length ratio for intrusion systems detected in the (a) NH and (b) SH. The black (grey) bars show boreal winter (summer) frequencies of the period July 1983–June 2006. The total numbers for each season and region are given in brackets. Regions are defined in Fig. 9.1a.

Considering the distribution of LWR values of the TP episodes, in Table 10.1 the regional numbers of episodes with a maximum LWR value of more and less than 3 are listed. Note that here only TP episodes are considered that do not cross the equator. 43% of all TP episodes (that do not cross the equator) are characterized by maximum LWR values of 3 or more. These TP episodes form the data base for further investigations such as composite studies of upper circulation anomalies in relation to the occurrence of TP episodes (see Chap. 12).

	N-Ind	NW-Pac	NE-Pac	NE-Atl	S-Afr	S-Ind	Austr	SW-Pac	S-Atl
LWR$\geq$3	138	306	664	653	217	355	274	810	554
LWR<3	212	379	519	374	561	554	406	671	703

Table 10.1: Number of TP episodes with maximum LWR value ≥ 3 or < 3 (see Section 3.2 for a definition of this parameter) detected in boreal winter (Oct.-March) in the selected regions during the CLAUS investigation period (July 1983 to June 2006). Regions are defined in Fig. 9.1a.

10.3 Horizontal tilt

In this subsection the horizontal tilt of the TP events is analysed based on TP events identified with the original TP identification routine (that means which are part of a TP episode with maximum LWR value of 3 or more). The horizontal tilt of a TP is estimated from the tilting angle towards the meridian of the smallest rectangle bordering a cloud band (see Fig. 3.3 in Chap. 3.2) i.e. north-south aligned cloud structures are not tilted and west-east (north-south) orientated TPs in the NH (SH) are characterized by a maximum angle of 90° (-90°). Note, the described definition of the tilting angle is in contrast to the definition of the tilting angle for intrusion systems.
The normalized distribution of TP horizontal tilt in Figs. 10.3a and 10.3b shows that most of the TPs in the NH/SH are positively/negatively tilted. Maximum TP frequencies are observed between 60° and 70° in the NH during winter and summer. A second maximum appears during summer for tilting angles between 80° and 90°, which is primarily due to NE-Pac TPs (Fig. A.7 in the Appendix) and points to more west-east orientated TP events detected more often at this time of the year. In the SH most TP events are characterized by tilting angles between -60° and -50° in winter as well as in summer, which implies that SH TP events display on average a slightly greater angle towards the equator than NH events. This maximum is even more pronounced during austral winter and is also observed on a regional scale in the S-Afr, Austr and S-Atl regions.

(a) Northern Hemisphere

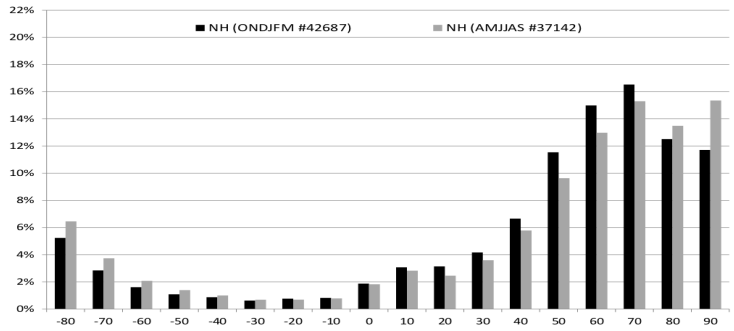

(b) Southern Hemisphere

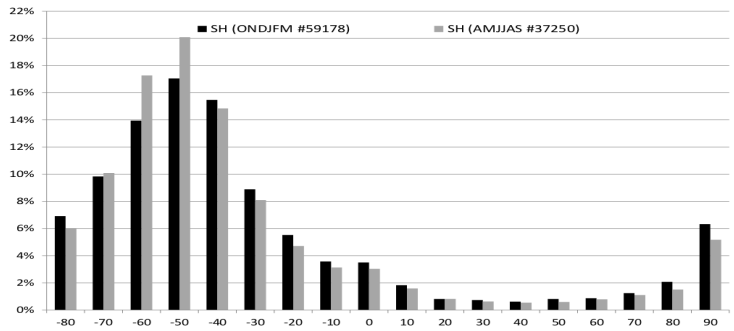

Figure 10.3: Normalized distributions of TP horizontal tilt for TPs detected in (a) the NH and (b) the SH. The black (grey) bars show boreal winter (summer) TP frequencies of the period July 1983–June 2006. The total numbers for each season and region are given in brackets. Regions are defined in Fig. 9.1a.

Overall, the distribution of horizontal tilt, especially on a regional scale corresponds well with the orientation of the main f_{TP} maxima in the grid-point based TP climatology in Fig. 9.1.

11 Trends and inter-annual variability

In this chapter the regional time series of seasonal TP frequencies, depicted in Fig. 11.1, are analysed with respect to long-term trends and inter-annual variability within the investigation period from winter 1983/84 to summer 2005. Some of the regions exhibit large year-to-year fluctuations in seasonal TP occurrences. Largest variations are observed in the NE-Pac during winter, where TP frequencies vary between nearly 20% in the winter of 1997/98 and 75% in the winter of 1993/94 (Fig. 11.1c). Variations in summer in this region are only slightly smaller with a frequency minimum of about 15% in the summer of 1998 and a maximum of 55% in the summer of 1985. The NW-Pac region also exhibits strong inter-annual fluctuations, primarily during summer (Fig. 11.1b). TP frequencies range from 60% in the summer of 1985 to nearly 10% in the summer of 1987. Fluctuations in the remaining regions are generally smaller. For example the SW-Pac region is characterized by constantly high TP frequencies of above 60% (40%) during austral summer (winter) throughout the investigation period (Fig. 11.1h). In the NE-Atl region the majority of winters exhibit values between 35% and 55% (Fig. 11.1d); however, there is one outstanding TP frequency of 60% in the winter of 1991/92.
In the following the long-term trends in these time series are evaluated based on a Mann-Kendall described in Sec. 3.5. To visualize the trend calculations, the linear regression lines of the time series of seasonal TP frequencies are added in Fig. 11.1 (black and grey dashed lines). In Fig. 11.1 it is evident that all regions display a downward trend in the seasonal mean TP frequencies in summer and winter except for the Australian sector. In boreal winter these trends in TP occurrence are statistically significant on a 95% level in the SW-Pac, N-Ind and S-Ind and on a 90% level in the S-Atl. Long-term trends calculated for the global and SH TP frequencies are statistically significant at a 99% level in summer and winter.

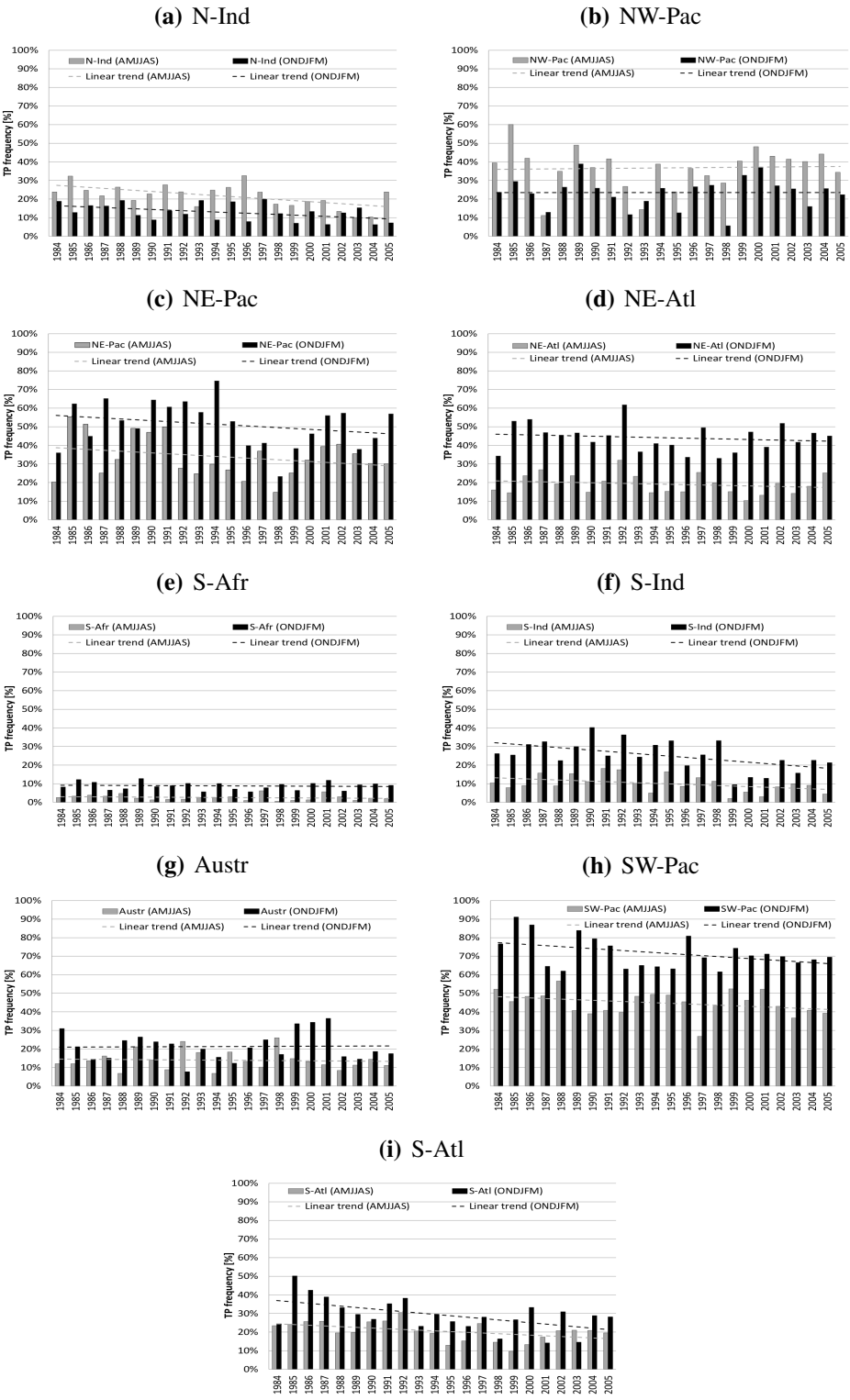

Figure 11.1: Seasonal mean TP frequencies in [%] for the (a) N-Ind, (b) NW-Pac, (c) NE-Pac, (d) NE-Atl, (e) S-Afr, (e) S-Ind, (f) Austr, (g) SW-Pac and (h) S-ATl regions. Black (grey) bars show boreal winter (summer) frequencies between winter 1983/84 and summer 2005. "1984" corresponds to the 1983/84 winter mean. Dashed black (grey) lines are the corresponding linear trend lines of the winter (summer) TP time series. Regions are defined in Fig. 9.1a.

Explanations for these trends are found in a paper by Evan et al. (2007), who argue that long-term trends in cloudiness in the **I**nternational **S**atellite **C**loud **C**limatology **P**roject (ISCCP) data, the source data for the CLAUS project (see Chap. 2.2), are satellite viewing geometry artifacts (due to limb darkening) and not related to physical changes in the atmosphere. Evan et al. (2007) present a time series of ISCCP total cloud amount from 1983 to 2006 averaged over 60°N and 60°S. This time series is characterized by a significant decrease in cloud amount between about 1987 and 2000. Furthermore, they found that the regional cloud amounts correlate differently with this time series depending on the viewing satellite geometry (Evan et al. 2007, their Fig. 2). Furthermore, these regional correlations reveal several areas in the Tropics and Subtropics over the Indian Ocean, western Atlantic and central Pacific that contribute most to the decrease in global cloudiness. These conspicuous regions coincide with the N-Ind, S-Ind, SW-Pac, S-Atl and NE-Pac regions defined in the present work. Apparently these regions are characterized by strongest negative trends in TP occurrences, which is consistent with the results of Evan et al. (2007). Finally, the authors advise against the application of ISCCP data in its current form for studying long-term trends.

11.1 Association with ENSO

In this section year-to-year fluctuations in the TP frequencies in association with the El Niño-Southern Oscillation (ENSO) are examined. For these investigations the regional time series of seasonal TP frequencies are compared with two time series of ENSO indices, the Niño3.4 and the SO index (for further information see Sec. 2.3) via correlation analysis. The resulting correlation coefficients, presented for boreal winter in Tab. 11.1, reveal four areas with statistically significant (99% level) high correlations between the seasonal TP frequencies and ENSO. The strongest relationship is observed in the NW-Pac region with a negative correlation coefficient of -0.88 based on the Niño3.4 index pointing to a decrease/increase in TP events during the warm/cold phase of ENSO (El Niño/La Niña). Based on the SO index the link between TP frequencies over the Northwest Pacific and ENSO is only slightly smaller with a correlation coefficient of 0.85. According to these high correlations, more than 70% of the winter-to-winter variance in TP activity in this region is explained by ENSO. In the Austr and SW-Pac regions statistically significant correlation coefficients of -0.69 and -0.68 are achieved with the

	N-Ind	NW-Pac	NE-Pac	NE-Atl	S-Afr	S-Ind	Austr	SW-Pac	S-Atl
Niño3.4	0.22	**-0.88**	0.06	0.04	-0.23	0.43	**-0.69**	**-0.68**	-0.16
SOI	0.24	**0.85**	-0.12	-0.02	0.22	**-0.61**	**0.77**	0.41	-0.01

Table 11.1: Correlation coefficients between regional TP frequencies (cp. Fig. 11.1) and the ENSO indices Niño3.4 and SOI for boreal winter season from 1983/84 until 2005/06 (23 winters). Statistically significant (99% level) correlation coefficients are bold. Regions are defined in Fig. 9.1a.

Niño3.4 index. Compared to the NW-Pac these correlations are of the same sign but weaker. In comparison to the Niño3.4 index the correlation coefficient on the basis of the atmospheric SO index is higher in the Australian region (r=0.77) and lower in the SW-Pac (r=0.41, statistically not significant). However, for the S-Ind this index reveals a statistically significant relationship with ENSO (r=0.61), which indicates more TP events during El Niño.
The correlation analysis reveals a very low connection between TP occurrence and ENSO for the NE-Pac, NE-Atl and S-Atl. In these regions correlations are higher considering the northern summer TP frequencies (see Table A.2 in the Appendix), although these correlations are not significant. In the remaining regions correlation coefficients between summer TP frequencies and the ENSO indices are generally low.

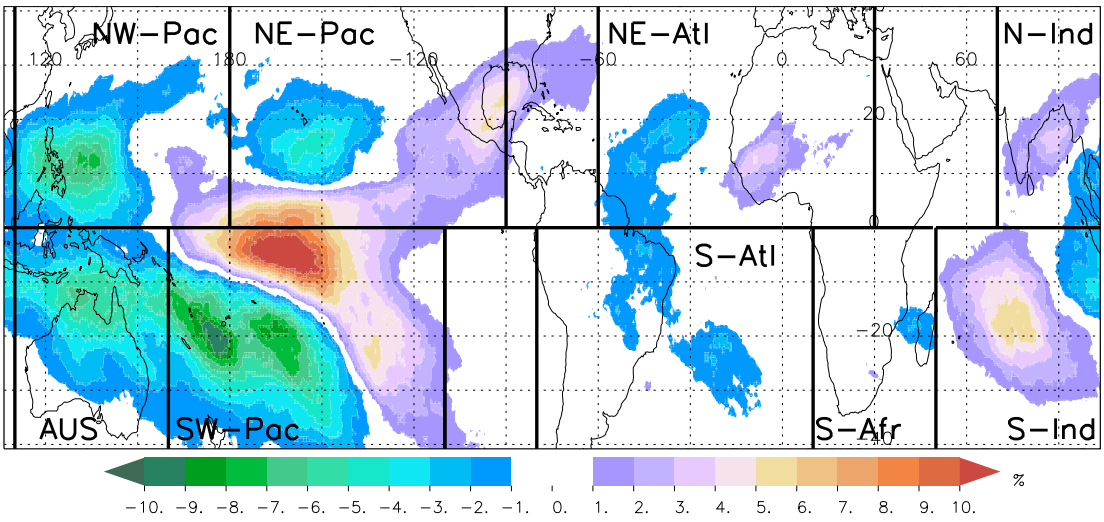

Figure 11.2: Differences in the TP frequency [%, percentage points] (shaded) between El Niño minus La Niña winter from 1980 until 2001. For ENSO winter classification see 2.1.

In the following the results of the correlation analysis are compared with differences between the two phases of ENSO in the grid-point based, global TP climatologies. Therefore two TP climatologies were constructed (see Fig. A.8 in the appendix) on the basis of 6 El Niño and 5 La Niña winter within the investigation period (see Sec. 2.3). The differences between both climatologies (El Niño minus La Niña) are presented in Fig. 11.2 without significance test due to the very small sample size. Fig. 11.2 reveals that ENSO-induced differences in the TP frequencies are most pronounced in the Pacific ocean with the strongest signal very close to the main activity region of ENSO. During El Niño TP frequencies increase in a large area over the tropical central Pacific which is in agreement with the ENSO-induced shift of the main convective regions from the western to the central equatorial Pacific. At its eastern end this area is expanded by two branches of enhanced TP frequencies reaching north- and south-eastward into the northern or southern Subtropics. Further west over the equatorial Pacific, TP occurrences are reduced during El Niño. This area of ENSO-reduced TP frequencies expands to the North over the western Pacific into the northern Subtropics and to the Southeast over Australia and

large parts of the Southwest Pacific into the southern Subtropics. Hence, over the southwestern Pacific a dipole with a sharp nearly northwest-southeast orientated boundary forms in relation to ENSO that indicates an eastward shift of TP occurrence during El Niño (leading to a shift of the SPCZ). Over the southern Indian Ocean a distinct region of enhanced TP activity during the warm phase of ENSO appears. Finally over the North Atlantic, slightly more events occur to the east (over southern West Africa) and less to the west although the signal is weaker compared to the other regions.
In Fig. 11.2 ENSO-induced differences are greatest in the SW-Pac in contrast to the calculated correlation coefficients in Table 11.1. This is due to the fact that areas of increasing and decreasing TP frequencies occur at the same time within the SW-Pac box. The same is true for the NE-Pac and NE-Atl regions. Hence, for investigations in association with ENSO the regional classifications are not always optimal for correlations between TP frequencies and ENSO.
In Fig. 11.3 the mean numbers of TP episodes and life times are presented for the two different ENSO winter phases (no test of significance). Figure 11.3 reveals that ENSO does not only change the number but also the persistence of the TP episodes. This fact becomes most obvious in the S-Ind region, where the mean life time of the TP episodes increases from 1.4 days during the cold phase to 2.1 during the warm phase of ENSO, while the number of TP episodes stays almost unchanged. The reversed is observed over Australia where the negative correlation to ENSO is primarily a result of shorter TP episodes. Finally, Fig. 11.3 reveals for the NW-Pac region, the region that has the strongest negative correlation with ENSO in Tab 11.1, less and shorter TP episodes during El Niño.

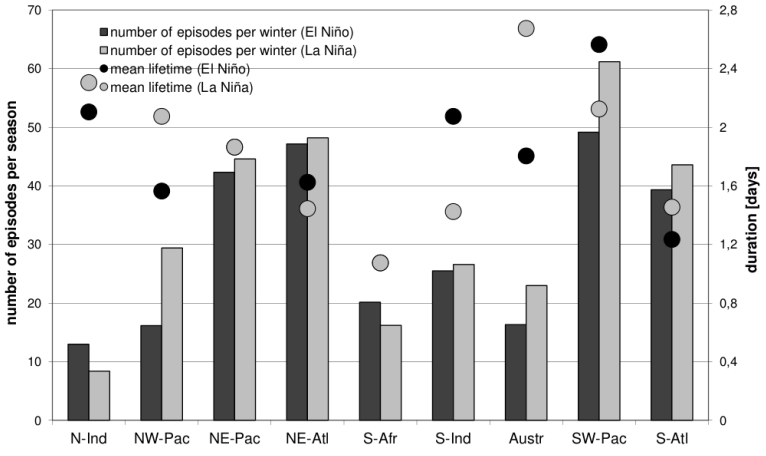

Figure 11.3: Mean number per season and mean lifetime [days] of TP episodes per region El Niño (black) and La Niña (grey) during the period 1983 – 2005. Regions are defined in Fig. 9.1a.

Discussion

Investigation of long-term trends in the regional time series of seasonal TP frequencies yield a significant downward trend in most regions, with the strongest signal in the N-Ind, S-Ind and S-Atl sector. Similar observations in relation to the ISCCP data set were made in former studies and are, according to Evan et al. (2007), a result of inhomogeneities in the satellite viewing geometries rather than a presentation of real atmospheric changes. As the authors suggest, data from ISCCP is homogeneous enough for long-term trend analysis. Further studies are on the way, in which the TP identification algorithm will be applied to the more homogeneous Patmos-X[1] data set.

Despite of the inhomogeneities in the ISCCP data inter-annual variability in association with ENSO has been investigated. The resulting differences in the global TP frequencies between both phases of ENSO in Fig. 11.2 represent well the results of former studies (e.g., McGuirk et al. 1987, Kuhnel 1989, Iskenderian 1995). For example, Kuhnel (1989) compared regional numbers of tropical-extratropical cloud bands with the SO index via correlation analysis on a monthly basis (including lag correlations) and received strongest correlations for two regions over the Southern Pacific: The first region is located over the eastern South Pacific (140°W – 80°W) and exhibits a strong negative correlation with the SO index (indicating more cloud bands during El Niño). The second region is located over the central South Pacific (170°E–140°W) and is characterized by an opposite correlation. These findings are in accordance with the ENSO-induced differences over the South Pacific in the present TP climatology in Fig. 11.2. The third strongest (positive) correlation is found in this study of Kuhnel (1989) over the central North Pacific between 150°E and 155°W with the SO index leading cloud band activity by six month. This is also in agreement with Fig. 11.2 that shows a negative tendency over the central North Pacific pointing to reduced TP frequencies during El Niño.

In the climatology of Iskenderian (1995) a strong reduction in Tropical Plume occurrences over the north-eastern Pacific is observed in the winter of 1982/83. In the same cool season, McGuirk et al. 1987 detected less cloud bands with the location of occurrence shifted eastward. Due to the fact that cloud band formation in this region is often associated with equatorward propagating troughs from the extratropics, these changes are explained by ENSO-induced modulations in the strength and position of the westerly duct and the North Pacific subtropical jet and in the low-latitude trough activity over the tropical eastern Pacific (see also Chap. 6.1). Fig. 11.2 displays for the Northern Atlantic a shift in the location of TP occurrence to the east similar to the NE-Pac. However, over the North Atlantic, where low-latitude trough activity is significant enhanced during El Niño (see Chap. 6.1), a significant increase in TP events is not observed in the present study.

Correlation between the TP time series and other atmospheric climate state indices such as the NAO and PNA are low (see Tab. A.2) except for the NW-Pac and Australian region that display a strong correlation with the PNA index (-0.8 and -0.68). It is suggested

[1] http://cimss.ssec.wisc.edu/patmosx/overview.html

that these strong correlations are due to the strong relationship between ENSO and PNA (e.g., Straus and Shukla 2002).

12 Composited evolution of Tropical Plumes

In this chapter the evolution of Tropical Plumes is described via composite analysis (see Sec. 3.4) of upper circulation anomalies. For that reason composites of the statistically significant (95% level) VAPV (vertically between 400 and 100 hPa averaged PV) anomalies in relation to the occurrence of a TP episode during boreal winter are displayed in Fig. 12.1 for the nine high-TP activity regions. The VAPV anomalies are used here as an indicator for circulation anomalies in the upper troposphere, which may lead to TP formation. Furthermore, in these composites the corresponding T_b anomalies (less than -5 K) are drawn to represent the position and the shape of the climatological mean Tropical Plume.

In the NE-Pac region (Fig.12.1c) a positive PV anomaly is evident west of the climatological TP, which is part of a northwest-southeast orientated wave train across the North Pacific and points to an upper-level trough at low latitudes with extratropical origin. Fig. 12.1c suggest that in this region TPs develop primarily along the eastern flank of an upper-level trough. Negative PV anomalies overlap with the mean TP, which indicates that the wave train has propagated further south-eastward across the region of convection. Noticeable is also a significant signal south of the equator that indicates wave dispersion in the South Pacific from the Northern Hemisphere. All these observations are broadly in agreement with the findings of e.g. Iskenderian (1995) and Kiladis and Weickmann (1992b, their Fig. 2), who argue that cloud systems in the eastern Pacific are forced by transient Rossby waves that originate in the Asian jet region and propagate south-eastward from the mid-latitudes through the westerly duct in the eastern Pacific. A similar wave train is apparent in association with TPs in the NE-Atl, the S-Atl, SW-Pac, S-Ind and S-Afr regions (see Fig. 12.1). In the SH regions the PV trough directly related to TP genesis is located further away from the equator than the respective NH troughs, which is assumed to be due to the mean position of the ITCZ south of the equator during boreal winter.

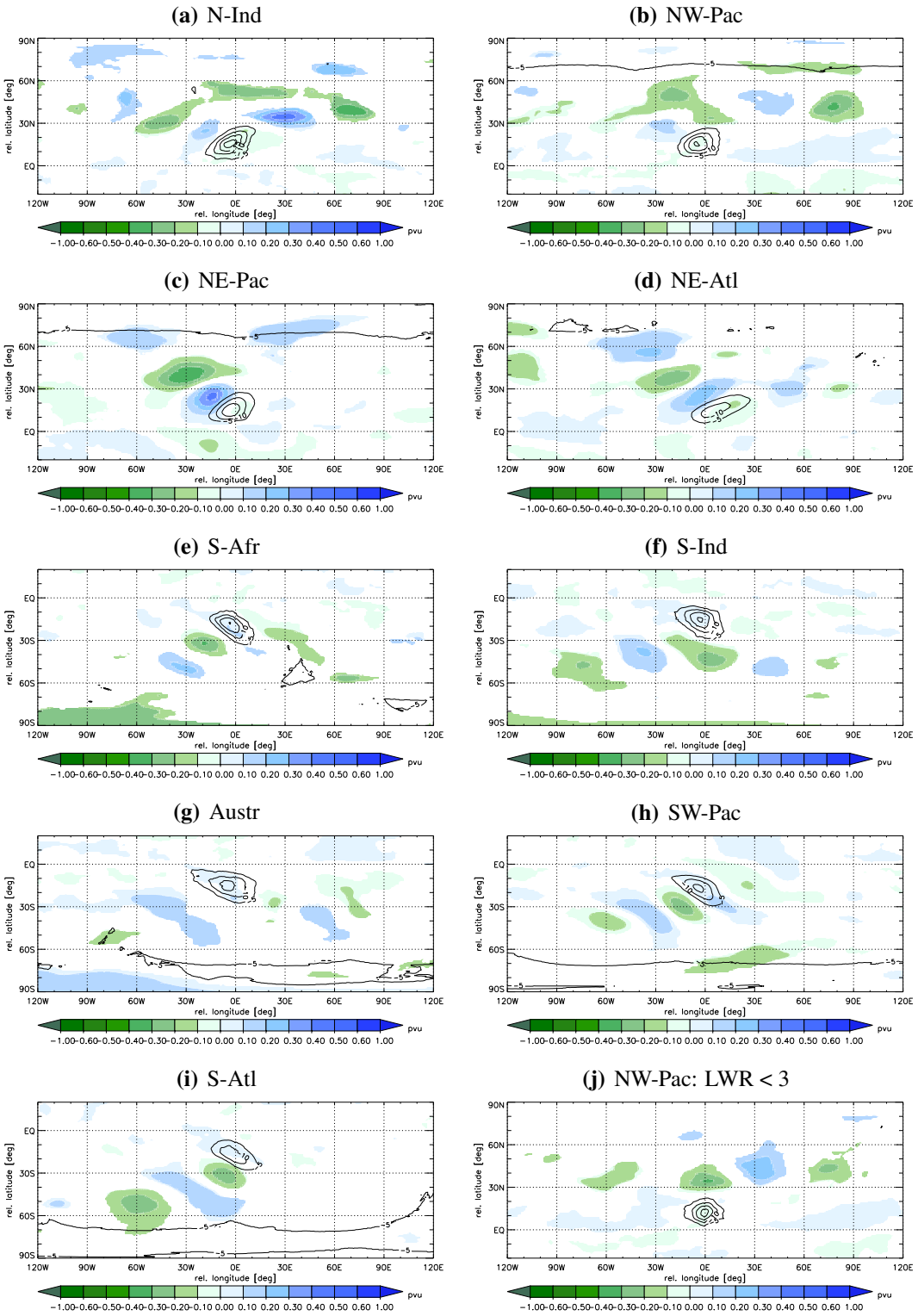

Figure 12.1: Composites of statistically significant (95% level) VAPV anomalies [PVU] (shaded) and negative T_b anomalies [°K] (lines) less than -5 K (indicator for the mean TP) for TP episodes with maximum LWR value of 3 or more in the (a) N-Ind, (b) NW-Pac, (c) NE-Pac, (d) NE-Atl, (e) S-Afr, (f) S-Ind, (g) Austr, (h) SW-Pac, (i) S-Atl region and (j) for TP episodes with maximum LWR value less than 3 in the NW-Pac region during boreal winter (October to March) within the TP investigation period. Regions are defined in Fig. 9.1a.

In contrast to these regions, the NW-Pac composite (Fig. 12.1b) is dominated by downstream development, i.e. a distinct wave like structure of positive and negative PV anomalies is found east of the TP. This signal is even more pronounced considering cloud bands in the NW-Pac with low LWR values (less than 3) in Fig. 12.1j. These observations are similar to circulation anomalies found in a study of Kiladis and Weickmann (1997, their Fig. 4b) in relation to enhanced convection in the western tropical Northwest Pacific. According to these authors, it is assumed that divergent outflow from the region of enhanced convection leads to the generation of a subtropical anticyclone, which acts as a Rossby wave source, i.e. eastward propagating midlatitude wave trains are generated. Lagged relationships suggest that these circulation anomalies are strongest after the convection maximized, which implies that the circulation is forced by the convection (Kiladis and Weickmann 1997).
In the N-Ind region (Fig. 12.1a) upstream as well as downstream developments are seen in association with TP occurrence, which indicates that some of the TPs are related to disturbances from the extratropics and some are the result of equatorial heating anomalies, as described above, which induce circulation anomalies downstream over the western North Pacific. The PV anomalies in relation to TPs over Australia show a positive anomaly in the midlatitudes to the Southwest of the TP, pointing to a wave disturbance in the midlatitudes with a northeast-southwest orientation, which is observed in a similar way in the S-Atl and SW-Pac regions (see also Kiladis and Weickmann 1997, their Fig. 2c). However, in this region there is no trough at low-latitudes that can directly be involved in TP formation as in e.g. the SW-Pac or NE-Pac regions. Kiladis and Weickmann (1997) describe that the upper-level circulations associated with convection over Australia are dominated by signals of outflow into Asian jet wave trains. Looking at circulation anomalies in the NH in relation with TPs over Australia a similar pattern is obtained in this work (not shown).

Fig. 12.1 reveals that in the majority of the regions cold clouds associated with TPs are a result of equatorward propagating Rossby wave trains. This is, in some regions, in contrast to the distinction between transient convection in regions with mean easterly and westerly winds over the equator made by e.g. Kiladis and Weickmann (1997). They argued that convection in regions of mean upper easterly winds are associated with patterns of meridional outflow into subtropical anticyclones and in regions of mean westerly winds with troughs at low latitudes. In regions with mean easterly winds over the equator (see Fig. 4.1) this idea appears to be only true for circulation anomalies in relation to TPs in the NW-Pac and partly in the N-Ind region. It is suggested that these differences arise from the implementation of the LWR criterion (see Sec. 3.2) in the TP identification routine that requires an elongated shape of the cold cloud anomalies. This idea is confirmed by looking at composites of upper circulation anomalies based on TP episodes with LWR values less than 3 (as shown for the NW-Pac in Fig. 12.1). These composites generally show enhanced downstream development. Consequently, elongated cloud bands appear to be the result of cloud anomalies induced by an transient upper-level troughs from the extratropics despite the mean upper easterlies.

	N-Ind	NW-Pac	NE-Pac	NE-Atl	S-Afr	S-Ind	Austr	SW-Pac	S-Atl
Oct.-March	0.9%	2.6%	18.1%	24.0%	3.4%	1.4%	1.8%	10.9%	8.7%
April-Sept.	0.9%	8.8%	19.1%	9.8%	6.7%	2.9%	3.9%	5.5%	8.5%

Table 12.1: Percentage of TP events in the vicinity (within -15° and +10° relative to the southern-most point of a detected TP) of a detected intrusion event at the same analysis time. Regions are defined in Fig. 9.1a.

Finally, the TP occurrence is briefly compared with the intrusion climatology, described in the first part of this thesis, in the following way: All intrusion events are counted that occur at the same time and in the same hemisphere within -15° and +10° relative to the southern-most point of a detected TP. It has to be mentioned that due to the different temporal resolution of the CLAUS and ERA-40 data sets (see Chap. 2), only every second analysis time of the CLAUS data set is considered. In Tab. 12.1 the percentage of TPs with an intrusion system in the vicinity are listed. The greatest percentages of 24% is found in the NE-Atl, which means that nearly every fourth TP event coincides with an intrusion event. High values are also found in the NE-Pac, SW-Pac and S-Atl regions. Note that these calculations consider TP and intrusion events instead of episodes. It is assumed that the portion of TPs near an intrusion would increase looking at episodes or using time lags between the detection of both phenomena. However, these findings are a further evidence that convection is activated by equatorward propagating troughs from the extratropics preferentially in regions with mean upper westerly flow over the equator.

13 Conclusions

13.1 Summary

13.1.1 Identification and climatology of troughs at low latitudes

In the first part of this thesis a novel climatology of upper-level troughs at low-latitudes was presented. These troughs are a common feature of the tropical upper troposphere and they are important due to their impacts on global momentum and moisture transports. The latter occasionally leads to heavy rainfall events in the Tropics or subtropics. The climatology of low-latitude troughs was constructed on the basis of a novel algorithm based upon vertical averages of the upper-tropospheric PV field. This way the detection is less sensitive to seasonal variations and only responds to intense troughs with coherent signals throughout the upper troposphere in contrast to prior studies. Continuous regions between 17° North and South with PV values of |2 PVU| or more are defined as intrusion events. The detected systems were tracked and attributes such as lifetime, vertical depth and horizontal tilt were assessed. Applying the algorithm to the ERA-40 reanalysis data from 1980 to 2001, a 22-year intrusion climatology was constructed. The resulting climatology reveals that intrusion occurrence is confined to the Pacific and Atlantic Oceans in both hemispheres. During boreal winter the absolute maximum in intrusion frequency of 12% is found over the eastern subtropical North Atlantic followed by the eastern South Pacific. In boreal summer the geographical distribution pattern is quite similar, but intrusion activity is generally reduced with the exception of the central North Pacific, where long-lived, shallow and strongly tilted systems frequently occur. The over-all geographical distribution and seasonal variations reflect the previously documented relation to mean westerly winds in the low-latitude upper troposphere. The mean lifetime of an intrusion system is nearly two days with a maximum in summer in both hemispheres. The vertical depth is on average larger during winter

and in the Southern Hemisphere. The majority of intrusion systems are positively tilted, i.e. southwest-northeast orientated in the NH and northwest-southeast in the SH. The detection is sensitive to the chosen latitudinal and VAPV thresholds with biggest effects on frequency and seasonality, while the geographical distribution is rather robust.
Inter-annual variations of intrusion frequency in boreal winter show a clear association with the El Niño-Southern Oscillation (ENSO): Over the North Pacific, negative correlations with the Niño3.4-index of -0.83 are directly related to the eastward shift of the tropical convection maximum and the associated wind changes, i.e. a weakening of the upper-tropospheric "westerly duct" over the tropical eastern Pacific and an eastward extension of the Pacific jet stream. Statistically significant positive correlations between the atmospheric Southern Oscillation index and intrusions numbers over the North Atlantic of -0.86 and over the South Atlantic of -0.7, however, must be the result of teleconnections, which lead to opposite changes in the mean upper wind field over the neighbouring ocean basin. In addition intrusion frequency over the North Atlantic shows a positive correlation to the North Atlantic Oscillation (NAO) of +0.4 (not statistically significant). The link between intrusion activity and ENSO is less pronounced in the South Pacific region and in summer.
With the help of composite studies the typical evolution upstream of a PV intrusion was investigated. For intrusions in the north-east Atlantic five days prior to intrusion detection a Rossby wave train was found upstream reaching from the north-eastern Pacific across North America. At the same time a northwest-southeast oriented dipole with a large PV reservoir over the North Atlantic and a negative anomaly, possibly indicative of a blocking, over Europe are observed. In the following days the Rossby wave intensifies and approaches the rather stationary dipole from the west. A negative PV anomaly appears east of the approaching Rossby wave, which explosively amplifies and helps to move air with high PV values from the PV reservoir toward low latitudes. This leads to a quick intensification of the positive PV anomaly, which later becomes the intrusion system. During the intrusion occurrence the upper-tropospheric PV anomaly field displays a meridional tripole structure with the northern two nodes reflecting a positive phase of the NAO as has been found in earlier work.
In the remaining regions a similar south-eastward propagating Rossby wave train is found upstream in the storm track region up to six days prior to intrusion occurrence. However, the large PV reservoir and the PV ridgeI were not found in these regions.
Composite analysis of meridional moisture flux anomalies associated with intrusion systems over the tropical north-eastern Atlantic show positive values with maxima between 750 and 500 hPa on the eastern flank of the wave disturbance. The intensity of the anomalous moisture flux depends on the vertical extension of the intrusion systems. Upstream, in the region of the North Atlantic storm track considerable anomalous transport of water vapour towards the pole can be noticed as well, which is, however, most pronounced in the lower troposphere (1000 to 800 hPa). These areas might be related to the Warm Conveyor Belt of an extratropical cyclone. Composites for intrusions in other regions are similar except for the north-eastern Pacific, where the poleward moisture fluxes are most pronounced in the lower troposphere.

13.1.2 Identification and climatology of tropical plumes

In the second part of this thesis a novel climatology of Tropical Plumes (TPs) is presented. Tropical Plumes are bands of high and mid-level clouds that often develop along the eastern flank of low-latitudes troughs and extent from the Tropics into the Subtropics and even into midlatitudes. They are important e.g. due to their effects on the global radiation budget. Previous TP studies were based on a visual inspection of infra-red satellite images and were therefore quite elaborate with respect to climatological investigations.

In this study a first objective identification algorithm has been developed that allows a flexible and quick processing of large datasets. The new algorithm was applied to the 10.8 μm brightness temperatures (T_b) of the Cloud Archive User Service (CLAUS), which provides global data on a uniform latitude-longitude grid at a spatial resolution of 0.5 by 0.5 degrees and a temporal resolution of three hours for the time period July 1983 to June 2006.

Following the classical definition by McGuirk et al. (1987) TPs were defined as extended bands (length > 2000 km) with BT anomalies below -30 K that cross 15° North or South. The detected systems were tracked in time based on spatial overlap. This way TP episodes were defined and attributes such as lifetime and horizontal tilt were determined. Additionally a criterion for the elongatedness of TP has been developed, which is based on the length-to-width ratio (LWR) of the smallest rectangle that contains the TP. Finally, only those TP events are retained that are part of a TP episode with a maximum LWR value of 3 or more.

The resulting winter (Oct.-March) climatology reveals that TP occurrence is largely confined to the oceanic regions with the main maximum located over the Central South Pacific close to the South Pacific convergence zone (SPCZ). Further TP frequency maxima are found over the eastern parts of the North Pacific and North Atlantic and over the South Atlantic near the South Atlantic convergence zone (SACZ). In summer (April-Sep.) the geographical distribution of TP occurrence is similar, although the TP frequency is generally reduced except for the Bay of Bengal and the Northwest Pacific. TP episodes last nearly one and a half day on average. Over Australia the most persistent TP episodes are detected during austral summer with a mean duration of nearly two and a half days. In this region even more than 4% of all TPs persist 10 days or longer. Most of the detected TPs are positively (negatively) tilted in the NH (SH), which means that they are southwest-northeast (northwest-southeast) orientated.

The TP identification algorithm is sensitive to the implementation of the LWR criterion in such a way that TP frequencies are more strongly reduced in regions where circularly shaped cloud structures are predominant, while the overall geographical distribution is rather robust.

A long-term trend analysis reveals a significant downward trend in TP occurrence in most regions, which appears to be a technical artefact caused by limb darkening due to changes in the satellite viewing geometries (Evan et al. 2007).

Inter-annual variations in TP frequency are related to ENSO, primarily over the Pacific

and Indian Oceans and over Australia with a maximum correlation with the Niño3.4 index of -0.88 found over the Northwest Pacific.
Based on composite analysis, two main conditions for TP genesis are detected in the upper-tropospheric circulation. While TP development for example in the North Atlantic and North Pacific regions is linked to the propagation of extra-tropical upper-level troughs into low latitudes, in the North Indian Ocean and Northwest Pacific tropical convective processes related to tropical heating anomalies are mainly responsible for TP formation.
Finally, the TP occurrence was briefly compared with the intrusion climatology. The greatest percentages of 24.0% and 18.1% of TP events coinciding with a intrusion event were found over the North Atlantic and the North Pacific during boreal winter. This is a further evidence that tropical convection in these regions is preferentially forced by intrusions of stratospheric air into the tropical troposphere.

13.2 Discussion and Rèsumè

The results of this thesis have been discussed in detail in comparison to other research results at the end of each chapter. Here only those results are highlighted again that are most important, most interesting, most surprising and/or deserve further research.
The new climatology of low-latitude troughs constructed in this thesis largely confirms results of former studies in terms of location, seasonality and relation to mean winds in the tropical upper troposphere (e.g., Waugh and Polvani 2000). Looking at interannual variations, the strong relationship between ENSO and transient disturbances in the Northeast Pacific found in this work had already been documented in several former studies (e.g., Matthews and Kiladis 1999a, Abatzoglou and Magnusdottir 2006b).
A remarkable new result, however, is the strong correlation between intrusion frequencies over the North Atlantic and the Southern Oscillation index of -0.86, pointing to substantially more intrusions during El Niño winters. Such a strong correlation is exceptional regarding the great distance between both centres of action. This strong relationship is assumed to be the result of ENSO-induced changes in (i.) the spatial extent of the westerly duct over the tropical Atlantic, (ii) the strength and position of the subtropical jet and (iii) the frequency of wave disturbances reaching into the North Atlantic sector due to ENSO-related changes in the strength of the wave guide over the North Pacific. Further studies are needed to find out which of these processes contributes most to the strong association between intrusion frequencies over the North Atlantic and ENSO.

A great novelty of the algorithm developed here was the classification of intrusion systems by their vertical thickness. Based on several composite studies, it was shown that anomalies induced by disturbances with larger vertical extent are generally more pronounced. This confirms our initial expectation that the vertical thickness of an intrusion system can be used as an indicator for its intensity. Looking at moisture flux anomalies, this also supports, in a climatological sense, the argument of Knippertz (2007) that only

intrusion systems that reach deep enough in the troposphere can initiate poleward moisture fluxes substantial enough to feed significant precipitation events.

The well-known linkage between the formation of troughs at low latitudes and east- and equatorward propagating coherent Rossby wave trains from the extratropics (e.g., Kiladis and Weickmann 1992a) was demonstrated here with the help of composite studies. Specifically for intrusions over the North Atlantic composites of upper circulation anomalies five days prior to intrusion detection revealed two previously undocumented coherent PV structures: A reservoir of high PV over the extratropical North Atlantic and a PV ridge over Europe. Based on numerical sensitivity experiments, Meier and Knippertz (2009) showed for a case study of heavy precipitation in the Cape Verde region (tropical Northwest Africa) that these two precursors were instrumental for the development of the unusually intense intrusions associated with the highly anomalous rainfalls. A combination of the present statistical study and the sensitivity study of Meier and Knippertz (2009) points to a high relevance of the PV dipole over the North Atlantic and Europe up to five days ahead of the event. These findings indicate a relatively high predictability of PV intrusions over the North Atlantic, when these precursors are present. It should be stressed that these results appear to be specific to the North Atlantic and cannot be applied to intrusion development in other regions due to the absence of such PV precursors in the corresponding composites. Further numerical studies are needed to better understand the main processes responsible for wave amplification in these regions.

A second main achievement of this thesis is the development of an objective algorithm for the detection of Tropical Plumes. Using this algorithm, the first ever long-term (23-year) objective climatology of Tropical Plumes was constructed, which is in broad agreement with previous TP climatologies (e.g., McGuirk et al. 1987, Kuhnel 1989, Iskenderian 1995), but statistically much more robust. The new TP climatology can now serve as a much improved basis for further investigations into this interesting phenomenon.
The analysis of the TP time series revealed a remarkable strong correlation (-0.88, Niño3.4) between TP frequencies in the Northwest Pacific and ENSO. A similar but weaker relationship to ENSO in this region had already been documented in prior studies, e.g. by Kuhnel (1989). However, over the eastern North Pacific and Atlantic the correlations between ENSO and TP occurrences are weak. In these regions, TP activity is mainly shifted zonally while the total numbers are nearly invariant between both phases of ENSO. This is in contrast to the ENSO-related changes in the intrusion time series and to some extent to the results of former studies based on much shorter time periods (e.g., McGuirk et al. 1987, Kuhnel 1989, Iskenderian 1995). The discrepancy might be explained by differences in the seasonality between intrusion and TP activity: While in the North Atlantic TP activity is strongest in the transition seasons, intrusion frequencies maximize between December and January, the most active time of ENSO. However, there are other possible reasons such as differences in the moisture availability and poleward moisture transport between both phases of ENSO.

Another unexpected result are the upper circulation anomalies associated with Tropical Plume occurrence. Based on composites it was shown that the elongated TP cloud bands are associated with transient upper-level troughs from the extatropics even in regions with mean upper easterly winds in the Tropics. This is inconsistent with the linear theory of stationary Rossby waves (Hoskins and Ambrizzi 1993), which requires westerlies for wave propagation. It is not clear whether there are occasional sufficiently persistent westerly episodes on synoptic or intraseasonal time scales or whether the linear Rossby wave theory is too simplistic to describe the wave propagation in some of these cases.

13.3 Future research aspects

The new identification algorithms for low-latitude disturbances and Tropical Plumes and the associated climatologies form the basis for numerous follow-up studies, which deepen the analysis presented here or add new research aspects.

- For example, Knippertz and Martin (2007a) revealed that the midlevel moisture transport from the deep Tropics is often too slow to produce significant rainfall in the outer Tropics or subtropics. They suggest that such events require a persistent disturbance or two disturbances in short succession. The intrusion climatology constructed in this thesis can serve as a basis for statistical investigations of heavy subtropical rainfall events in relation to trough occurrence to verify this idea.

- Recently a new reanalysis dataset has been released from the ECMWF, called ERA-Interim, which covers the time period from 1979 to present (Dee et al. 2011). Overall, various difficulties encountered in the production of ERA-40 have been improved in this data set. However, over tropical regions, the changes between both data sets are minor. So it is assumed that ERA-40 is still an appropriate data set for the construction of a climatology of low-latitude troughs. Trough detection on the basis of the ERA-Interim data set would be interesting due to comparison reasons and to extend the investigation period.

- The reasons for the discrepancy in the seasonality between TP and intrusion activity as described just above are not clear yet. Differences in the moisture availability and fluxes are possible causes, which could be investigated on the basis of composites of water vapour or moisture flux anomalies constructed for the different seasons.

- Matthews and Kiladis (1999b) showed that in winter equatorward propagating, transient waves over the central North Pacific are influenced by the Madden-Julian oscillation (MJO, see Madden and Julian 1994 for a review). This signal is also seen in the tropical convection, that is induced by these waves. It would be interesting to see if there is a similar relationship between the MJO and the intrusion and TP frequencies detected in this region or if in another region intrusion or TP frequencies are affected by the different phases of the MJO.

- Due to the artificial long-term trend caused by limb darkening (Chap. 11) in the TP time series, the TP identification algorithm will be applied to the more homogeneous Patmos-X data set. The novel TP climatology will be compared with the TP climatology based on the CLAUS data set and long-term trends are calculated.
- Based on the TP climatology the impact of TPs on the global radiation budget would be interesting to estimate.
- At the end a further interesting point in relation with the intrusion climatology based on the modified algorithm (see Chap. 4.2): The inter-annual variability of the intrusion frequencies detected over the North Atlantic with the modified algorithm are less correlated with ENSO (+0.61, Niño3.4) and more with the NAO (+0.57). Furthermore, this time series shows two outstanding maxima in the winters 1982/83 and 1991/91. These winters follow two major volcano eruptions in spring (the El Chinchòn in April 1982, Mexico and Mount Pinatubo in June 1991, Philippines). It is already known that aerosol heating increases the Equator-Pole temperature gradient, which leads to a stronger polar vortex and an amplified NAO (e.g., Robock 2000). It would be interesting to analyse the modified intrusion climatology in this context.

References

Abatzoglou, J. T. and G. Magnusdottir, 2006a: Opposing Effects of Reflective and Non-reflective Planetary Wave Breaking on the NAO. *J. Atmos. Sci.*, **63**, 3448–3457.

— 2006b: Planetary Wave Breaking and Nonlinear Reflection: Seasonal Cycle and Interannual Variability. *J. Climate*, **19**, 6139–6152.

Ackerman, S. A., W. Smith, H. Revercomb, and J. Spinhirne, 1990: The 27-28 October 1986 FIRE IFO Cirrus Case Study: Spectral Properties of Cirrus Clouds in the 8-12 μm Window. *Mon. Wea. Rev.*, **118**, 2377–2388.

Allen, G., G. Vaughan, D. Brunner, P. T. May, W. Heyes, P. Minnis, and J. K. Ayers, 2009: Modulation of tropical convection by breaking Rossby waves. *Q.J.R. Meteorol. Soc.*, **135**, 125–137.

Ambrizzi, T., B. J. Hoskins, and H. H. Hsu, 1995: Rossby-wave propagation and teleconnection patterns in the austral winter. *J. Atmos. Sci.*, **52**, 3661–3672.

Appenzeller, C., H. C. Davies, and W. A. Norton, 1996: Fragmentation of stratospheric intrusions. *J.Geophys.Res.-Atmos.*, **101**, 1435–1456.

Arkin, P. A., 1982: The Relationship Between Interannual Variability In the 200 Mb Tropical Wind-field and the Southern Oscillation. *Mon. Wea. Rev.*, **110**, 1393–1404.

Bao, J. W., S. A. Michelson, P. J. Neiman, F. M. Ralph, and J. M. Wilczak, 2006: Interpretation of enhanced integrated water vapor bands associated with extratropical cyclones: Their formation and connection to tropical moisture. *Monthly Weather Review*, **134**, 1063–1080.

Barnston, A. G. and R. E. Livezey, 1987: Classification, Seasonality and Persistence of Low-frequency Atmospheric Circulation Patterns. *Monthly Weather Review*, **115**, 1083–1126.

Bates, J. J., D. L. Jackson, F. M. Breon, and Z. D. Bergen, 2001: Variability of tropical upper tropospheric humidity 1979-1998. *Journal of Geophysical Research-atmospheres*, **106**, 32271–32281.

Benedict, J. J., S. Lee, and S. B. Feldstein, 2004: Synoptic view of the North Atlantic Oscillation. *Journal Of The Atmospheric Sciences*, **61**, 121–144.

Bengtsson, L., K. I. Hodges, and S. Hagemann, 2004: Sensitivity of the ERA40 reanalysis to the observing system: determination of the global atmospheric circulation from reduced observations. *Tellus Series A-Dynamic Meteorology And Oceanography*, **56**, 456–471.

Blackwell, K. G., 2000: Tropical plumes in a barotropic model: A product of rossby wave generation in the tropical upper troposphere. *Monthly Weather Review*, **128**, 2288–2302.

Brown, R. G. and C. D. Zhang, 1997: Variability of midtropospheric moisture and its effect on cloud-top height distribution during TOGA COARE. *Journal of the Atmospheric Sciences*, **54**, 2760–2774.

Browning, K. A., 1990: Organization of clouds and precipitation in extratropical cyclones. *Newton, C., Holopainen, E. (Eds.), Extratropical Cyclones: The Erik H. Palmén Memorial Volume. American Meteorological Society, Boston, MA*, 129–153.

Brönnimann, S., 2007: Impact of El Nino Southern Oscillation on European climate RID A-5737-2008. *Reviews of Geophysics*, **45**, RG3003.

Cau, P., J. Methven, and B. Hoskins, 2005: -Representation of dry tropical layers and their origins in ERA-40 data. *Journal Of Geophysical Research-Atmospheres*, **110**, D06110.

— 2007: Origins of dry air in the tropics and subtropics. *Journal of Climate*, **20**, 2745–2759.

Chang, C.-P. and K. M. Lau, 1982: Short-Term Planetary-Scale Interactions over the Tropics and Midlatitudes during Northern Winter. Part I: Contrasts between Active and Inactive Periods. *Monthly Weather Review*, **110**, 933–946.

Chang, P., L. Ji, and H. Li, 1997: A decadal climate variation in the tropical Atlantic Ocean from thermodynamic air-sea interactions. *Nature*, **385**, 516–518.

Chiang, J. C. H. and D. J. Vimont, 2004: Analogous Pacific and Atlantic meridional modes of tropical atmosphere-ocean variability. *Journal of Climate*, **17**, 4143–4158.

Dee, D. P., S. M. Uppala, A. J. Simmons, P. Berrisford, P. Poli, S. Kobayashi, U. Andrae, M. A. Balmaseda, G. Balsamo, P. Bauer, P. Bechtold, A. C. M. Beljaars, L. van de Berg, J. Bidlot, N. Bormann, C. Delsol, R. Dragani, M. Fuentes, A. J. Geer, L. Haimberger, S. B. Healy, H. Hersbach, E. V. Holm, L. Isaksen, P. Kallberg, M. Koehler, M. Matricardi, A. P. McNally, B. M. Monge-Sanz, J. . J. Morcrette, B. . K. Park, C. Peubey, P. de Rosnay, C. Tavolato, J. . N. Thepaut, and F. Vitart, 2011: The ERA-Interim reanalysis: configuration and performance of the data assimilation system. *Quarterly Journal of the Royal Meteorological Society*, **137**, 553–597.

Eckhardt, S., A. Stohl, H. Wernli, P. Janes, C. Forster, and N. Spichtinger, 2004: A 15-Year Climatology of Warm Conveyor Belts. *Journal of Climate*, **17**, 218–237.

Eliassen, A. and E. Kleinschmidt, 1957: Dynamic Meteorology. *Handbuch der Physik*, **58**, 1–154.

Erickson, C. O. and J. S. Winston, 1972: Tropical Storm, Mid-Latitude Cloud-Band Connections and the Autumnal Buildup of the Planetary Circulation. *Journal of Ap-*

plied Meteorology, **11**, 23–36.

Ertel, H., 1942: Ein neuer hydrodynamischer Wirbelsatz. *Meteorologische Zeitschrift*, **52 (2)**, 277–281.

Evan, A. T., A. K. Heidinger, and D. J. Vimont, 2007: Arguments against a physical long-term trend in global ISCCP cloud amounts. *Geophysical Research Letters*, **34**, L04701.

Ferreira, R. N. and W. H. Schubert, 1999: The role of tropical cyclones in the formation of tropical upper-tropospheric troughs. *Journal of the Atmospheric Sciences*, **56**, 2891–2907.

Fink, A. H. and P. Knippertz, 2003: An extreme precipitation event in southern Morocco in spring 2002 and some hydrological implications. *Weather*, **58**, 377–387.

Froehlich, L. and P. Knippertz, 2008: Identification and global climatology of upper-level troughs at low latitudes. *Meteorologische Zeitschrift*, **17**, 565–573.

Garreaud, R. D., 2001: Subtropical cold surges: Regional aspects and global distribution. *International Journal of Climatology*, **21**, 1181–1197.

Gray, T. I. and P. F. Clapp, 1978: Interaction Between Low-latitude and High Latitude Cloud Bands As Recorded On Goes-1 Imagery. *Bulletin of the American Meteorological Society*, **59**, 808–809.

Hart, N. C. G., C. J. C. Reason, and N. Fauchereau, 2010: Tropical-Extratropical Interactions over Southern Africa: Three Cases of Heavy Summer Season Rainfall. *Monthly Weather Review*, **138**, 2608–2623.

Held, I. M., S. W. Lyons, and S. Nigam, 1989: Transients and the Extratropical Response To El-Niño. *Journal of the Atmospheric Sciences*, **46**, 163–174.

Hodges, K. I., D. W. Chappell, G. J. Robinson, and G. Yang, 2000: An improved algorithm for generating global window brightness temperatures from multiple satellite infrared imagery. *Journal Of Atmospheric And Oceanic Technology*, **17**, 1296–1312.

Hohberger, E., 2008: Development of an objective method for the identification of tropical plumes in infra-red satellite imagery. *Diploma thesis in german, University of Mainz, Germany, University of Mainz, Germany*, 75 p.

Horel, J. D. and J. M. Wallace, 1981: Planetary-scale Atmospheric Phenomena Associated With the Southern Oscillation. *Monthly Weather Review*, **109**, 813–829.

Hoskins, B. J. and T. Ambrizzi, 1993: Rossby-Wave Propagation On A Realistic Longitudinally Varying Flow. *Journal Of The Atmospheric Sciences*, **50**, 1661–1671.

Hoskins, B. J. and D. J. Karoly, 1981: The Steady Linear Response of A Spherical Atmosphere To Thermal and Orographic Forcing. *Journal of the Atmospheric Sciences*, **38**, 1179–1196.

Hoskins, B. J., M. E. McIntyre, and A. W. Robertson, 1985: On the Use and Significance of Isentropic Potential Vorticity Maps. *Quarterly Journal of the Royal Meteorological Society*, **111**, 877–946.

Hurrell, J. W., 1995: Decadal Trends In the North-atlantic Oscillation - Regional Temperatures and Precipitation. *Science*, **269**, 676–679.

Inoue, T., 1987: A Cloud Type Classification With Noaa 7 Split-window Measurements. *Journal of Geophysical Research-atmospheres*, **92**, 3991–4000.

Iskenderian, H., 1995: A 10-Year Climatology of Northern Hemisphere Tropical Cloud Plumes and Their Composite Flow Patterns. *Journal of Climate*, **8**, 1630–1637.

Jones, C., D. E. Waliser, K. M. Lau, and W. Stern, 2004: The Madden-Julian oscillation and its impact on Northern Hemisphere weather predictability. *Monthly Weather Review*, **132**, 1462–1471.

Kalnay, E., M. Kanamitsu, R. Kistler, W. Collins, D. Deaven, L. Gandin, M. Iredell, S. Saha, G. White, J. Woollen, Y. Zhu, M. Chelliah, W. Ebisuzaki, W. Higgins, J. Janowiak, K. C. Mo, C. Ropelewski, J. Wang, A. Leetmaa, R. Reynolds, R. Jenne, and D. Joseph, 1996: The NCEP/NCAR 40-year reanalysis project. *Bulletin of the American Meteorological Society*, **77**, 437–471.

Kendall, M., 1975: Rank correlation methods. *4th ed. Charles Griffin, London*.

Kiladis, G. N., 1998: Observations of Rossby waves linked to convection over the eastern tropical Pacific. *Journal Of The Atmospheric Sciences*, **55**, 321–339.

Kiladis, G. N. and S. B. Feldstein, 1994: Rossby-wave Propagation Into the Tropics In 2 Gfdl General-circulation Models. *Climate Dynamics*, **9**, 245–252.

Kiladis, G. N. and K. M. Weickmann, 1992a: Circutlation Anomalies Associated with Tropical Convection during Northern Winter. *Monthly Weather Review*, **120**, 1900–1923.

— 1992b: Extratropical Forcing of Tropical Pacific Convection during Northern Winter. *Monthly Weather Review*, **120**, 1924–1938.

— 1997: Horizontal structure and seasonality of large-scale circulations associated with submonthly tropical convection. *Monthly Weather Review*, **125**, 1997–2013.

Knippertz, P., 2005: Tropical-extratropical interactions associated with an Atlantic tropical plume and subtropical jet streak. *Monthly Weather Review*, **133**, 2759–2776.

— 2007: Tropical-extratropical interactions related to upper-level troughs at low latitudes. *Dynamics Of Atmospheres And Oceans*, **43**, 36–62.

Knippertz, P. and A. H. Fink, 2009: Prediction of Dry-Season Precipitation in Tropical West Africa and Its Relation to Forcing from the Extratropics. *Weather and Forecasting*, **24**, 1064–1084.

Knippertz, P. and J. E. Martin, 2005: Tropical plumes and extreme precipitation in subtropical and tropical West Africa. *Quarterly Journal Of The Royal Meteorological Society*, **131**, 2337–2365.

— 2007a: A Pacific moisture conveyor belt and its relationship to a significant precipitation event in the semiarid southwestern United States. *Weather And Forecasting*, **22**, 125–144.

— 2007b: The role of dynamic and diabatic processes in the generation of cut-off lows over Northwest Africa. *Meteorology And Atmospheric Physics*, **96**, 3–19.

Knippertz, P. and H. Wernli, 2010: A Lagrangian Climatology of Tropical Moisture Exports to the Northern Hemispheric Extratropics. *Journal of Climate*, **23**, 987–1003.

Kodama, Y., 1992: Large-scale Common Features of Subtropical Precipitation Zones (the Baiu Frontal Zone, the Spcz, and the Sacz) .1. Characteristics of Subtropical Frontal Zones. *Journal of the Meteorological Society of Japan*, **70**, 813–836.

Kodama, Y. M., 1993: Large-Scale Common Features Of Subtropical Convergence

Zones (The Baiu Frontal Zone, The Spcz, And The Sacz) .2. Conditions Of The Circulations For Generating The Stczs. *Journal Of The Meteorological Society Of Japan*, **71**, 581–610.

Kossin, J. P. and D. J. Vimont, 2007: A more general framework for understanding Atlantic hurricane variability and trends. *Bulletin of the American Meteorological Society*, **88**, 1767–+.

Kuhnel, I., 1989: Tropical-extratropical cloudband climatology based on satellite data. *International Journal of Climatology*, **9**, 441–463.

L'Heureux, M. L. and D. W. J. Thompson, 2006: Observed relationships between the El Nino-Southern Oscillation and the extratropical zonal-mean circulation. *Journal of Climate*, **19**, 276–287.

Li, Y. and N.-C. Lau, 2011: Impact of ENSO on the Atmospheric Variability over the North Atlantic in Late Winter – Role of Transient Eddies. *J. Climate*, –.

Liebmann, B. and D. L. Hartmann, 1984: An Observational Study of Tropical-Midlatitude Interaction on Intraseasonal Time Scales during Winter. *Journal of Atmospheric Sciences*, **41**, 3333–3350.

Madden, R. A. and P. R. Julian, 1994: Observations of the 40-50-day Tropical Oscillation - A Review. *Monthly Weather Review*, **122**, 814–837.

Mann, H. B., 1945: Nonparametric Tests Against Trend. *Econometrica*, **13**, 245–259.

Martius, O., C. Schwierz, and H. C. Davies, 2007: Breaking Waves at the Tropopause in the Wintertime Northern Hemisphere: Climatological Analyses of the Orientation and the Theoretical LC1/2 Classification. *Journal of the Atmospheric Sciences*, **64**, 2576–2592.

Massacand, A. C., H. Wernli, and H. C. Davies, 2001: Influence of Upstream Diabatic Heating upon an Alpine Event of Heavy Precipitation. *Monthly Weather Review*, **129**, 2822–2828.

Matthews, A. J. and G. N. Kiladis, 1999a: Interactions between ENSO, transient circulation, and tropical convection over the Pacific. *Journal Of Climate*, **12**, 3062–3086.

— 1999b: The tropical-extratropical interaction between high-frequency transients and the Madden-Julian oscillation. *Monthly Weather Review*, **127**, 661–677.

May, W. and L. Bengtsson, 1998: The signature of ENSO in the Northern Hemisphere midlatitude seasonal mean flow and high-frequency intraseasonal variability. *Meteorology and Atmospheric Physics*, **69**, 81–100.

McGuirk, J. P., A. H. Thompson, and J. R. Schaefer, 1988: An Eastern Pacific Tropical Plume. *Monthly Weather Review*, **116**, 2505–2521.

McGuirk, J. P., A. H. Thompson, and N. R. Smith, 1987: Moisture Bursts over the Tropical Pacific Ocean. *Monthly Weather Review*, **115**, 787–798.

McGuirk, J. P. and D. J. Ulsh, 1990: Evolution of Tropical Plumes in VAS Water Vapor Imagery. *Monthly Weather Review*, **118**, 1758–1766.

Mecikalski, J. R. and G. J. Tripoli, 1998: Inertial Available Kinetic Energy and the Dynamics of Tropical Plume Formation. *Monthly Weather Review*, **126**, 2200–2216.

Meier, F. and P. Knippertz, 2009: Dynamics and Predictability of a Heavy Dry-Season Precipitation Event over West Africa-Sensitivity Experiments with a Global Model.

Monthly Weather Review, **137**, 189–206.

Moore, R. W., O. Martius, and H. C. Davies, 2008: Downstream development and Kona low genesis. *Geophysical Research Letters*, **35**, L20814.

Neiman, P. J., F. M. Ralph, G. A. Wick, J. D. Lundquist, and M. D. Dettinger, 2008: Meteorological characteristics and overland precipitation impacts of atmospheric rivers affecting the West Coast of North America based on eight years of SSM/I satellite observations. *Journal of Hydrometeorology*, **9**, 22–47.

Peixoto, J. P. and A. Oort, 1992: *Physics of Climate*. American Institute of Physics, New York.

Postel, G. A. and M. H. Hitchman, 1999: A climatology of Rossby wave breaking along the subtropical tropopause, journal = Journal Of The Atmospheric Sciences. *Journal Of the Atmospheric Science*, **56**, 359–373.

Ralph, F. M., P. J. Neiman, and G. A. Wick, 2004: Satellite and CALJET aircraft observations of atmospheric rivers over the eastern north pacific ocean during the winter of 1997/98. *Monthly Weather Review*, **132**, 1721–1745.

Robock, A., 2000: Volcanic eruptions and climate. *Reviews Of Geophysics*, **38**, 191–219.

Rossby, C. G., 1940: Planetary flow patterns in the Atmosphere. *Quarterly Journal Of The Royal Meteorological Society*, **66**, 68–97.

Rubin, S., B. Ziv, and N. Paldor, 2007: Tropical Plumes over Eastern North Africa as a Source of Rain in the Middle East. *Monthly Weather Review*, **135**, 4135–4148.

Ryoo, J.-M., D. W. Waugh, and A. Gettelman, 2008: Variability of subtropical upper tropospheric humidity. *Atmospheric Chemistry and Physics Discussions*, **8**, 1041–1067.

Saunders, R. W. and K. T. Kriebel, 1988: An Improved Method For Detecting Clear Sky and Cloudy Radiances From Avhrr Data. *International Journal of Remote Sensing*, **9**, 123–150.

Schwierz, C., M. Croci-Maspoli, and H. C. Davies, 2004: Perspicacious indicators of atmospheric blocking. *Geophysical Research Letters*, **31**, L06125.

Seager, R., N. Harnik, Y. Kushnir, W. Robinson, and J. Miller, 2003: Mechanisms of hemispherically symmetric climate variability. *Journal of Climate*, **16**, 2960–2978.

Slingo, J. M., 1998: Extratropical forcing of tropical convection in a northern winter simulation with the UGAMP GCM. *Quarterly Journal Of The Royal Meteorological Society*, **124**, 27–51.

Steenburgh, W. J. and C. F. Mass, 1994: The Structure and Evolution of A Simulated Rocky-mountain Lee Trough. *Monthly Weather Review*, **122**, 2740–2761.

Straus, D. M. and J. Shukla, 2002: Does ENSO force the PNA? *Journal of Climate*, **15**, 2340–2358.

Strong, C. and G. Magnusdottir, 2008: Tropospheric Rossby wave breaking and the NAO/NAM. *Journal of the Atmospheric Sciences*, **65**, 2861–2876.

Thepenir, R.-M. and D. Cruette, 1981: Formation of Cloud Bands Associated with the American Subtropical Jet Stream and Their Interaction with Midlatitude Synoptic Disturbances Reaching Europe. *Monthly Weather Review*, **109**, 2209–2220.

Thorpe, A. J., H. Volkert, and D. Heimann, 1993: Potential Vorticity of Flow along the

Alps. *Journal of the Atmospheric Sciences*, **50**, 1573–1590.

Tomas, R. A. and P. J. Webster, 1994: Horizontal And Vertical Structure Of Cross-Equatorial Wave-Propagation. *Journal Of The Atmospheric Sciences*, **51**, 1417–1430.

Trenberth, K. E., 1997: The definition of El Niño. *Bulletin of the American Meteorological Society*, **78**, 2771–2777.

Uppala, S., P. Kallberg, A. Hernandez, S. Saarinen, M. Fiorino, X. Li, K. Onogi, N. Sokka, U. Andrae, and V. Da Costa Bechtold, 2004: ERA-40: ECMWF 45-year reanalysis of the global atmosphere and surface conditions 1957-2002. *ECMWF Newsletter*, **101**, 2–21.

Vimont, D. J. and J. P. Kossin, 2007: The Atlantic Meridional Mode and hurricane activity. *Geophysical Research Letters*, **34**, L07709.

Vincent, D. G., 1994: The South-pacific Convergence Zone (SPCZ) - A Review. *Monthly Weather Review*, **122**, 1949–1970.

Wallace, J. M. and D. S. Gutzler, 1981: Teleconnections In the Geopotential Height Field During the Northern Hemisphere Winter. *Monthly Weather Review*, **109**, 784–812.

Waugh, D. W., 2005: Impact of potential vorticity intrusions on subtropical upper tropospheric humidity. *Journal Of Geophysical Research-Atmospheres*, **110**, D11305.

Waugh, D. W. and B. M. Funatsu, 2003: Intrusions into the tropical upper troposphere: Three-dimensional structure and accompanying ozone and OLR distributions. *Journal Of The Atmospheric Sciences*, **60**, 637–653.

Waugh, D. W. and L. M. Polvani, 2000: Climatology of intrusions into the tropical upper troposphere. *Geophysical Research Letters*, **27**, 3857–3860.

Webster, P. J. and J. R. Holton, 1982: Cross-Equatorial Response To Middle-Latitude Forcing In A Zonally Varying Basic State. *Journal Of The Atmospheric Sciences*, **39**, 722–733.

Weickmann, K. M., G. R. Lussky, and J. E. Kutzbach, 1985: Intraseasonal (30–60 Day) Fluctuations of Outgoing Longwave Radiation and 250 mb Streamfunction during Northern Winter. *Monthly Weather Review*, **113**, 941–961.

Wernli, H. and C. Schwierz, 2006: Surface Cyclones in the ERA-40 Dataset (1958-20019. Part I: Novel Identification Method and Global Climatology. *Journal of Atmospheric Sciences*, **63**, 2486–2507.

Wernli, H. and M. Sprenger, 2007: Identification and ERA-15 Climatology of Potential Vorticity Streamers and Cutoffs near the Extratropical Tropopause. *Journal of the Atmospheric Sciences*, **64**, 1569–1586.

Wiegand, L., 2008: Transport of stratospheric airmasses into the tropical troposphere - climatology and influence on the ozone budget. *Diploma thesis in German. University of Mainz.*

Woollings, T., B. Hoskins, M. Blackburn, and P. Berrisford, 2008: A new Rossby wave-breaking interpretation of the North Atlantic Oscillation. *Journal of the Atmospheric Sciences*, **65**, 609–626.

Wright, W. J., 1997: Tropical-extratropical cloudbands and Australian rainfall: 1. Climatology. *International Journal of Climatology*, **17**, 807–829.

Xie, S. P. and J. A. Carton, 2004: Tropical Atlantic variability: Patterns, mechanisms,

and impacts. *Earth's Climate: the Ocean-atmosphere Interaction*, **147**, Amer Geophys Union.

Xie, S. P. and S. G. H. Philander, 1994: A Coupled ocean-atmosphere model of relevance to the ITCZ in the eastern Pacific. *Tellus Series A-dynamic Meteorology and Oceanography*, **46**, MAX PLANCK INST METEOROL.

Yoneyama, K. and D. B. Parsons, 1999: A proposed mechanism for the intrusion of dry air into the Tropical Western Pacific region. *Journal of the Atmospheric Sciences*, **56**, 1524–1546.

Zhu, Y. and R. E. Newell, 1994: Atmospheric Rivers and Bombs. *Geophysical Research Letters*, **21**, 1999–2002.

— 1998: A proposed algorithm for moisture fluxes from atmospheric rivers. *Monthly Weather Review*, **126**, 725–735.

Ziv, B., 2001: A subtropical rainstorm associated with a tropical plume over Africa and the Middle-East. *Theoretical And Applied Climatology*, **69**, 91–102.

A Additional figures and tables

	Niño3.4	SOI	NAO	PNA	AMM	
					SST	WIND
N-Atl	0.09	-0.11	0.40	0.28	**-0.67**	-0.21
NE-Pac	-0.27	0.34	0.15	-0.22	0.28	0.01
S-Atl	0.16	-0.11	0.36	0.06	-0.31	0.12
SE-Pac	-0.12	0.03	0.24	-0.37	-0.18	-0.14

Table A.1: Correlation coefficients between regional intrusion frequencies (cp. Fig. 6.1) and different climate state indices based on boreal winter seasons from 1980/81 until 2000/01 (21 winters). Statistically significant (99% level) correlation coefficients are bold. For the correlation coefficients in the first two rows (Niño3.4 & SOI) the summer intrusion frequencies are considered. Regions are defined in Fig. 4.1a.

	Niño3.4	SOI	NAO	PNA
N-Ind	-0.14	-0.03	0.22	0.18
NW-Pac	**-0.62**	**0.63**	0.22	**-0.80**
NE-Pac	-0.42	0.37	0.46	0.25
NE-Atl	0.37	-0.46	0.15	0.16
S-Afr	-0.14	0.26	-0.04	-0.28
S-Ind	0.39	-0.41	0.33	0.48
Austr	0.29	-0.38	-0.03	**-0.68**
SW-Pac	-0.12	0.14	-0.10	**-0.60**
S-Atl	0.12	-0.36	0.30	-0.08

Table A.2: Correlation coefficients between regional TP frequencies (cp. 11.1) and several climate state indices based on time series of the boreal winter TP frequencies between 1983/84 and 2005/06 (23 winter). For the correlation coefficients in the first two rows (Niño3.4 and SOI) the summer TP frequencies are considered. Statistically significant correlations coefficients (99% level) are bold.

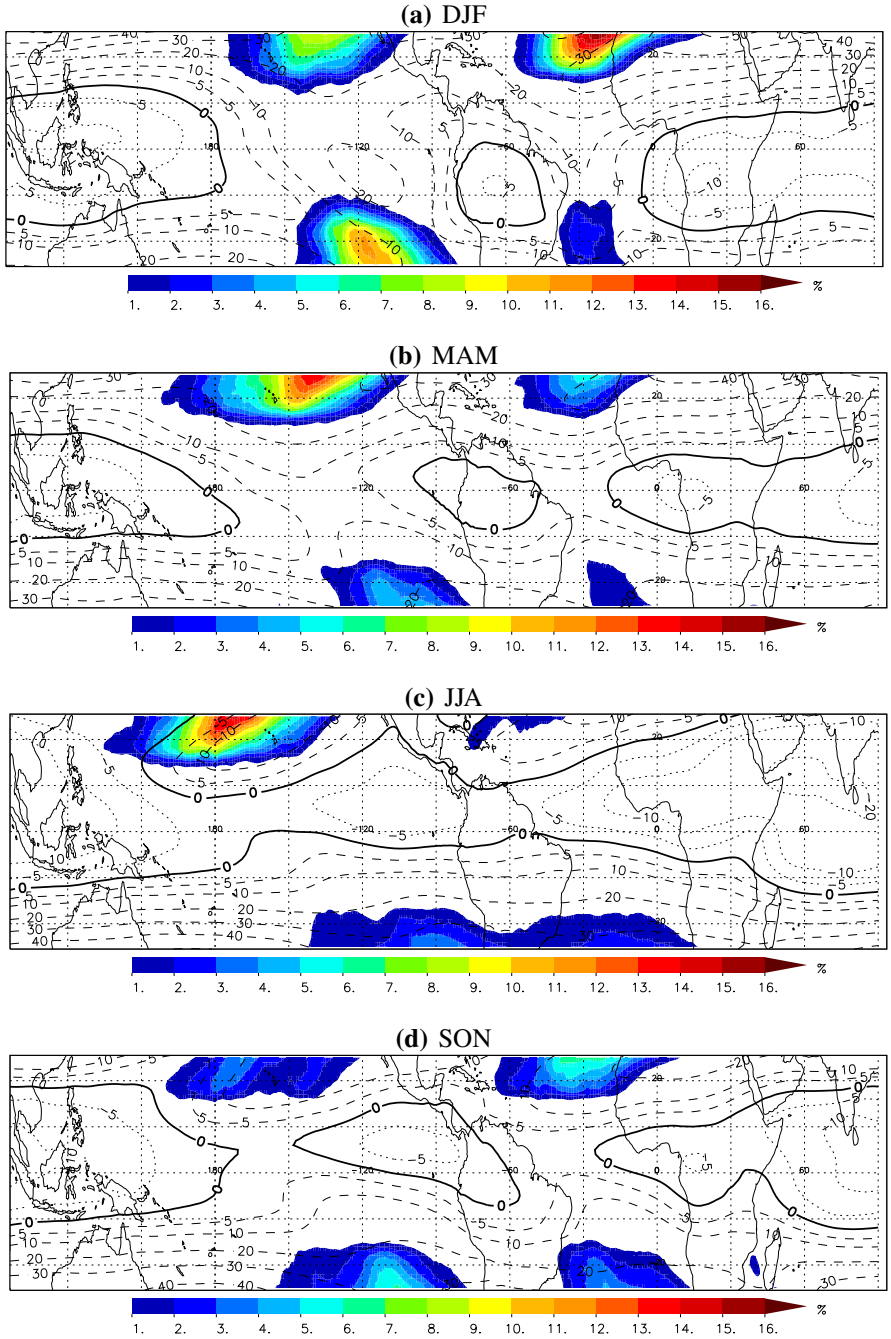

Figure A.1: Mean intrusion frequency [%] (shaded) and mean zonal wind at 200 hPa [m/s] (dashed contours for westerlies and dotted contours for easterlies with the zero contour in bold) averaged from (a) December to February, (b) March to May, (c) June to August and (d) September to November in the period 1980–2001.

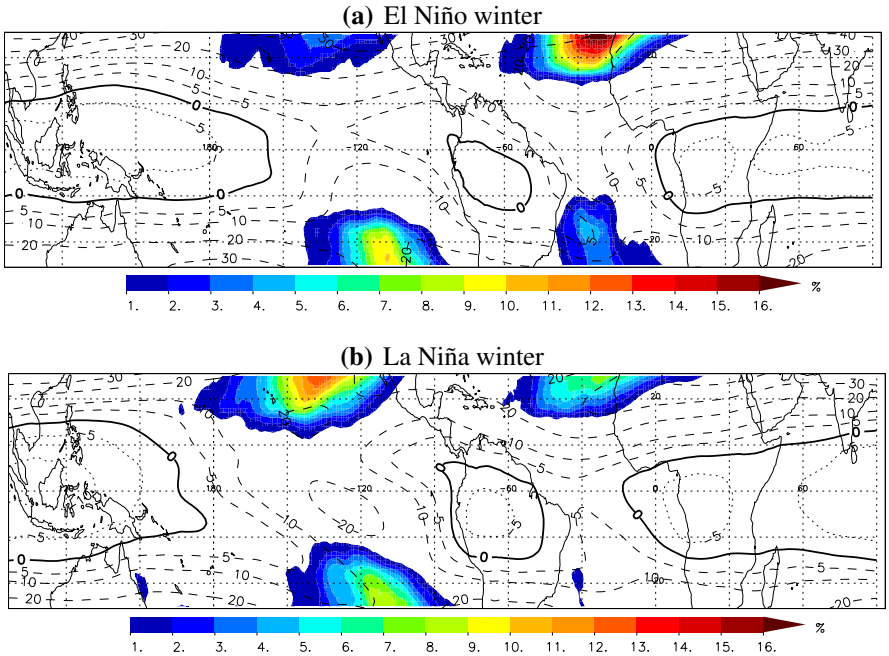

Figure A.2: Mean intrusion frequency [%] (shaded) and mean zonal wind at 200 hPa [m/s] (dashed contours for westerlies and dotted contours for easterlies with the zero contour in bold) for (a) the 6 El Niño and (b) 5 La Niña winter between 1980–2001. The classification of the ENSO winter is defined in 2.1.

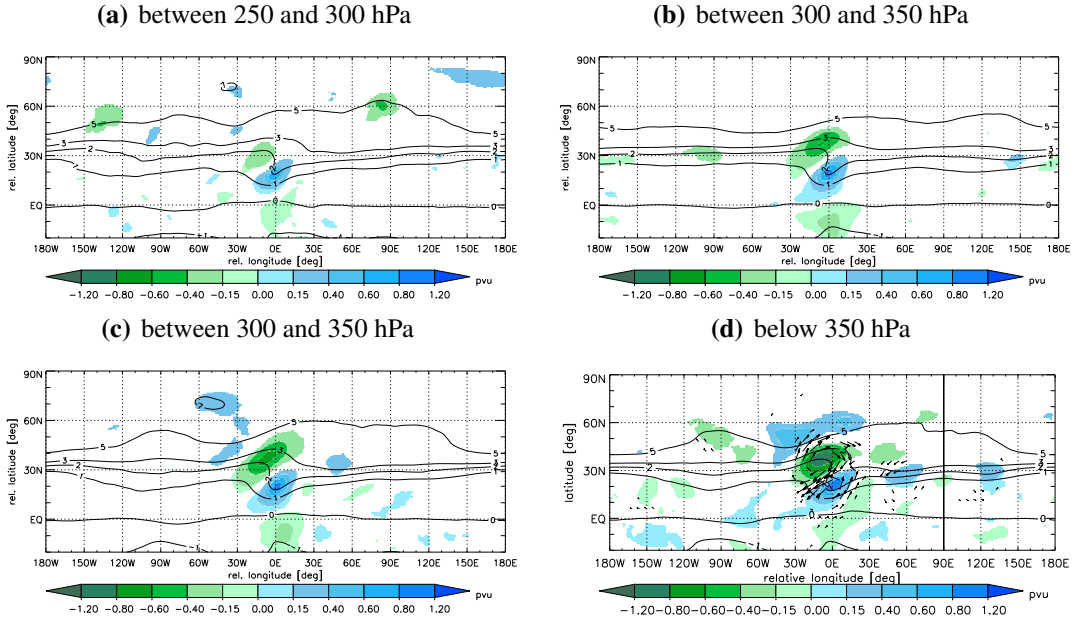

Figure A.3: Composite of statistically significant (95% sign. level) VAPV anomalies (shaded) and VAPV values (lines) [pvu] averaged over intrusion episodes with the lowest vertical level (lowest level of 1.5PVU-surface within the intrusion system) between (a) 200 and 250 hPa (b) 250 and 300 hPa (c) 300 and 350 hPa and (d) below 350 hPa detected in the N-Atl region between 1980-2001 (Oct. to March).

(a) S-Atl **(b)** SE-Pac

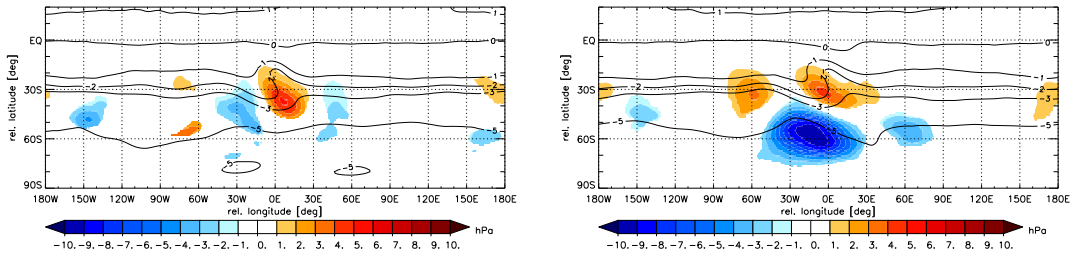

Figure A.4: Composite of statistically significant (95% level) SLP anomalies (shaded) [hPa] and VAPV values (lines) [PVU] averaged during the occurrence of the most intense intrusion episodes in the (a) S-Atl and (b) SE-Pac regions between 1980–2001 from April to September (#81 and #60).

(a) day -5 **(b)** day -3

(c) day -1 **(d)** day 0

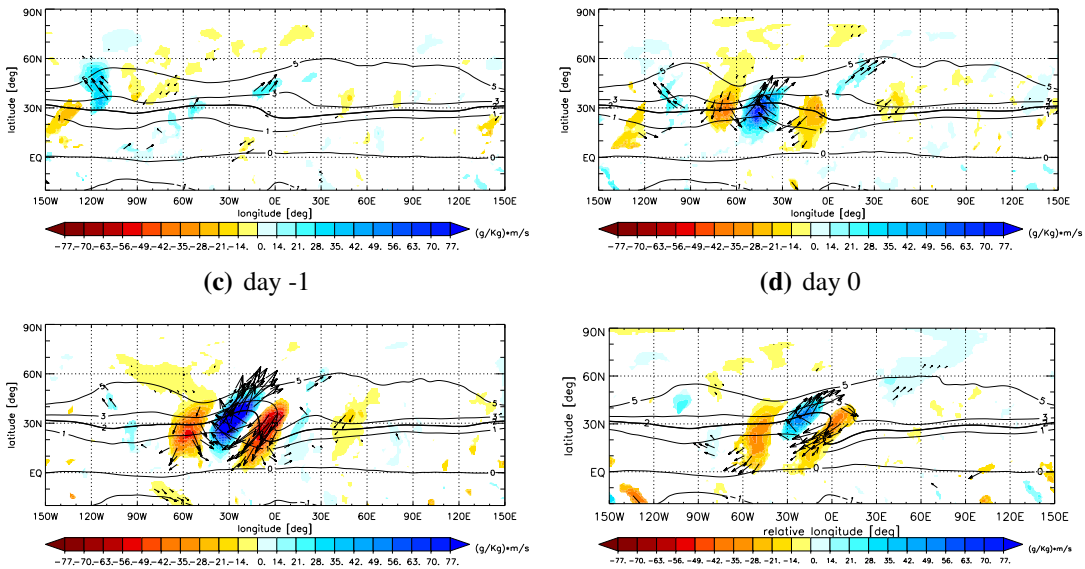

Figure A.5: Composite of statistically significant (95% level) moisture flux anomalies (vectors and meridional component shaded) and VAPV values (lines) [pvu] averaged (a) five days (b) three days, (c) one day before and (d) during the occurence of intense intrusion episodes in the N-Atl region from October to March between 1980-2001 (#102).

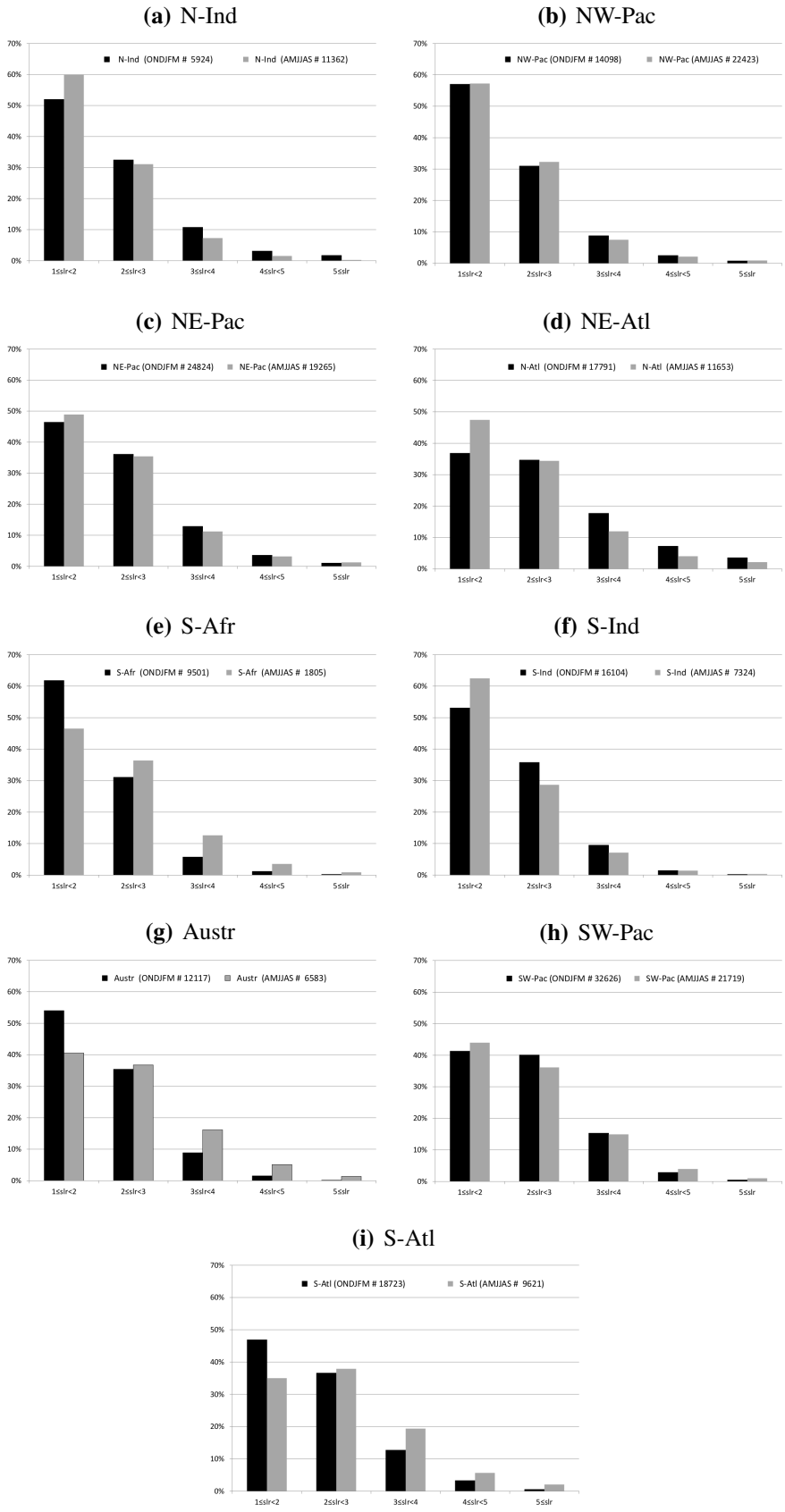

Figure A.6: Normalized distributions of TP side length ratio for the (a) N-Ind, (b) NW-Pac, (c) NE-Pac, (d) NE-Atl, (e) S-Afr, (f) S-Ind, (g) Austr, (h) SW-Pac and (i) S-Atl region. The black (grey) bars show boreal winter (summer) frequencies of the period July 1983–June 2006. The total numbers for each season and region are given in brackets. For more information about the calculation of LWR see Chap. 3.2. Regions are defined in Fig. 9.1a

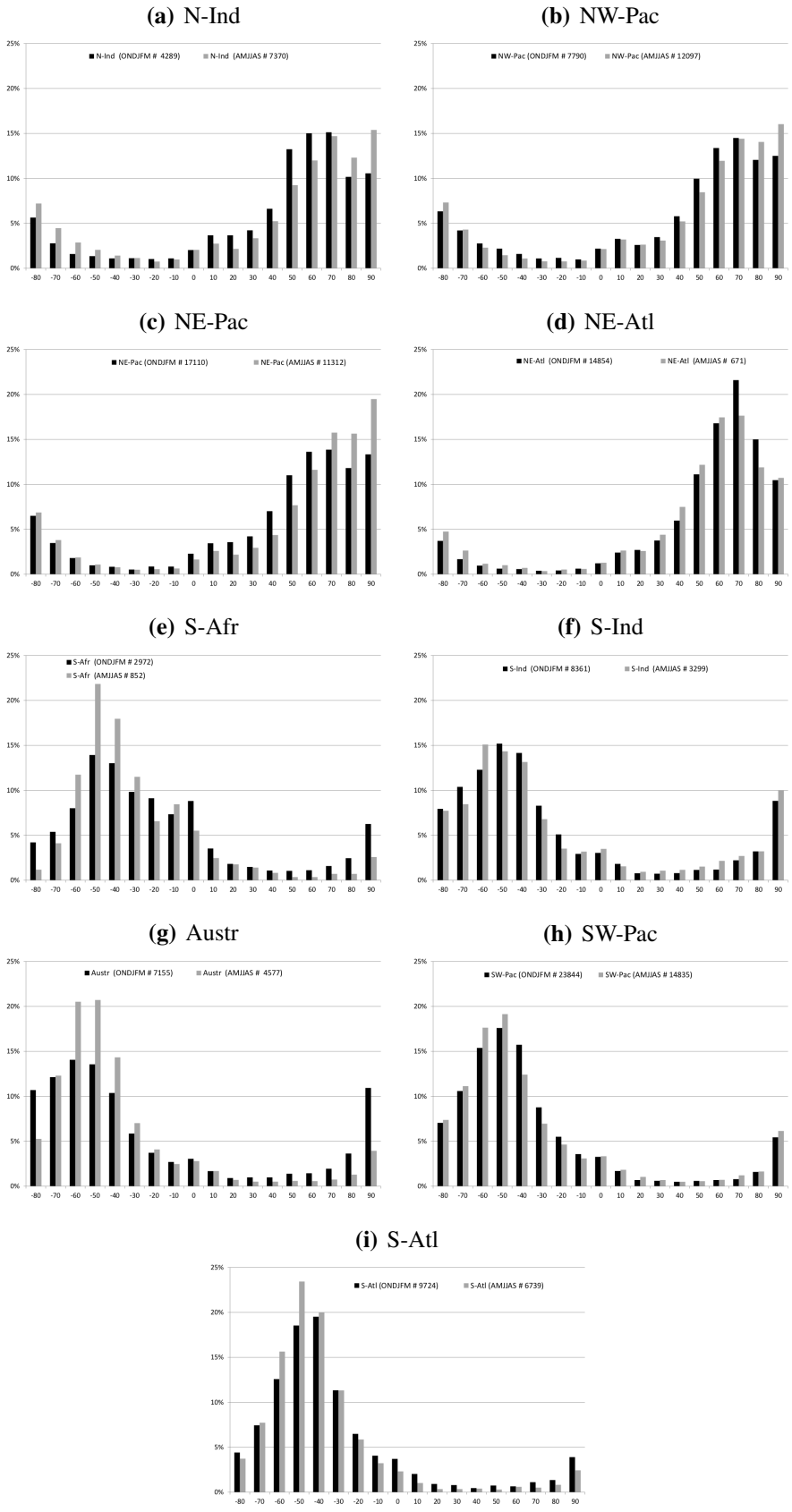

Figure A.7: Normalized distributions of TP horizontal tilt in (a) N-Ind, (b) NW-Pac, (c) NE-Pac, (d) NE-Atl, (e) S-Afr, (f) S-Ind, (g) Austr, (h) SW-Pac and (i) S-Atl region. The black (grey) bars show boreal winter (summer) frequencies of the period July 1983–June 2006. The total numbers for each season and region are given in brackets. For more information about the tilt calculation see Chap. 3.2. Regions are defined in Fig. 9.1a

(a) El Niño winter

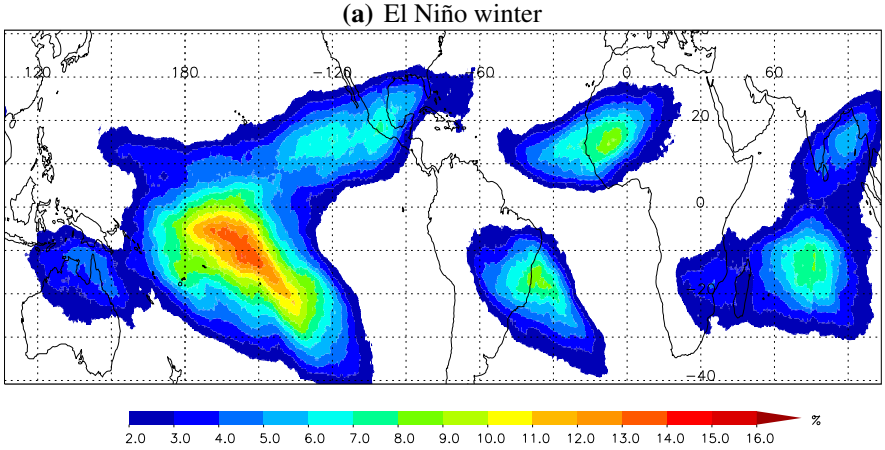

(b) La Niña winter

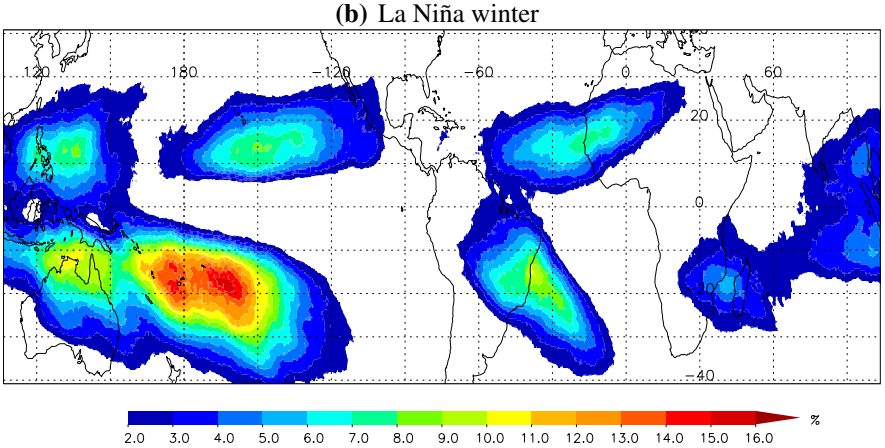

Figure A.8: Mean TP frequency [%] (shaded) averaged for the (a) 6 El Niño winter and (b) 5 La Niña winter between Jul. 1983 and Jun. 2006. ENSO winter are defined in Tab. 2.1.

Erklärung

Ich versichere, dass ich die von mir vorgelegte Dissertation selbständig angefertigt, die benutzten Quellen und Hilfsmittel vollständig angegeben und die Stellen der Arbeit – einschließlich Tabellen, Karten und Abbildungen–, die anderen Werken im Wortlaut oder dem Sinn nach entnommen sind, in jedem Einzelfall als Entlehnung kenntlich gemacht habe; dass diese Dissertation noch keiner anderen Fakultät oder Universität zur Prüfung vorgelegt hat; dass sie – abgesehen von unten angegebenen Teilpublikationen – noch nicht veröffentlicht worden ist sowie, dass ich eine solche Veröffentlichung vor Abschluss des Promotionsverfahrens nicht vornehmen werde.
Die Bestimmungen dieser Promotionsordnung sind mir bekannt. Die von mir vorgelegte Dissertation ist von Herrn Dr. habil. P. Knippertz und Prof. Dr. A. Fink betreut worden.

Teilpublikationen:
Fröhlich, L.; Knippertz, P., 2008: Identification and global climatology of upper-level troughs at low latitudes. Meteorol. Zeitschr., 17(5), 565-573

Ich versichere, dass ich alle gemachten Angaben wahrheitsgemäß nach besten Wissen und Gewissen gemacht habe und verpflichte mich, jedmögliche, die obigen Angaben betreffenden Veränderungen, dem Dekanat unverzüglich mitzuteilen.

Köln, den 30 November 2011

(Luise Fröhlich)